©Copyright 2017
Austin J. Phillips

Spatial Models as Powerful Tools for Climate Change Ecology

Austin J. Phillips

A dissertation
submitted in partial fulfillment of the
requirements for the degree of

Doctor of Philosophy

University of Washington

2017

Reading Committee:

Mark Kot, Chair

James Anderson

Lauren Buckley

Sándor Tóth

Program Authorized to Offer Degree:
Quantitative Ecology and Resource Management

University of Washington

Abstract

Spatial Models as Powerful Tools for Climate Change Ecology

Austin J. Phillips

Chair of the Supervisory Committee:
Dr. Mark Kot
Department of Applied Mathematics

Many scientists suggest that the Earth has entered a new geologic epoch, the Anthropocene, defined by human influence on nearly every physical and biological system. Climate change is perhaps the most widespread human impact. One ecological effect of climate change is the movement of species' habitats due to changes in temperature, precipitation, and other environmental variables. Populations may either track their habitats using dispersal, acclimate to new conditions with phenotypic plasticity, or adapt in place by rapid evolution. Though paleontological records give some clues about past responses to abrupt environmental change, the rapid pace of current climate trends leaves the fate of many species somewhat unknown.

Ecologists must, therefore, rely on predictive models to anticipate the dynamics of populations adjusting to their moving habitats. In this work, I focus on a number of spatial models that describe populations responding to their moving habitats. In the first two studies, I use integrodifference equations to describe populations that grow and disperse in distinct stages. Researchers have already used integrodifference equations to model populations tracking their habitats. My goal is to extend their work by (a) adding spatial realism and (b) comparing the long-term and short-term population dynamics that can be observed. In a third study, I use an optimization model based on reserve design to explore optimal management strategies for a population tracking its habitat. The model offers a prescriptive plan for allocating conservation resources under a limited budget.

In the first study, I model a population in two-dimensional space. I find that the shape of the population's moving habitat has a strong influence on the population's fate. The pattern of dispersal determines whether the population does best in a long habitat, a wide habitat, or a square habitat. Moreover, the study shows that simplified spatial models can greatly overestimate persistence compared to spatially realistic ones.

In the second study, I focus on the short-term dynamics of a population tracking its habitat. The model shows that a mismatch can occur between short-term and long-term population trends, which creates a confounding effect for prediction and management. I focus on understanding when and why such a mismatch occurs, depending on the population's biology, environment, and spatial distribution.

Finally, the third study highlights that management of vulnerable species during climate change must be dynamic. I focus on an at-risk population that grows, disperses, and acclimates as temperature increases over time. The model identifies, among a collection of habitat sites, the sequence of management actions that maximizes a conservation metric related to total population size. While many models incorporate dispersal into management decision analysis, this study makes an important advancement by including acclimation in an explicit way.

My approach with these three studies is to develop models that (a) advance the mechanistic understanding of population dynamics during climate change, (b) are easy to parameterize with data from a wide variety of species, and (c) make testable predictions. In doing so, I hope to inspire further interdisciplinary work between theoretical and applied ecologists as we confront the challenges of climate change.

TABLE OF CONTENTS

LIST OF FIGURES

LIST OF TABLES

ACKNOWLEDGMENTS

I would like to give heartfelt thanks to Mark Kot and Sándor Tóth for careful mentoring, inspiration, and financial support throughout my time at the University of Washington. I also wish to thank all of my committee members for helpful guidance and critiques. My graduate studies were funded through the National Science Foundation and the Seattle Chapter of the ARCS Foundation, to whom I am greatly indebted.

DEDICATION

To Rhona, for whom this seed is planted

Chapter 1

INTRODUCTION

1.1 The challenge of climate change

As a discipline, ecology is increasingly shaped by human impacts on biological systems. This trend is likely to continue, as many scientists suggest that the Earth has entered a new geologic epoch, the Anthropocene, defined by widespread human influence on natural systems [210, 215]. We no longer have the luxury of being natural historians who collect and observe from the outside. For ecosystems, the dimensions of human impact include pollution, overharvesting, habitat destruction, and climate change, with significant overlap between them [25]. Climate change is especially potent, since atmospheric and oceanic circulation amplify local forcing, such as CO_2 emission, to a global level. The emerging subfield of climate change ecology develops the theory of how environmental changes affect the abundance, distribution, behavior, and physiology of organisms [see, e.g., 94].

The goal of this work is to explore two types of models that advance climate change ecology. Because climate change is linked to geographic and spatial patterns, the models I consider will be spatial in nature. I first give a brief overview of recent and projected climate changes, as well as how those changes are anticipated to affect species. Next, I review a selection of spatial models used to address problems in climate change ecology. Finally, I give a more in-depth description of two types of models that lay the foundation for the remainder of this work.

The full breadth of projected climate changes is wider than my scope here. I narrow my attention to trends in mean temperature, mean precipitation, and the frequency and magnitude of extreme weather events. Mean temperature is projected to increase by 2–5 °C by the end of this century, with variation depending on the extent of future CO_2 emissions

[see, e.g., 111]. Regional variation is expected to cause much greater warming in certain regions such as the Arctic [175]. Precipitation changes are harder to project, but the general expectation is that wet areas will become wetter and dry areas will become drier. The frequency of high-magnitude weather events such as droughts and floods is very likely to increase [111].

Environmental changes have already altered the location and shape of species' suitable habitats. Temperature and moisture play a role in determining species' fundamental niches, so (under niche conservatism) environmental changes will affect where species can persist [242]. For example, global warming has pushed many habitats poleward and upslope [42, 221]. The cumulative effects of different stressors is an active area of research [80, 235].

One way to quantify habitat movement is the velocity of climate change, which is the ratio of the spatial and temporal gradients of an environmental variable such as mean temperature or precipitation [140, 141]. That is, it is the speed and direction an individual would have to move to maintain equal mean environmental conditions over time. Earlier studies emphasized the speed component, and more recent works consider the directional component and associated vector field properties [32, 61].

Apart from extinction, species may respond in three different ways to changing habitat availability. They may track their habitats using dispersal, acclimate using phenotypic plasticity, or adapt in place with rapid evolution [4, 107, 109]. Dispersal has led to observed range shift in many populations that coincides with habitat movement. Similarly, changes in phenology are widespread in many species as the dates of life-history events have changed in recent years [170]. Phenological shift allows species to track suitable conditions through time rather than over space. Rapid evolution due to climate change is supported by more restricted evidence so far [155].

The overall prediction for biodiversity is not simply that it will change, but that it will suffer [214]. As many as one in six species are at risk of extinction due to climate change [229]. While biota have survived multiple extreme environmental swings in geologic past, the current rate of change will be too high for many species [182]. Current temperature changes

differ from those during glacial–interglacial cycling, for example, in that the trend is global and made worse by factors such as habitat fragmentation. Climate change is projected to select for traits such as high fecundity, long-distance dispersal, and short generation time [173]. Hence, many species will do well under climate change, though the net outlook for biodiversity is grim.

1.2 Rising to the challenge with spatial models

1.2.1 Survey of approaches

To anticipate the effects of climate change on species, researchers have developed a spectrum of tools ranging from the statistical to the analytical. Species distributions models (SDMs) statistically correlate realized niches with environmental variables and then project future ranges based on climatic changes [64]. SDMs were originally used for other purposes, such as interpolating species occurrence across a region based on limited observations. The use of SDMs to extrapolate to novel climatic conditions warrants caution [249], but recent improvements (e.g., including biotic interactions and dispersal) have assured that SDMs remain useful spatial models for climate change ecology [23, 81, 223].

Individual-based models (IBMs) are another class of spatial models, and rely on simulation. To simulate a population tracking a moving habitat, an IBM includes rules for population growth and dispersal between discrete locations [26]. An environmental gradient that shifts over time represents climate change [22, 180]. IBMs can achieve a high degree of realism, but often at a heavy computational cost.

Reaction–diffusion equations (RDEs) represent an analytical approach to spatial ecology. Long before their use in the context of climate change, RDEs were used to describe the shape and speed of invasion waves, pattern formation, and the critical habitat size for a population to persist [see, e.g., 168, 208]. RDEs use partial differential equations with terms for growth and Gaussian-based diffusion in continuous space and time. The addition of shifting environmental gradients brought RDEs into the climate change ecology literature

[18, 17, 137]. RDEs are most appropriate when long-distance dispersal is negligible and movement can be described with diffusion, advection, and other kinetics-inspired processes.

1.2.2 Integrodifference equations

I will base the majority of this work on integrodifference equations (IDEs), which are complementary spatial models to those described above. IDEs model populations with distinct growth and dispersal phases [130]. They are the discrete-time analogs of RDEs and can accommodate a wider range of dispersal patterns. As with RDEs, research on IDEs led to advancements in characterizing invasions [126, 49], spatial pattern formation [166], chaotic dynamics [207], and critical patch sizes [135].

The canonical IDE has the form

$$n_{t+1}(x) = \int_{\Omega} k(x,y)\, f[\, n_t(y)\,]\, dy, \tag{1.1}$$

where $n_t(x)$ describes the population density over every location x at generation t. First, the population grows and reproduces according to the function $f[n_t(x)]$, which can take on a wide variety of density-dependent forms. Common examples include the Beverton–Holt stock-recruitment curve (compensation), the discrete-time logistic function (overcompensation), and functions with an Allee effect (depensation) [see, e.g., 131].

In the second stage, offspring disseminate according to the dispersal kernel $k(x,y)$, which is the relative frequency distribution of destinations x for source location y. A common (but not necessary) assumption is that dispersal only depends on the distance between source and destination, so that $k(x,y) = k(|x-y|)$. The dispersal kernel makes IDEs advantageous because it can accommodate a wide variety of movement patterns. Modelers can use field data, derivations from mechanistic first principles, or pre-existing probability distributions to derive dispersal kernels [30, 55, 163].

After dispersal, only offspring that land in the suitable habitat $\Omega \subseteq \mathbb{R}$ count toward the next generation. If $\Omega = \mathbb{R}$, all habitat is suitable for growth and IDE (1.1) describes the dynamics of an invasion. For a finite suitable habitat of length L, such as $\Omega = [-L/2, L/2]$,

the dynamics occur on a single patch. A natural question is whether the patch is large enough for the population to persist [135]. Similar formulations have been studied with alternating good and bad patches [60].

Model (1.1) and its extensions continue to be successful in ecology for three reasons. First, they generate mechanistic explanations for spatial patterns, For example, long-distance dispersal kernels in IDEs offer an explanation for accelerating waves of invasion that quickly advance populations over broad regions [126]. Coupled systems of IDEs (such as predator–prey systems) help explain how spatial patterns in population abundance can arise in homogeneous environments [166].

Second, model (1.1) can be modified to describe more nuanced aspects of biology such as stage-structure, demographic stochasticity, and optimal harvesting. Using stage-structured integrodifference models, researchers have explored the sensitivity of invasion speed to demographic parameters in species spanning a wide spectrum of life-histories [165]. The addition of demographic stochasticity to model (1.1) shows that invasion speeds are robust to the randomness inherent in individual reproduction and mortality [127]. Researchers have also used techniques from optimal control theory to describe the most profitable strategy for harvesting an IDE-governed population [114].

Third, IDEs are flexible enough to describe a wide variety of species. Although model (1.1) applies most directly to semelparous species with distinct life stages, it may also be considered a sampling of a continuously changing population at discrete time intervals. Applications span many taxa, including insects [126], crustaceans [116], weeds [209], trees [96], birds [236], non-human mammals [224], and humans [72]. An extensive literature exists on parameterizing IDEs given information on demography and dispersal [38, 79, 138].

1.2.3 Moving-habitat models

Recently, Zhou and Kot [252] used model (1.1) for an application in climate change ecology. By setting $\Omega = [-L/2 + ct, L/2 + ct]$, they considered a habitat of length L that moves at a speed of c per generation. Only individuals that land in the moving habitat

contribute to the next generation. The governing IDE is then

$$n_{t+1}(x) = \int_{-L/2+ct}^{L/2+ct} k(x-y) f[\, n_t(y)\,]\, dy. \tag{1.2}$$

where c is the velocity of climate change. Model (1.2) has become known as a moving-habitat model [95]. Zhou and Kot [252] showed that a population governed by model (1.2) will either persist and track its moving habitat or decline toward extinction. They calculated the critical speed of climate change, c^*, above which the population cannot persist. Importantly, c^* may be much less than the population's invasion speed (the speed at which it would move given unlimited suitable habitat). Thus, a population's risk level cannot be predicted by simply comparing the speed of climate change to its invasion speed.

Model (1.2) can easily morph into more complex forms that address different aspects of climate change. I will spend the next two chapters of this work showing just that. In Chapter 2, I analyze a moving-habitat model with two spatial dimensions. Chapter 3 explores the (often substantial) differences in short-term vs. long-term dynamics of model (1.2).

1.3 Reserve design: a spatial management approach

Climate change ecology is arguably marked more by synthesis than by new theory. The discussion above draws heavily from spatial ecology and population ecology, for instance. An equally important line of research comes from conservation ecology. Given current threats, understanding biodiversity should only be a precursor to safeguarding it. Managing species requires both descriptive and prescriptive tools.

1.3.1 History

Reserve design, or reserve selection, is a decision analysis framework used in conservation biology [35]. It begins with the assumption that different species or populations occur in different areas across a landscape. A land manager may apply some conservation action at each area. Depending on the situation, the action may include active processes such as

weeding or planting seeds; or, it may include passive processes such as building fences or disallowing urban development. Each action has an associated cost, and the general goal is to maximize some metric of conservation while minimizing cost. The number of possible combinations of when and where to apply action increases exponentially with the number of land areas and time steps. In response, reserve design draws on various mathematical tools to navigate the combinatorial explosion and find reasonable (if not optimal) solutions.

Formally, a reserve selection problem consists of an objective function, decision variables, and constraints. Early formulations of the problem focused on selecting sites (the decisions) such that the selected sites represent the greatest number of species (the objective), given that only a certain number of sites can be selected (the constraint) [48]. A similar approach, including multiple objectives, simultaneously maximizes species coverage and minimizes the total associated cost [50]. These formulations are examples of the maximal set covering problem, a classic problem in linear programming [47].

I will focus on a slightly different way to formulate the reserve selection problem that can incorporate some aspects of climate change ecology more naturally. Suppose there are N sites, and each site $i \in \{1, 2, \ldots, N\}$ has an associated ecological benefit a_i and cost of selection c_i. The benefit could be a metric of biodiversity, population abundance, or habitat quality. Take the binary decision variable X_i to equal 1 if site i is selected and zero otherwise. Assume the available budget is B. Then the objective is to

$$\text{maximize} \qquad \sum_{i=1}^{N} a_i X_i, \tag{1.3}$$

subject to

$$\sum_{i=1}^{N} c_i X_i \leq B. \tag{1.4}$$

This is a simple example of a knapsack problem—that of selecting which items to include in a "knapsack" (or set) so that the total value is largest and the items do not exceed the capacity of the set [147]. In a conservation context, the knapsack formulation differs from

the maximal covering formulation in that it assumes the values of selected sites are non-overlapping (i.e., that the benefit cannot be "double-counted" between sites).

The reserve selection literature quickly adapted to serve management needs [145]. It also began to include more ecologically nuanced assumptions. For example, sequential selection assumes that management decisions occur over time and are subject to time-varying costs, benefits, and constraints [34, 53, 158]. Models can include stochasticity when there is uncertainty around future land prices and extinction risks [7, 219, 226]. Other models incorporate population dynamics such as growth and dispersal between sites [20, 106].

Solving problems such as model (1.3–1.4) means finding the combination of decision variables that maximizes the objective function, if doing so is possible. Techniques from linear programming (and integer programming, when some variables are constrained to be integers) are suitable approaches [see, e.g., 246]. Model (1.3–1.4) is a binary integer program since the decision variables are binary. The branch-and-bound method works well for integer programs and guarantees an exact optimal solution. As the problem formulation and size grows in complexity, it is not always feasible to find an exact solution, however. Researchers have relied on simulated annealing, genetic algorithms, and a wide variety of other heuristic methods to tackle large-scale reserve selection problems [15, 143, 157].

1.3.2 Reserve selection and climate change

Climate change raises questions about the future efficacy of reserve design methods. First, will populations leave protected areas as their habitats move, rendering the areas ineffective? Preliminary studies suggest that some populations will, though the size of the effect is uncertain [9, 83, 176]. Second, how should reserve selection models anticipate the variety of species' responses to climate change? Dispersal is relatively well-represented in models, but few quantitative frameworks deal with acclimation or adaptation [92, 161].

In Chapter 4, I develop a mixed-integer linear program to address some of issues that climate change poses for reserve selection. ("Mixed-integer" implies that some variables are constrained to be integer, while others may be non-integer.) Technically, the model I propose

is not a proper reserve selection model, since it allows sites to be selected and unselected through time in a way that is uncharacteristic of actual reserves. Hence, I refer to it simply as a "site selection model" from now on, with the understanding that additional constraints could make it a reserve selection model.

Conceptually, the model follows a knapsack-like approach and allows sequential selection. That is, the decision variable $X_{i,t}$ is 1 if site i is selected at time t, and zero otherwise. Management occurs over the time horizon $t \in \{1, 2, \ldots, T\}$. The objective function, rather than being a linear combination of decision variables as in (1.3), is a linear combination of accounting variables $M_{i,t}$ that track the population size at each site over time. The purpose of creating such a roundabout objective is to allow the population sizes to depend dynamically on both previous population sizes and previous management decisions. I keep the financial side of the model fairly simple by assuming a fixed total budget B and site-specific selection costs $c_{i,t}$. The model has the form

$$\text{maximize} \qquad \sum_{i=1}^{N} \sum_{t=1}^{T} M_{i,t}, \tag{1.5}$$

subject to

$$M_{i,t+1} = \mathcal{F}(M_{1,t}, M_{2,t}, \ldots, M_{N,t}, X_{1,t}, X_{2,t}, \ldots, X_{N,t}) \tag{1.6}$$

and

$$\sum_{i=1}^{N} \sum_{t=1}^{T} c_{i,t} X_{i,t} \leq B. \tag{1.7}$$

The objective function (1.5) reflects the idea of retention—that the real goal is to maximize ecological benefit across the whole landscape, not just the selected sites. The "$\mathcal{F}$" in constraint (1.6) suggests a large and complicated function. Specifically, $\mathcal{F}$ will account for dispersal between sites, density-dependent growth, mortality due to whether a site is selected, and mortality due to environmental effects. The population has a limited ability to acclimate to environmental conditions, which change at a fixed rate to represent climate change. Now, admittedly, the knapsack analogy is strained: the objective is to maximize

the value of *all* items (selected or not), given that selecting one item changes the value of all others, and that the order of selection matters.

Climate change is already happening, to the detriment of many ecological systems. The purpose of this work is to advance climate change ecology with spatial models. I will show that the models provide conceptual understanding, make use of field data from a variety of species, and generate testable hypotheses.

Chapter 2

PERSISTENCE IN A TWO-DIMENSIONAL MOVING-HABITAT MODEL

2.1 Introduction

Species now face many environmental changes that affect survival. Habitat loss, overexploitation, pollution, and invasive species threaten many populations [33, 68, 104]. In addition, changes in temperature, precipitation, and other climate variables are moving habitats [42, 171, 170]. To avoid local extinction, organisms can track suitable conditions by dispersing, acclimate by changing their phenotypes, or adapt by evolving [4, 44, 107]. Constraints on these three responses vary and may prove deadly for many populations [29, 43, 109, 115, 182, 193, 194, 238]. Can scientists model climate-driven changes and help species survive?

Many studies focus on populations that track their habitats. Species distribution models relate climate variables, such as temperature, precipitation, and edaphic conditions, to realized niches and use climate projections to predict future ranges [13, 64, 86]. Individual-based models simulate individuals or populations on lattices with rules for population dynamics, dispersal, habitat, and climate change [19, 26, 133]. Reaction–diffusion approaches analyze the solutions of partial differential equations describing continuous growth and diffusion with moving range boundaries [18, 137, 178].

Integrodifference equations (IDEs) provide yet another approach to modeling population movement. Recently, Zhou and Kot [252, 253] used a one-dimensional IDE to study whether a population can track a moving habitat. They, in effect, assumed that organisms live in an infinitely long strip and leave the habitat in the direction perpendicular to the long axis of the strip. Using information on reproduction, dispersal, and habitat length, they calculated

the critical speed of climate change, above which the population goes extinct. Their model is an example of a one-dimensional moving-habitat model [95].

In this work, I generalize moving-habitat models to two dimensions. Having two spatial dimensions is advantageous. A modeler may wish to describe anisotropic dispersal across a landscape [190, 191, 209]. A land manager may wish to determine the best length and width for a rectangular migration corridor [54, 58, 82, 90, 139, 179, 228]. A two-dimensional moving-habitat model allows researchers to explore these scenarios. I will measure how a second dimension, i.e., width, changes the risk of extinction and find which habitat lengths and widths lead to persistence under climate change.

In section 2.2 , I will present the two-dimensional moving-habitat model. In section 2.3, I derive an eigenvalue problem that determines persistence. I will use numerical methods (section 2.4) and analytical approximations (section 2.5) to solve the eigenvalue problem. In section 2.6, I will explore how reproduction, dispersal, and habitat dimensions influence persistence. In section 2.7, I will illustrate the model using the Rocky Mountain Apollo butterfly (*Parnassius smintheus*) as a case study. Section 2.8 will discuss model limitations and future work.

2.2 Model formulation

Consider the integrodifference equation

$$n_{t+1}(x,y) = \int_{-L/2+ct}^{L/2+ct} \int_{-W/2}^{W/2} k(x-x', y-y')\, f[\, n_t(x',y')\,]\, dy'\, dx'. \tag{2.1}$$

Here, $n_t(x,y)$ describes the population density at location (x,y) at discrete generation t. The habitat is a rectangle of length L and width W, initially centered at the origin. The population changes from one non-overlapping generation to the next by a simple two-stage process. During the sedentary stage, individuals in the habitat grow, reproduce, and die according to some growth function, $f(n_t)$, such as the Beverton–Holt stock-recruitment curve

[21]. The growth function maps parent density n_t to offspring density $f(n_t)$. Here, I assume there is no Allee [5] effect.

During the dispersal stage, offspring (or propagules) with coordinates (x', y'), where $x' \in [-L/2 + ct, L/2 + ct]$ and $y' \in [-W/2, W/2]$, disseminate according to a dispersal kernel, $k(x-x', y-y')$. The kernel is the relative frequency distribution of propagule displacements. Common dispersal kernels include the bivariate Gaussian, Cauchy, and Laplace distributions [14, 132].

Each generation, the habitat moves c units in the positive x-direction (i.e., in the direction of habitat length) due to climate change. Habitat boundaries are fixed in the y-direction (in the direction of width). The velocity of climate change, c, may be to due to factors such as isotherm movement [31, 32, 140]. I assume c is constant.

The goal now is to analyze when integrodifference equation (2.1) leads to persistence or extinction.

2.3 Stability analysis

Since the habitat moves at a constant speed, it is helpful to shift the dynamics using the transformation

$$n_t(x, y) = \bar{n}_t(x - ct, y). \tag{2.2}$$

Rewriting governing equation (2.1) in terms of the new coordinates

$$\bar{x} \equiv x - ct - c, \qquad \bar{x}' \equiv x' - ct, \qquad \bar{y} \equiv y, \qquad \bar{y}' \equiv y' \tag{2.3}$$

and using substitution (2.2) gives

$$n_{t+1}(x, y) = \int_{-L/2}^{L/2} \int_{-W/2}^{W/2} k(x + c - x', y - y')\, f[\, n_t(x', y')\,]\; dy'\; dx', \tag{2.4}$$

where I have now dropped all bars for convenience. For units to make sense, please note that c is actually $c\Delta t$ with $\Delta t = 1$. The limits of integration in recursion (2.4) no longer depend on t, and the kernel is shifted by c in the x-direction.

The trivial equilibrium of system (2.4), $n_t(x, y) \equiv 0$, corresponds to local extinction. The local stability of the trivial solution determines whether extinction occurs. To determine stability, linearize system (2.4) about zero to get

$$n_{t+1}(x, y) = R_0 \int_{-L/2}^{L/2} \int_{-W/2}^{W/2} k(x + c - x', y - y')\; n_t(x', y')\; dy'\; dx', \tag{2.5}$$

where $R_0 \equiv f'(0)$ is the net reproductive rate.

In the spirit of separation of variables, I look for perturbations of the form

$$n_t(x, y) = \lambda^t\, u(x, y). \tag{2.6}$$

Recursion (2.5) now becomes

$$\lambda u(x, y) = R_0 \int_{-L/2}^{L/2} \int_{-W/2}^{W/2} k(x + c - x', y - y')\, u(x', y')\; dy'\; dx', \tag{2.7}$$

where λ is an eigenvalue with associated eigenfunction $u(x, y)$. Equation (2.7) a homogeneous Fredholm integral equation of the second kind [174].

Another way to write equation (2.7) is

$$\lambda u(x, y) = \mathcal{K}[\, u(x, y)\,], \tag{2.8}$$

where $\mathcal{K}$ is the linear integral operator

$$\mathcal{K}: \quad u(x, y) \to R_0 \int_{-L/2}^{L/2} \int_{-W/2}^{W/2} k(x + c - x', y - y')\, u(x', y')\; dy'\; dx'. \tag{2.9}$$

Persistence depends on the operator's spectral radius, $\rho(\mathcal{K})$. If $\rho(\mathcal{K}) < 1$, perturbations from zero decay over time and the population goes extinct. Persistence only occurs if $\rho(\mathcal{K}) > 1$. What determines $\mathcal{K}$'s spectrum? If the integral operator is compact, its spectrum is a discrete set [110, 118]. If, in addition, the dispersal kernel is positive and has infinite support, a generalization of Jentzsch's theorem guarantees $\mathcal{K}$ has a simple, positive dominant eigenvalue with a positive corresponding eigenfunction [117]. Jentzsch's theorem generalizes the Perron–Frobenius theorem from positive matrices to positive integral operators [108, 113]. I consider only compact operators and positive dispersal kernels, so there is guaranteed a simple, positive dominant eigenvalue that is the spectral radius.

The case $\rho(\mathcal{K}) = 1$ separates extinction and persistence. The goal is to find the critical speed c^* that makes $\rho(\mathcal{K}) = 1$. Solving eigenvalue problem (2.7) for c^* after setting $\rho(\mathcal{K}) = 1$ is difficult for an arbitrary dispersal kernel since the problem is infinite-dimensional. However, if problem (2.7) is approximated as finite-dimensional, it reduces to a matrix eigenvalue problem. The following two sections explore such approximations.

2.4 Numerical techniques

One way to reduce the dimension of problem (2.7) is to use Nyström's method to discretize the integrals on the right-hand side. Nyström's method relies on a quadrature rule such as the trapezoidal method to approximate the operator $\mathcal{K}$ with a matrix $\mathbf{A}$ [59, 181]. Dividing $[-L/2, L/2]$ into n equal subintervals, $[-W/2, W/2]$ into m equal subintervals, and evaluating the integrand in problem (2.7) only at grid points produces a matrix eigenvalue problem,

$$\lambda u = \mathbf{A}u. \tag{2.10}$$

Here, u is an $(m+1)(n+1) \times 1$ vector, and $\mathbf{A}$ is an $(m+1)(n+1) \times (m+1)(n+1)$ matrix. (Please see Appendix A.1.1 for a derivation of the elements of $\mathbf{A}$.) Since $\mathbf{A}$ is a positive matrix, its dominant eigenvalue is equal to its spectral radius, $\rho(\mathbf{A})$. I first calculate $\rho(\mathbf{A})$ and then use a root-finding routine such as the bisection method [181] to find the critical

speed c^* such that $\rho(\mathbf{A}) = 1$. Options for calculating $\rho(\mathbf{A})$ include the power method and routines such as `eig` or `spec` in computing environments such as MATLAB or R.

Three issues complicate solving eigenvalue problem (2.10). First, the size of $\mathbf{A}$, $O(n^2m^2)$, can create memory and speed issues. Fortunately, the assumption that the kernel has the form $k(x - x', y - y')$ means not all entries of $\mathbf{A}$ are unique. By storing only unique values of displacements, one can reduce the size to $O(nm)$.

Second, $\mathbf{A}$ is often nearly imprimitive. The dispersal kernels I consider have infinite support, so $\mathbf{A}$ is primitive. But if a subdominant eigenvalue is close to $\rho(\mathbf{A})$, the power method may converge very slowly or not at all. The method of Collatz is similar to the power method but calculates tight successive error bounds on $\rho(\mathbf{A})$ [51, 248, 247]. I follow the technique of Harsch [96], who used the Collatz method with a spectral shift to find dominant eigenvalues of imprimitive matrices.

Third, many common two-dimensional dispersal kernels are unbounded at the origin. For instance, the two-dimensional Laplace kernel contains a modified Bessel function of the second kind, which behaves logarithmically near zero [1, 241]. Other kernels become unbounded when converting a distribution of dispersal distances to a distribution of propagule locations [55]. Since elements of $\mathbf{A}$ require calculating $k(x + c - x', y - y')$, one simple way to avoid singularities is to shift y' grid points so that the routine never evaluates $k(0, 0)$ (see Appendix A.1.2).

2.5 Analytical approximations

Basis functions consisting of orthogonal polynomials, such as Legendre polynomials, have been used to solve integral equations [136, 240, 250] and are an alternative to Nyström's method. Legendre polynomials $P_i(x)$ form an orthogonal sequence in the Hilbert space $L^2[-1, 1]$. I follow Sansone [189] by rescaling $P_i(x)$ to fit intervals different than $[-1, 1]$. First, define two rescaled sets of polynomials, $X_i(x) = P_i(2x/L)$ and $Y_i(y) = P_i(2y/W)$, which are orthogonal on $[-L/2, L/2]$ and $[-W/2, W/2]$, respectively.

$$\int_{-L/2}^{L/2} X_i(x)X_j(x)\ dx = \frac{L}{2i+1}\delta_{ij}, \tag{2.11}$$

$$\int_{-W/2}^{W/2} Y_i(y)Y_j(y)\ dy = \frac{W}{2i+1}\delta_{ij}, \tag{2.12}$$

where δ_{ij} is the Kronecker delta function. The spans of $X_i(x)$ and $Y_i(y)$ are dense in their respective spaces, so the dispersal kernel has an expansion

$$k(x+c-x', y-y') = \sum_{i,j,k,\ell=0}^{\infty} b_{ijk\ell}X_i(x)X_j(x')Y_k(y)Y_\ell(y') \tag{2.13}$$

for some unique expansion coefficients $b_{ijk\ell}$. Note that there is a quadruple sum in (2.13), which I write with one sum for simplicity. One can recover the coefficients by using orthogonality properties (2.11)–(2.12) on expansion (2.13) (see Appendix A.2.1).

By truncating each sum in expansion (2.13) at some value N,

$$k(x+c-x', y-y') \approx \sum_{i,j,k,\ell=0}^{N} b_{ijk\ell}X_i(x)X_j(x')Y_k(y)Y_\ell(y'), \tag{2.14}$$

one can approximate the kernel as a separable function [135, 174]. Substituting the separable kernel approximation into integral eigenvalue problem (2.7) yields a matrix eigenvalue problem,

$$\lambda u = \mathbf{B}u. \tag{2.15}$$

Please see Appendix A.2.1 for a derivation of the elements of $\mathbf{B}$, which involve expansion coefficients $b_{ijk\ell}$.

Often, choosing $N = 0$, which treats $k(x+c-x', y-y')$ as a constant, estimates c^* well. System (2.15) becomes

$$\lambda\, u_{00} = R_0 LW b_{0000}\, u_{00}, \tag{2.16}$$

or

$$\lambda = R_0 LW b_{0000}. \tag{2.17}$$

At the critical speed, $\lambda = 1$, so

$$1 = R_0 LW b_{0000}. \tag{2.18}$$

Using the expression for b_{0000},

$$1 = \frac{R_0}{LW} \int_{-L/2}^{L/2} \int_{-L/2}^{L/2} \int_{-W/2}^{W/2} \int_{-W/2}^{W/2} k(x + c - x', y - y')\, dy\, dy'\, dx\, dx'. \tag{2.19}$$

The right-hand side of approximation (2.19) is the product of net reproductive rate and average dispersal success [67, 230, 231] with a shifted dispersal kernel. Since it arose from truncating the Legendre expansion at $N = 0$, I will refer to (2.19) as the $N = 0$ Legendre approximation.

To get an explicit approximation for c^*, expand $k(x + c - x', y - y')$ in a bivariate Taylor series around (x, y) in the $N = 0$ Legendre approximation. Keeping only quadratic terms and solving for c,

$$c^* = -\frac{\beta}{\gamma} + \sqrt{\left(\frac{\beta}{\gamma}\right)^2 - \frac{2\alpha}{\gamma} - \frac{(L^2\gamma + W^2\delta)}{12\gamma} + \frac{2}{R_0\gamma}}, \tag{2.20}$$

where α, β, γ, and δ are constants (see Appendix A.2.2). For radially symmetric kernels, β vanishes, but approximation (2.20) applies to anisotropic dispersal as well. As an alternative to the $N = 0$ Legendre approximation, truncate expansion (2.13) at higher terms

($N = 1, 2, \dots$) and solve the associated eigenvalue problem (2.15) numerically. I will refer to approximations using higher truncations in a similar way (e.g., the $N = 1$ Legendre approximation).

The Legendre method has some advantages over Nyström's method. The matrix $\mathbf{B}$ is much smaller than $\mathbf{A}$ in the associated eigenvalue problem. Legendre expansion also leads to an explicit approximation for c^*. However, there are some disadvantages.

First, elements of $\mathbf{B}$ are harder to compute. A quadruple integral is required rather than a single dispersal kernel evaluation. I used Monte Carlo integration to evaluate the expansion coefficients efficiently. With Monte Carlo integration, error decreases as $1/\sqrt{M}$ for M sample points, independent of the number of dimensions of integration, whereas the error in deterministic integration generally depends exponentially on the number of dimensions [93].

Second, there is no guarantee the truncated kernel expansion is everywhere nonnegative, even though the model requires a positive kernel [204]. As a result, often $\rho(\mathbf{B})$ does not correspond to a positive, real dominant eigenvalue, resulting in poor c^* approximations. One way to guarantee positivity to choose a higher value of N in truncation (2.14). Unfortunately, there is no *a priori* way to determine the necessary number of terms.

Another way to improve the Legendre method is to symmetrize the dispersal kernel before expanding in Legendre polynomials. Many studies have used symmetrization to bound maximal eigenvalues of nonnegative matrices [6, 123, 202]. For example, to bound the spectral radius of a nonnegative matrix $\mathbf{D}$, one can use the geometric mean to form the symmetric matrix $\mathbf{G}$, where $g_{ij} = \sqrt{d_{ij}d_{ji}}$. It is known that $\rho(\mathbf{G}) \leq \rho(\mathbf{D})$ and often gives a tight lower bound [6, 202]. Furthermore, symmetric matrices have the advantage of all real eigenvalues and orthogonal eigenvectors. Rather than constructing a matrix and then symmetrizing, one can take advantage of symmetry directly by constructing the geometrically symmetrized dispersal kernel,

$$k_G(x+c-x', y-y') \equiv \sqrt{k(x+c-x', y-y')\, k(x'+c-x, y'-y)}, \tag{2.21}$$

and using the kernel with either Nyström's method or the Legendre method.

Geometric symmetrization can also give an explicit approximation for c^* for some dispersal kernels [128]. Substituting $k_G(x+c-x', y-y')$ in eigenvalue problem (2.7) gives a new integral operator, $\mathcal{K}_G$. Since the kernel is symmetric, the spectral radius of the integral operator is the maximum value of the Rayleigh quotient

$$\rho(\mathcal{K}_G) = \max_{g \neq 0} \frac{\displaystyle\int_{-L/2}^{L/2}\int_{-L/2}^{L/2}\int_{-W/2}^{W/2}\int_{-W/2}^{W/2} k_G(x+c-x', y-y')\, g(x,y)\, g(x',y')\, dy'\, dy\, dx'\, dx}{\displaystyle\int_{-L/2}^{L/2}\int_{-W/2}^{W/2} g^2(x,y)\, dy\, dx} \tag{2.22}$$

[177]. I assume that $g(x,y)$ is square-integrable over its domain. To get a quick lower bound for $\rho(\mathcal{K}_G)$, set $g(x,y) \equiv 1$ to simplify the denominator to LW.

Setting $\rho(\mathcal{K}_G) = 1$ allows us to solve for c^* when the numerator of (2.22) is tractable. For example, symmetrizing the Gaussian kernel gives

$$k_G(x+c-x', y-y') = \frac{1}{2\pi\sigma^2} \exp\left[\frac{-c^2}{2\sigma^2}\right] \exp\left[\frac{-(x-x')^2}{2\sigma^2}\right] \exp\left[\frac{-(y-y')^2}{2\sigma^2}\right]. \tag{2.23}$$

Solving for c^* produces

$$c^* = \sigma\sqrt{2\ln\left(\frac{R_0 S_0}{2\pi\sigma^2 LW}\right)}, \tag{2.24}$$

where

$$S_0 = \left[\sqrt{2\pi}\sigma L \text{ erf}\left(\frac{L}{\sqrt{2}\sigma}\right) - 2\sigma^2 + 2\sigma^2 \exp\left(\frac{-L^2}{2\sigma^2}\right)\right] \times \left[\sqrt{2\pi}\sigma W \text{ erf}\left(\frac{W}{\sqrt{2}\sigma}\right) - 2\sigma^2 + 2\sigma^2 \exp\left(\frac{-W^2}{2\sigma^2}\right)\right]. \quad (2.25)$$

2.6 Results

How do reproduction, dispersal, and habitat dimensions affect persistence? I begin by describing the form of critical speed curves (plots of critical speed c^* vs. net reproductive rate R_0) and by comparing how different methods estimate these curves. Next, I explore the effects of habitat length and width on critical speed. Finally, I find the lengths and widths that lead to persistence and that maximize persistence.

2.6.1 Critical speed curves

If R_0 is below a certain threshold value, the population cannot withstand any climate change. Extinction below the threshold depends on the size, rather than the movement, of the habitat (as in the critical patch-size problem) [135]. Above the threshold, critical speed increases with the net reproductive rate R_0 (Fig. 2.1). These critical speed curves are qualitatively similar to those obtained by Zhou and Kot [252, 253], but they can differ quantitatively as the habitat width changes (see section 6.2).

When habitat length is small, there is close agreement between Nyström's method, the $N = 1$ Legendre approximation, and the symmetrization method (Fig. 2.1a). The Taylor expansion method is accurate for small c, but underestimates c^* as R_0 increases. For large L, the $N = 1$ Legendre approximation and Taylor expansion methods greatly overestimate c^* (Fig. 2.1b). The symmetrization method is immune to the large-L issue and gives a tight lower bound on c^*. These results on the accuracy of each method are similar to those in the one-dimensional moving-habitat model [128].

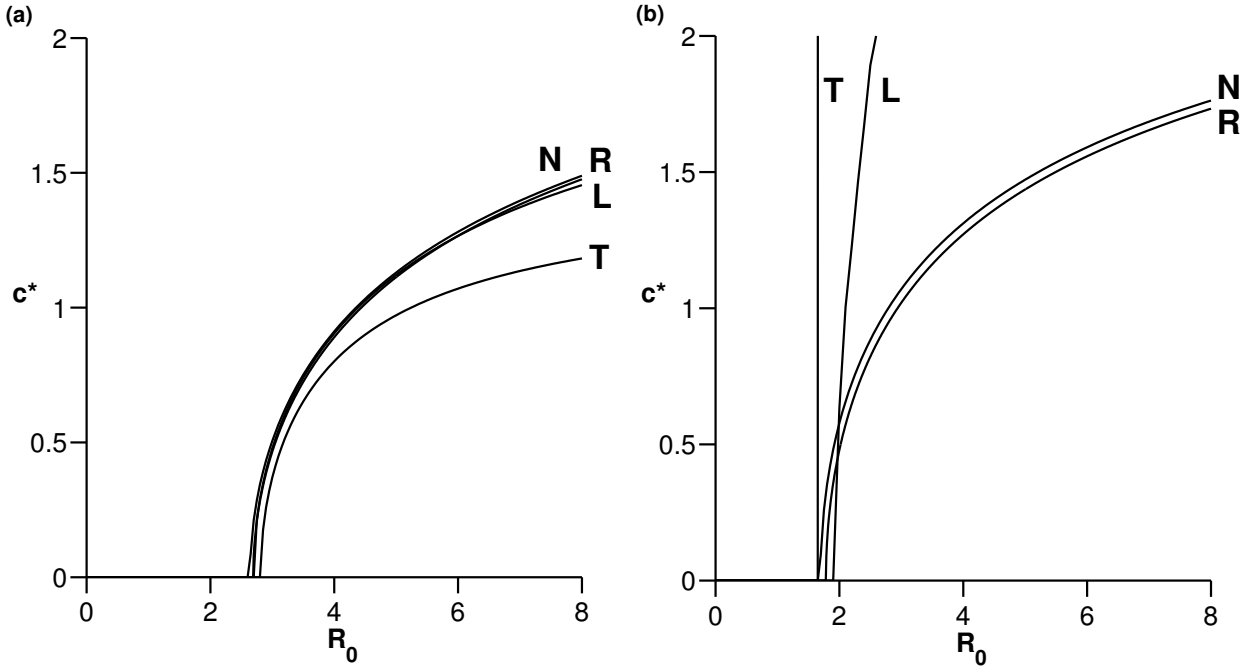

Figure 2.1: I compared **(a)** a small L-value of 2 km with **(b)** a large L-value of 10 km. $W = 2$ km in both plots. I used a two-dimensional Gaussian kernel with $\sigma = 1$ km. Techniques include Nyström's method with 10×10 grid points (N), Legendre expansion truncated at two terms (i.e., $N = 1$ approximation) (L), geometric symmetrization followed by a constant-eigenfunction Rayleigh quotient approximation (R), and a quadratic Taylor expansion (T). For small habitat length, the $N = 1$ Legendre approximation agrees closely with Nyström's method and the Rayleigh quotient. Taylor expansion is accurate for small c, but diverges for large c. However, when L is large, the $N = 1$ Legendre approximation and Taylor expansion method greatly overestimate persistence.

2.6.2 Effects of habitat size

How does the critical speed change as habitat length and width increase? As W increases with L fixed, the critical speed curve shifts to the left and the threshold R_0 decreases (Fig. 2.2a). Increasing W is of limited help, though: the curve approaches an envelope corresponding to a one-dimensional marginal distribution. For example, the curve found with a two-dimensional Gaussian kernel approaches the curve found by Zhou and Kot [252, 253] with a one-dimensional Gaussian kernel. Model (2.1) reduces to the one-dimensional moving-habitat model when width is infinite. Since the one-dimensional model effectively treats habitat as an infinitely long strip with finite length and infinite width, such a result is not surprising. However, if W is limited, ignoring habitat width can greatly overestimate persistence.

An envelope effect also occurs as L increases with W fixed (Fig. 2.2b). To understand why increasing L is of limited help, suppose length and width are infinite, as in the two-dimensional invasion problem [138] (Fig. 2.2c). Assume a finite speed of invasion, $\widehat{c}$. In the moving-habitat model, the population will never be able to move faster than $\widehat{c}$. Critical speed is bounded from above by the speed of invasion. For example, a population with Gaussian dispersal with variance σ^2 has a one-dimensional invasion speed of $\widehat{c} = \sqrt{2\sigma^2 \ln R_0}$ [126]. One can show a radially symmetric bivariate Gaussian kernel gives the same invasion speed in two dimensions using methods in Lewis [138]. This speed bounds c^* from above (Fig. 2.2c). The symmetrization technique (2.21) confirms the bound for Gaussian kernels, since the limit of expression (2.25) as L and W increase is $\sqrt{2\sigma^2 \ln R_0}$.

Some dispersal kernels do not lead to finite invasion speeds. Kernels with tails that are not exponentially bounded lead to accelerating waves of invasion [49, 126]. How do such kernels affect the dynamics of model (2.1)? For finite length and width, there is still a critical speed. As W increases with L fixed, the critical speed curve still approaches that of the one-dimensional marginal distribution. However, as L increases with W fixed, the curve approaches a vertical asymptote from the right. As both L and W increase, the vertical asymptote is $R_0 = 1$ (Fig. 2.2d). Thus, for kernels with tails that are not exponentially

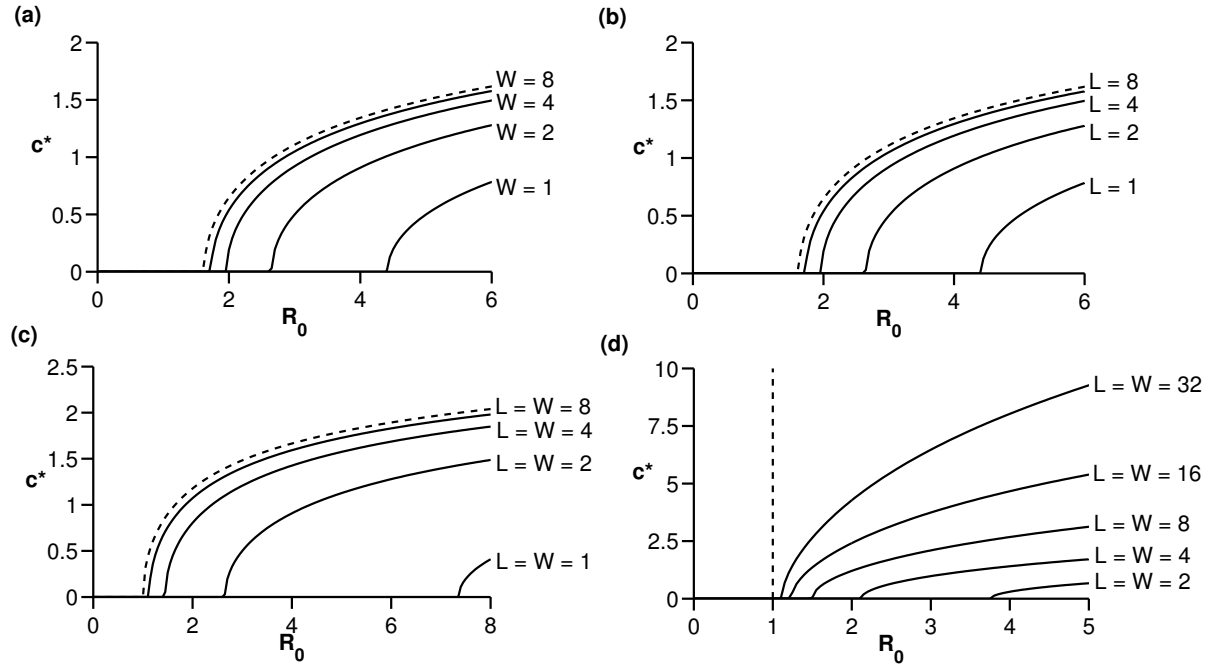

Figure 2.2: In **(a)**, $L = 2$ km is fixed and W increases. In **(b)**, $W = 2$ km and L increases. In **(c)** and **(d)**, both L and W increase. I used a Gaussian kernel with $\sigma = 1$ km in **(a)-(c)** and a Cauchy kernel (see Table 1) with dispersal parameter $\alpha = 1$ in **(d)**. In all four cases, curves shift left and approach envelopes (dashed) as habitat size increases, but envelopes differ qualitatively. In **(a)**, curves approach the critical speed curve associated with a one-dimensional Gaussian kernel. In **(b)**, increasing L increases persistence, but is limited. As both L and W increase **(c)**, critical speed approaches the invasion speed $\widehat{c} = \sqrt{2\sigma^2 \ln(R_0)}$ for the Gaussian kernel. For kernels with tails that are not exponentially bounded **(d)**, the critical speed curve approaches the asymptote $R_0 = 1$. Please note the different vertical scale in **(d)**. I used Nyström's method with 50×50 grid points for all computations.

bounded, increasing habitat length increases the critical speed without limit.

2.6.3 Importance of habitat length and width

I have shown that limiting habitat width lowers persistence. Width is important in another way. Although the habitat moves in the L-direction, habitat length is not always more important than width for persistence. There are two ways to compare the importance of L and W. First, I will describe the curve that separates persistence and extinction in (L, W) parameter space. Second, I will find the L and W values that maximize persistence.

In the one-dimensional critical patch-size problem, there is a habitat length below which persistence is impossible [121, 135]. The analog for a rectangular moving habitat is a curve in (L, W) parameter space (Fig. 2.3a–c, solid). I refer to such curves as critical size curves. Along each curve, the spectral radius is one.

I used the radially symmetric generalized Gaussian kernel,

$$k(r) = \frac{\beta}{\pi\,\Gamma(1/\beta)\,2^{1/\beta}\,\alpha^2} \exp\left[-\frac{1}{2}\left(\frac{r^2}{\alpha^2}\right)^{\beta}\right], \tag{2.26}$$

where $r = \sqrt{x^2 + y^2}$, to plot critical size curves for platykurtic ($\beta = 4$, Fig. 2.3a), mesokurtic ($\beta = 1$, Fig. 2.3b), and leptokurtic kernels ($\beta = 1/3$, Fig. 2.3c). Points above the curve lead to persistence, and points below the curve lead to extinction. The curves are not determined by habitat area. To show their symmetry, I reflected the curves across the diagonal $L = W$ (Fig. 2.3a–c, dashed). Some are symmetrical across the diagonal (Fig. 2.3b), meaning L and W are equally important for persistence. In such a case, switching L and W would not affect persistence. Other curves are tilted toward the W-axis (Fig. 2.3a) or the L-axis (Fig. 2.3c), meaning width or length are more important, respectively. For example, if a critical size curve is tilted toward the W-axis, a habitat with $W > L$ will lead to higher persistence than if length and width are switched. It is not always best to orient the longer side of a habitat parallel to the direction of climate change.

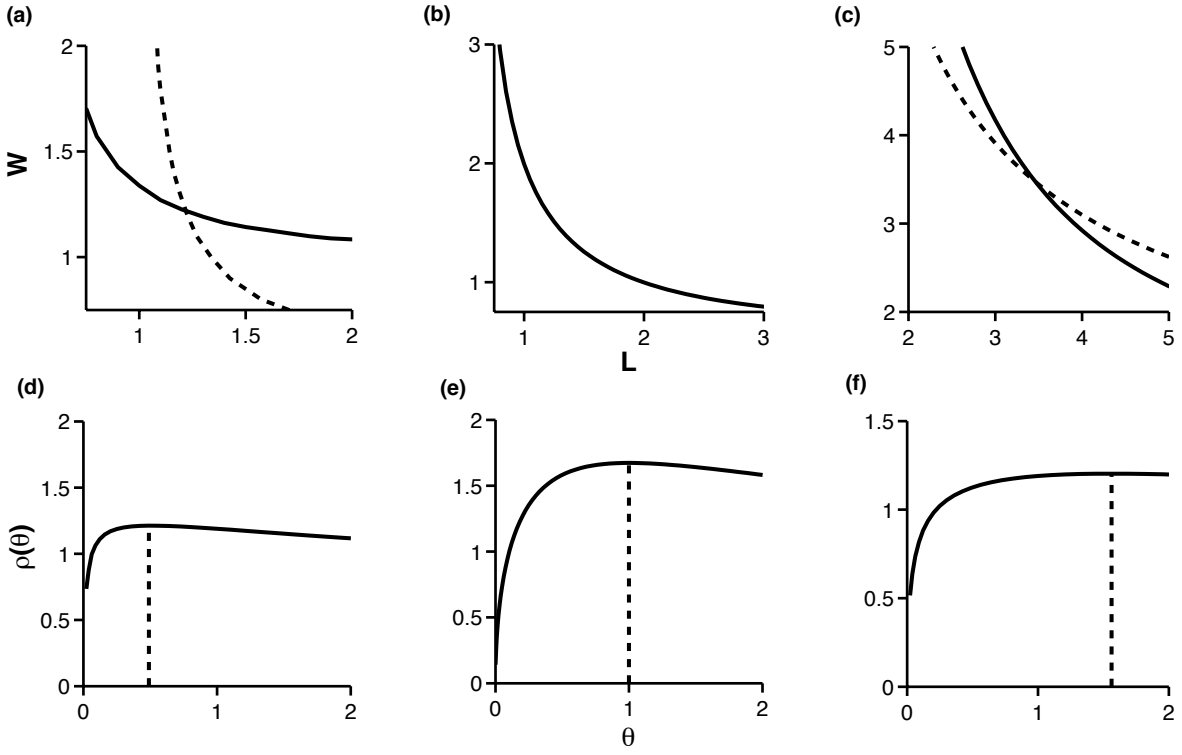

Figure 2.3: I varied β in the generalized Gaussian kernel (2.26) to make the kernel platykurtic in **(a)** and **(d)** ($\beta = 4$), mesokurtic in **(b)** and **(e)** ($\beta = 1$), and leptokurtic in **(c)** and **(f)** ($\beta = 1/3$). In **(a)-(c)**, solid curves are critical size curves and dashed curves are their reflections across the diagonal $L = W$ to show symmetry. In **(d)-(f)**, dashed lines show the location of the optimal aspect ratio under the constraint $LW = 4$ km^2. I used $c = 1$ km/yr, $R_0 = 6$/yr, and dispersal parameter $\alpha = 1$ km for all three kernels. I used Nyström's method with 15×15 grid points.

Another way to compare L and W is to constrain habitat area ($LW = A$ for some constant A) and to find which L- and W-values maximize spectral radius. An area constraint may arise when planning a conservation corridor with limited resources. With one free variable, the aspect ratio $\theta \equiv L/W$ defines each possible rectangular habitat. (Note that in some contexts aspect ratio cannot be less than one, but my usage here allows it.) Is there an optimal aspect ratio?

I used the dispersal kernels from Fig. 2.3a–c to plot spectral radius vs. aspect ratio under the constraint $LW = 4\,\mathrm{km}^2$. For some kernels, the optimal aspect ratio, θ_{opt}, is one (Fig. 2.3e). For others, $\theta_{\mathrm{opt}} < 1$ (Fig. 2.3d) or $\theta_{\mathrm{opt}} > 1$ (Fig. 2.3f). The location of θ_{opt} relative to one depends on the symmetry of the critical size curve. For example, suppose a curve is tilted toward the W-axis. If there exists an optimal aspect ratio, it must be less than one; otherwise, switching L and W would increase the spectral radius.

In addition to the generalized Gaussian dispersal kernel, I chose a number of other radially symmetric kernels and measured the optimal aspect ratio under an area constraint (Table 2.1). The kernels are grouped based on bivariate kurtosis, $\gamma_{2,2}$ (see below). In section 2.8, I hypothesize how kurtosis affects the relative importance of length and width. For now, I briefly review bivariate kurtosis and how to calculate it.

There are different interpretations of kurtosis as a distribution descriptor; most include peakedness, tail weight, and lack of shoulders. Distributions with low peaks, broad shoulders, and thin tails such as the uniform distribution are platykurtic; those with sharp peaks, low shoulders, and heavy tails such as the Laplace distribution are leptokurtic; and intermediate ones such as the Gaussian are mesokurtic. Many measures of bivariate kurtosis exist [148, 156, 212]. A suitable choice is given by Mardia [144],

$$\gamma_{2,2} = E\left[\frac{(x-\mu_1)^2}{\sigma_x^2} + \frac{(y-\mu_2)^2}{\sigma_y^2}\right]^2 - 8. \tag{2.27}$$

$E[\,\cdot\,]$ denotes expected value. In this case, x and y are the random variables for propagule displacement, μ_1 and μ_2 are their means, and σ_x^2 and σ_y^2 are their variances. The '-8 ' term

Table 2.1: Optimal aspect ratios for platykurtic, mesokurtic, and leptokurtic dispersal kernels. Kernels include only radially symmetric unimodal distributions. I constrained $LW = 4$ km^2 and set $c = 1$ km/yr in each case. I also calculated θ_{opt} for a range of different dispersal parameter values. In all cases, Conjecture 2 gave the correct prediction.

Kurtosis	Kernel	Functional Form $k(r)$	Parameter Values	$\gamma_{2,2}$	θ_{opt}
Platykurtic	Generalized Gaussian	$\dfrac{\beta}{\pi\,\Gamma(1/\beta)\,2^{1/\beta}\,\alpha^2}\exp\left[-\dfrac{1}{2}\left(\dfrac{r^2}{\alpha^2}\right)^{\beta}\right]$	$\alpha = 1$, $\beta = 4$	-4.808	0.49
	Uniform	$\begin{cases}\dfrac{1}{\pi\alpha^2} & \text{if } r < \alpha,\\ 0 & \text{otherwise}\end{cases}$	$\alpha = 1$	-2.665	0.7225
	Raised cosine	$\begin{cases}\dfrac{\pi}{\alpha^2(\pi^2-4)}\left[1+\cos\left(\dfrac{r}{\alpha}\pi\right)\right] & \text{if } r < \alpha,\\ 0 & \text{otherwise}\end{cases}$	$\alpha = 2$	-1.45	0.8100
Mesokurtic	Gaussian	$\dfrac{1}{2\pi\sigma^2}\exp\left(-\dfrac{r^2}{2\sigma^2}\right)$	$\sigma = 1$	0	1
Leptokurtic	Generalized Gaussian	same as above	$\alpha = 1$, $\beta = 1/3$	0.528	1.4400
	Cauchy	$\dfrac{\alpha}{2\pi}\dfrac{1}{(r^2+\alpha^2)^{3/2}}$	$\alpha = 1$	undefined	1.3225
	Laplace	$\dfrac{\gamma^2}{2\pi}K_0(\gamma r)$	$\gamma = 1$	6.3441	1.5625

is a correction to give $\gamma_{2,2} = 0$ for mesokurtic distributions. I have assumed $\mathrm{Cov}(x, y) = 0$. Further assuming $\mu_1 = \mu_2 = 0$, $\sigma_x^2 = \sigma_y^2 = \sigma^2$, and radial symmetry, Mardia's expression (2.27) simplifies to

$$\gamma_{2,2} = \frac{2\pi}{\sigma^4} \int_0^\infty k(r)\, r^5\, dr \; - \; 8, \tag{2.28}$$

where $r = \sqrt{x^2 + y^2}$. Negative $\gamma_{2,2}$ values correspond to platykurtic kernels and positive values to leptokurtic ones. For mesokurtic kernels, $\gamma_{2,2} = 0$.

The platykurtic kernels chosen gave optimal aspect ratios smaller than one, meaning highest persistence occurs when $L < W$. The leptokurtic kernels gave optimal aspect ratios larger than one, meaning highest persistence occurs when $L > W$. The mesokurtic Gaussian kernel gave an optimal ratio of one.

2.7 Application

Model (2.1) can easily incorporate data to quantify species' risk under climate change. As an example, I consider the Rocky Mountain Apollo butterfly (*Parnassius smintheus*). The species fits many (but not all) model assumptions. I first generate critical speed curves for different habitat sizes and dispersal parameters. Then, I calculate the optimal aspect ratio under an area constraint.

P. smintheus inhabits alpine and sub-alpine meadows in the Rocky Mountains of North America from Mexico to British Columbia [186]. It is not endangered, but other members of the *Parnassius* genus have been sources of conservation efforts [3]. It is semelparous, with one synchronous reproductive period per year. Larvae feed on a perennial obligate host plant, *Sedum lanceolatum*, from which they sequester a defensive toxin that keeps predation rates low [149]. Over fourteen flowering plant species spanning a range of flowering periods provide nectar for adults. Populations display no demographic Allee effect, and growth is greatest at low population densities [151].

Meadows are small in size [184] and are often located between the tree line and the tree limit [150]. Each meadow constitutes a population. Females fly less than males and often crawl on the ground, seeking oviposition sites [184]. Populations are effectively isolated if separated by more than 1 km of forest, the main dispersal barrier [185]. Dispersal kernels in the *Parnassius* genus have been fit with negative exponential distributions of dispersal distance [78, 152, 153, 184]. Converting from a distribution of dispersal distances to a two-dimensional kernel [55] gives

$$k(r) = \frac{\alpha}{2\pi r} \exp(-\alpha r), \tag{2.29}$$

where α is the inverse of mean dispersal distance.

P. smintheus is expected to respond to current climate change. Populations have moved upslope during interglacial periods and downslope during glaciation throughout the Pleistocene [57, 196]. Increasing temperatures are raising tree lines, which fragments populations and moves habitats upslope [185]. I converted tree line rise to distance along the mountainside to estimate the velocity of climate change c.

Will fragmented populations be able to track their moving habitats? Critical speed curves for three meadow sizes and two dispersal parameters give some insight (Fig. 2.4). For the estimate $c = 0.01$ km/year, small habitat size and high dispersal decrease persistence more than habitat movement. With an estimated $R_0 = 3.75$/yr, low-dispersing butterflies (Fig. 2.4, solid) could survive many habitat sizes. For high dispersal (Fig. 2.4, dashed), small habitats may result in local extinction. Habitat movement is slow enough that high dispersal causes too many individuals to be lost outside the habitat, especially for small meadows. The effect of $c = 0.01$ km/year on the threshold R_0 needed to survive is negligible (Fig. 2.4, solid horizontal). Model (2.1) suggests *P. smintheus* can track its moving habitat, but that small meadow size may decrease persistence.

Habitat length is more important than width for *P. smintheus* since the optimal aspect ratio is greater than one (Fig. 2.5). Despite the slowly shifting habitat, it is more helpful to

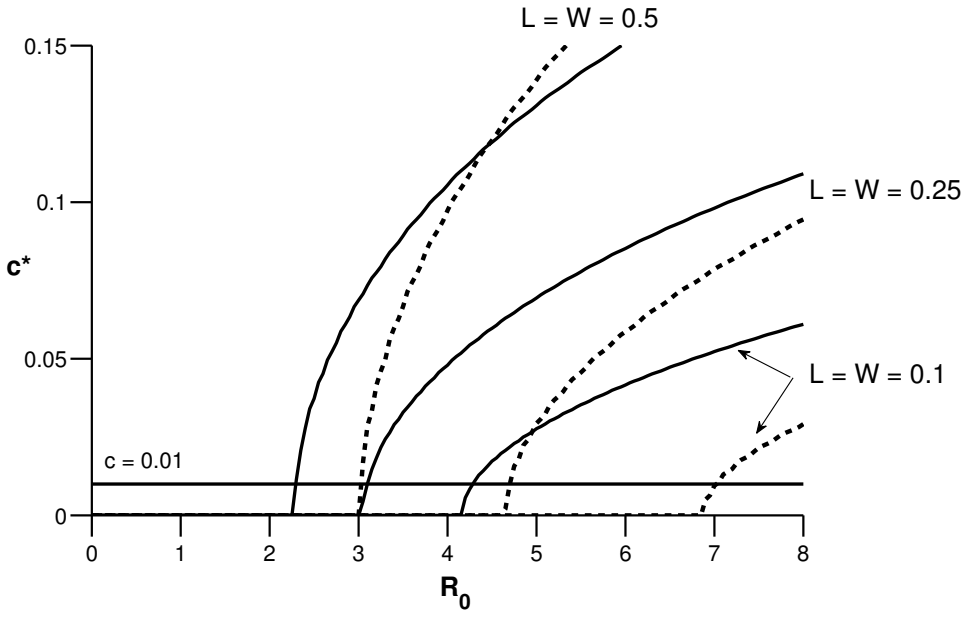

Figure 2.4: I used three different habitat sizes (0.5 km $\times$ 0.5 km, 0.25 km $\times$ 0.25 km, and 0.1 km $\times$ 0.1 km) with two different dispersal parameters for *P. smintheus*. Solid curves indicate low dispersal ($\alpha = 8.3$/km) and dashed curves indicate high dispersal ($\alpha = 4.3$/km) using the kernel (2.29). The estimate $c = 0.01$ km/yr (horizontal line) shows low habitat area and high dispersal are more detrimental than habitat movement. I used Nyström's method with 60×59 shifted grid points (see Appendix A.1.2)

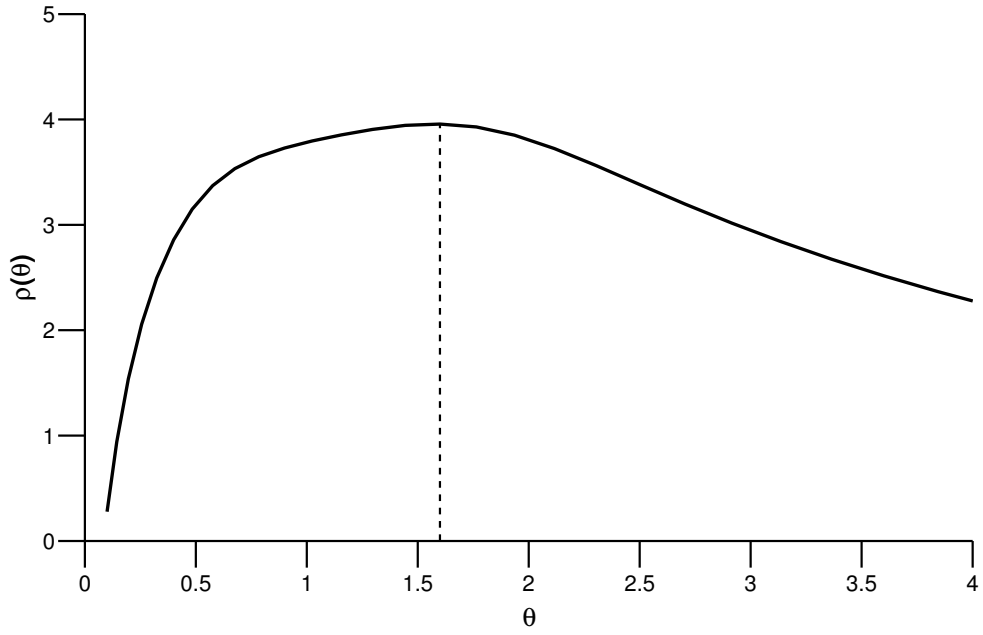

Figure 2.5: I used L values ranging from 0.1 km to 0.25 km and constrained habitat area $LW = 0.025$ km^2. I used $R_0 = 6$/yr, $c = 0.01$ km/yr, and $\alpha = 4.3$/km. The highest spectral radius occurs when $L > W$.

have habitat further upslope than along the same elevation.

2.8 Discussion

Species' habitats are likely to continue to move [32]. For some species, dispersal may be the only viable response [182]. The two-dimensional moving-habitat model (2.1) can test whether dispersal alone is enough to persist. The model is most salient when static dispersal barriers constrain habitat width and changing climate variables constrain habitat length. Many dispersal barriers are permanent and climate change continues, so the model should become increasingly applicable.

Having two dimensions comes at a computational cost (sections 4 and 5). Simulation and eigenvalue computation for model (2.1) requires double the integration and quadruple the matrix size compared to the one-dimensional moving-habitat model. The Legendre method

can be inaccurate when L is large or the truncation value N is small. Many two-dimensional dispersal kernels of interest are unbounded at the origin, making kernel evaluation difficult.

Fortunately, there ways around the above computational issues. The assumption that the dispersal kernel is only a function of displacement reduces the size of matrices. Monte Carlo integration outperforms deterministic quadrature rules for quadruple integration. Geometric symmetrization in combination with the Rayleigh quotient gives a tight lower bound on spectral radius. The method of Collatz combined with a spectral shift speeds up eigenvalue computations. Finally, shifting grid points sidesteps the problem of dispersal kernel singularities.

In Section 2.6.2, I showed that limiting habitat width lowers persistence compared to the one-dimensional moving-habitat model, which effectively assumes infinite width. Critical speed curves show the effects of increasing length and width. As width increases, moving-habitat model (2.1) reduces to the one-dimensional version. Thus, widening the habitat is of limited help for persistence. As both length and width increase, the model reduces to the two-dimensional invasion problem. For dispersal kernels with tails that are not exponentially bounded, lengthening the habitat increases persistence without limit. For kernels with exponentially bounded tails, lengthening the habitat is of limited help

The shape of the dispersal kernel changes the relative importance of length and width. The critical size curve separating persistence and extinction in (L, W) parameter space can be symmetrical; or, it can tilt toward either axis, indicating whether switching L and W would increase or decrease persistence. Under the area constraint $LW = A$, plotting spectral radius vs. aspect ratio L/W shows the optimal aspect ratio can change. The critical size curve's symmetry determines whether the optimal ratio will be larger than, smaller than, or equal to one.

I hypothesize that, for radially symmetric dispersal kernels, the kurtosis of the kernel controls the importance of length and width. Platykurtic kernels tilt the critical size curve toward the W-axis, making $\theta_{\text{opt}} < 1$. Leptokurtic kernels tilt the curve toward the L-axis, making $\theta_{\text{opt}} > 1$. For mesokurtic kernels, the curve is symmetrical and $\theta_{\text{opt}} = 1$. The

following conjectures state this hypothesis formally.

2.8.1 Conjecture 1a:

For each radially symmetric dispersal kernel, net reproductive rate, speed of climate change, and pair of habitat dimensions (L, W), let $\rho(L, W)$ be the corresponding spectral radius. Assume $L > W$. Then

$$\rho(L,W) \begin{cases} < \rho(W,L) & \text{if } \gamma_{2,2} < 0, \\ = \rho(W,L) & \text{if } \gamma_{2,2} = 0, \\ > \rho(W,L) & \text{if } \gamma_{2,2} > 0. \end{cases} \tag{2.30}$$

Conjecture 1a describes the effect of switching L and W, and thus the symmetry of the critical size curve. Given a rectangular habitat, the conjecture states that it is better to orient the long side perpendicular to the direction of habitat movement for platykurtic dispersers and parallel for leptokurtic dispersers. For mesokurtic dispersers, the two orientations are equivalent. Radial symmetry is necessary in the conjecture because, for example, one can construct a Gaussian kernel that is stretched in the L-dimension ($\sigma_x^2 > \sigma_y^2$). For such a kernel, $\gamma_{2,2} = 0$, but it is better to orient the long habitat side parallel to habitat movement.

2.8.2 Conjecture 1b:

For each radially symmetric dispersal kernel, net reproductive rate, speed of climate change, and habitat area, there is a single aspect ratio θ_{opt} that maximizes $\rho(\theta)$. Furthermore,

$$\theta_{\text{opt}} \begin{cases} < 1 & \text{if } \gamma_{2,2} < 0, \\ = 1 & \text{if } \gamma_{2,2} = 0, \\ > 1 & \text{if } \gamma_{2,2} > 0. \end{cases} \tag{2.31}$$

Conjecture 1a did not limit L- and W-values, in which case there is no "best" habitat design. Conjecture 1b assumes an area constraint and gives the location of θ_{opt} relative to one. When designing rectangular conservation corridors or other habitats with fixed area, there are many possibilities. For mesokurtic kernels, I conjecture that $L = W = \sqrt{A}$ is best. For platykurtic kernels, highest persistence occurs for some $W > L$. For leptokurtic kernels, the optimum occurs for some $L > W$. Please keep in mind that I assume the habitat moves at a constant speed. The optimal reserve or corridor designs the model suggests must be dynamic and move with the changing climate. For example, sequential reserve selection would be necessary to maintain a rectangular habitat that moves over time.

Statement (2.31) follows from Conjecture 1a plus the assumption that there exists a single optimal aspect ratio. The examples in Fig. 2.3 and Table 2.1 provide evidence, but not proof, of a single optimal aspect ratio for each dispersal kernel. An attempt to prove Conjecture 1a or 1b is beyond my scope here, but one can prove a weaker version of the mesokurtic case of 1b using geometric symmetrization of the Gaussian kernel (see Appendix A.3).

Model (2.1) made assumptions on biology, habitat, and climate change, many of which could be relaxed. Dispersal is not the only response to climate change, and it may occur in conjunction with evolutionary or plastic responses. Whether co-occurring responses help or hinder persistence in an integrodifference model is an open question.

Another line of future research is transient dynamics in model (2.1). Since habitat and

climate are heterogeneous over space and time, transient dynamics may be more important than asymptotic behavior. For example, a population moving through a spatial bottleneck may persist asymptotically on either side, but model (2.1) cannot address how much the bottleneck might reduce population levels temporarily. Species tracking habitats upslope, including *Parnassius smintheus*, will run out of space if change is constant. For such species, long-term behavior is uninformative. Metrics such as reactivity [39, 164] and the damping ratio [37] could quantify persistence in the short term.

Finally, Conjectures 1a and 1b are unproven. It remains an open challenge to prove the role of kurtosis or show another measure determines the importance of length and width. I hope to incorporate the above topics into future studies, and encourage researchers to continue seeking the rich patterns in spatial dynamics.

Chapter 3

WILL TRANSIENT DYNAMICS HELP OR HURT SPECIES DURING CLIMATE CHANGE?

3.1 Introduction

Climate change is forcing many species to track suitable conditions, adapt in place, or face extinction [80, 229]. Changes in temperature, precipitation, and other climate variables are moving habitats, often at unprecedented speeds [31, 42, 141, 170, 221]. Low dispersal rates and other constraints may prevent populations from keeping pace with their habitats [29, 52, 194]. The ability to predict whether populations can track their habitats is essential to developing risk assessments and management plans. As a result, spatial models of population dynamics are more important than ever.

Recent studies of populations tracking their moving habitats use integrodifference equations [95, 172, 252] or partial differential equations [18, 137, 178]. These models measure a population's risk by its long-term dynamics—whether local extinction occurs asymptotically. However, short-term, or *transient*, dynamics may be more important for developing ecological understanding than long-term dynamics [98]. Transient dynamics include a system's behavior before it approaches a long-term state such as an equilibrium point, limit cycle, or other attractor. Even in simple mathematical models, short-term and long-term trajectories may differ [39, 164]. For example, a population may grow in size initially (known as amplification) before declining toward extinction, or it may decrease initially (known as attenuation) before entering a long-term growth phase. Transient trajectories (or, simply, transients) can occur on the same timescale as the total time to approach equilibrium.

Transients are especially important for climate change ecology. First, environmental changes set many populations out of equilibrium with their habitats [220]. By definition,

transients will be prominent in the time period before populations regain equilibrium. Second, if perturbations such as extreme weather events are frequent enough to reset an ecological system before asymptotic dynamics set in, long-term behavior is less relevant [65]. Third, some species that are shifting poleward or upslope will run out of space if climate change continues [32, 63, 77]. Models should address whether such populations can survive in the short-term, before either humans reduce the effects of climate change or populations adapt in place.

Most studies of transient dynamics use non-spatial models of structured populations or multispecies systems [164, 211, 218]. In such systems, transient amplification and attenuation can occur because there are multiple states (ages, stages, or species) that interact and change at different rates. Researchers have also considered transients in spatial models, including transient chaos [99], transient persistence in spatially coupled predator–prey systems [97], the return time to equilibrium in metapopulation models [169], and sensitivity analysis of stage-structured invasion models [40, 165]. However, no studies have explored amplification and attenuation in a spatial model of a single, unstructured population. Is spatial structure enough to produce transient dynamics?

I will use an integrodifference equation (or IDE) to analyze the transient dynamics of a single, unstructured population tracking its moving habitat (hereafter called a moving-habitat model, MHM). In Section 3.2, I briefly review non-spatial models of transients and describe the MHM. Section 3.3 focuses on metrics for transients in the MHM. In Sections 3.4 and 3.5, I use Fender's blue butterfly (*Icaricia icarioides fenderi*) as a model species to discuss how a population's biology, environment, and distribution affect transients. In Section 3.6, I briefly discuss how transient metrics can be extended to stage-structured moving-habitat models, using four plant species as examples. Finally, Section 3.7 considers whether spatial transients will help or hurt a population tracking its habitat, with potential lessons for conservation during climate change.

3.2 Model formulation

Non-spatial models of structured populations or interacting species make up most of the literature on ecological transients, so I will briefly outline their features. Later, I show that the MHM exhibits transients because, in many ways, it is mathematically equivalent to the following non-spatial model.

Consider the linear, discrete-time model

$$\mathbf{n}_{t+1} = \mathbf{A}\mathbf{n}_t \tag{3.1}$$

with initial condition $\mathbf{n}_0$. The vector $\mathbf{n}_t$ represents the number or density of individuals in each of a number of states at discrete time t. The states may represent different ages or stages within a single population, in which case $\mathbf{A}$ is a population projection matrix (PPM) that describes the transition between different ages or stages over time [37]. Alternatively, the states may correspond to different species, in which case $\mathbf{A}$ is a Jacobian (or community) matrix describing the effect of one species on another [211]. Recursion (3.1) proceeds by matrix multiplication each time step, so the solution is

$$\mathbf{n}_t = \mathbf{A}^t\mathbf{n}_0. \tag{3.2}$$

Now consider the dynamics of a single, unstructured population tracking its habitat over one-dimensional space,

$$n_{t+1}(x) = R_0 \int_{-L/2+ct}^{L/2+ct} k(x-y)\, n_t(y)\, dy. \tag{3.3}$$

Here, $n_t(x)$ is the population density at location x at discrete generation t. The habitat is modeled as a line segment of length L, initially centered at the origin. The population changes from one non-overlapping generation to the next by a simple two-stage process. First, during the sedentary stage, individuals in the habitat grow, reproduce, and die with net reproductive rate R_0.

Then, during the dispersal stage, offspring (or propagules) in the habitat $[-L/2+ct, L/2+ct]$ disseminate according to a dispersal kernel $k(x-y)$. The kernel is the relative frequency distribution of destinations x for source y. Common dispersal kernels include the Gaussian, Laplace, and Cauchy distributions [125].

Each generation, the habitat moves c units in the positive x-direction due to climate change. The constant velocity of climate change c may be due to isotherm movement, precipitation changes, or other environmental trends. Since individuals outside the habitat do not contribute to the next generation, the population must track its habitat to survive. Model (3.3) is identical to that of [252], except that it contains a linear growth function.

With the right transformation, IDE (3.3) resembles recursion (3.1). Changing variables so that $\bar{x} = x - ct$, $\bar{y} = y - ct$, and then setting

$$n_t(x) = \bar{n}_t(x - ct), \tag{3.4}$$

IDE (3.3) can be rewritten as

$$n_{t+1}(x) = R_0 \int_{-L/2}^{L/2} k(x + c - y)\, n_t(y)\, dy. \tag{3.5}$$

Here, I have dropped bars for convenience. Please note that, for units to make sense, c is actually $c\Delta t$ with $\Delta t = 1$. The limits of integration are no longer time-dependent, and the kernel has been shifted by c. Transformation (3.4) forces the reference frame to follow the habitat, so that now x and y are locations in the moving habitat.

Another way to write recursion (3.5) is

$$n_{t+1}(x) = K[n_t(x)], \tag{3.6}$$

where K is the linear integral operator defined by

$$K[n(x)] \equiv R_0 \int_{-L/2}^{L/2} k(x+c-y)\, n(y)\, dy. \tag{3.7}$$

For most dispersal kernels $k(x)$, the operator K is compact and behaves much like a matrix [110]. In particular, recursion (3.5), together with some initial population density distribution $n_0(x)$, resembles recursion (3.1), with the exception that the population vectors are now functions. Each "state" corresponds to a location within the moving habitat rather than a discrete age, stage, or species. In effect, model (3.5) is an integral projection model with "stage" replaced by "location" [see Ch. 8 of 66].

One quick way to simulate model (3.5) is to discretize space. Divide the moving habitat interval $[-L/2, L/2]$ into N subintervals of length Δx with grid points at x_i, $i = 0, 1, \ldots, N$. Defining $y_i \equiv x_i$ and using a Riemann sum approximation for operator (3.7) gives

$$\begin{bmatrix} n_{t+1}(x_0) \\ n_{t+1}(x_1) \\ \vdots \\ n_{t+1}(x_N) \end{bmatrix} \approx R_0\, \Delta x \begin{bmatrix} k(x_0+c-y_0) & \cdots & k(x_0+c-y_N) \\ k(x_1+c-y_0) & \cdots & k(x_1+c-y_0) \\ \vdots & \ddots & \vdots \\ k(x_N+c-y_0) & \cdots & k(x_N+c-y_N) \end{bmatrix} \begin{bmatrix} n_t(y_0) \\ n_t(y_1) \\ \vdots \\ n_t(y_N) \end{bmatrix}, \tag{3.8}$$

or, grouping the constants and matrix on the right hand side,

$$\mathbf{n}_{t+1} \approx \mathbf{K}\mathbf{n}_t. \tag{3.9}$$

When discretized, model (3.5) really is a matrix model. In the limit as $N \to \infty$, system (3.8) becomes system (3.5). I will use system (3.8) as an approximation shortly.

3.3 Methods

How do metrics of transient dynamics in matrix models translate to the MHM? The main metrics I consider are amplification and attenuation. Amplification occurs when the population size increases in the first time step. In matrix model (3.1), amplification is only possible if the ratio

$$\bar{\rho}_1 \equiv \max_{\mathbf{n}_0 \neq 0} \frac{||\mathbf{n}_1||}{||\mathbf{n}_0||} = \max_{\mathbf{n}_0 \neq 0} \frac{||\mathbf{A}\mathbf{n}_0||}{||\mathbf{n}_0||} \tag{3.10}$$

is greater than one. The maximum is taken over all possible (nonzero) initial population vectors $\mathbf{n}_0$, and $||\cdot||$ is a norm, which measures the size of a population vector. The 1-norm,

$$||\mathbf{n}||_1 = \sum_{i=1}^{N} n_i, \tag{3.11}$$

is common since it gives the total population size [218].

The over-bar of $\bar{\rho}_1$ indicates amplification and the subscript indicates measurement over the first time step. If $\bar{\rho}_1 > 1$, there exists an initial population vector that increases in size in the first time step. Conveniently, $\bar{\rho}_1$ is the definition of the matrix norm $||\mathbf{A}||$, which, for the 1-norm, is the maximum column sum of $\mathbf{A}$,

$$\bar{\rho}_1 = \max_j \sum_i |a_{ij}|. \tag{3.12}$$

Similarly, a population that shrinks in the first time step has undergone attenuation. Attenuation can only occur if

$$\underline{\rho}_1 \equiv \min_{\mathbf{n}_0 \neq 0} \frac{||\mathbf{A}\mathbf{n}_0||}{||\mathbf{n}_0||} < 1, \tag{3.13}$$

in which case there exists an initial vector that decreases in size. By a similar argument, $\underline{\rho}_1$ is the minimum column sum of $\mathbf{A}$, which I abbreviate as minCS($\mathbf{A}$). Note that the minimum column sum is not a norm, since a nonzero matrix can have a minimum column sum of zero.

Returning to the moving-habitat model (3.5), there are two ways to quantify the system's amplification and attenuation. First, discretize space using approximation (3.8) so that the dynamics follow recursion (3.9). Then

$$\bar{\rho}_1 \approx ||\mathbf{K}||, \tag{3.14}$$

$$\underline{\rho}_1 \approx \text{minCS}(\mathbf{K}). \tag{3.15}$$

The accuracy of metrics (3.14) and (3.15) increases with the number of spatial grid points.

Alternatively, one can extend the concept of maximum and minimum column sums to operator K (3.7). Amplification and attenuation are

$$\bar{\rho}_1 = \max_{n_0(x)\neq 0} \frac{||K[n_0(x)]||}{||n_0(x)||} = \max_{-L/2\leq y\leq L/2} R_0 \int_{-L/2}^{L/2} k(x+c-y)\,dx, \tag{3.16}$$

$$\underline{\rho}_1 = \min_{n_0(x)\neq 0} \frac{||K[n_0(x)]||}{||n_0(x)||} = \min_{-L/2\leq y\leq L/2} R_0 \int_{-L/2}^{L/2} k(x+c-y)\,dx. \tag{3.17}$$

Here, $||\cdot||$ is the L^1-norm, which gives the total population size over the moving habitat,

$$||n(x)|| = \int_{-L/2}^{L/2} n(x)\,dx, \tag{3.18}$$

and $\bar{\rho}_1$ is equal to the operator norm, $||K||$. Formulas (3.16) and (3.17) come from the fact that, in the discretized form (3.8), each matrix column corresponds to a unique y-value. In the limit as the the number of subintervals N increases, column sums become integrals over the x-values and approximations (3.14) and (3.15) converge to metrics (3.16) and (3.17), respectively. I consider continuous or piecewise-continuous dispersal kernels $k(x)$, assuring that the integrals in (3.16) and (3.17) are continuous and that the corresponding maxima and minima exist. For some common dispersal kernels, amplification and attenuation can be calculated analytically using metrics (3.16) and (3.17) (Table 3.1).

Table 3.1: Amplification and attenuation for three common dispersal kernels, when used in model (3.5).

	$k(x)$	$\bar{\rho}_1$	$\underline{\rho}_1$
Gaussian	$\frac{1}{\sqrt{2\pi}\sigma}\exp\left(-\frac{x^2}{2\sigma^2}\right)$	$\begin{cases} R_0\sqrt{\frac{\sigma}{\pi}}\operatorname{erf}\left(\frac{L}{2\sqrt{2}\sigma}\right), & \text{if } 0 \le c \le L/2, \\ \frac{R_0}{2}\sqrt{\frac{\sigma}{\pi}}\left[\operatorname{erf}\left(\frac{L-c}{\sqrt{2}\sigma}\right)+\operatorname{erf}\left(\frac{c}{\sqrt{2}\sigma}\right)\right], & \text{if } c \ge L/2 \end{cases}$	$\frac{R_0}{2}\sqrt{\frac{\sigma}{\pi}}\left[\operatorname{erf}\left(\frac{L+c}{\sqrt{2}\sigma}\right)-\operatorname{erf}\left(\frac{c}{\sqrt{2}\sigma}\right)\right]$
Laplace	$\frac{\alpha}{2}\exp\left(-\alpha\lvert x\rvert\right)$	$\begin{cases} R_0\left[1-\exp\left(-\frac{\alpha L}{2}\right)\right], & \text{if } 0 \le c \le L/2, \\ R_0-\frac{R_0}{2}\left[\exp\left(-\alpha L(1-c)\right)+\exp(-\alpha Lc)\right], & \text{if } L/2 \le c \le L, \\ \frac{R_0}{2}\left[\exp(-\alpha L(1-c))-\exp(-\alpha Lc)\right], & \text{if } c \ge L \end{cases}$	$\frac{R_0}{2}\left[\exp(-\alpha Lc)-\exp(-\alpha L(c+1))\right]$
Cauchy	$\frac{1}{\pi\alpha}\frac{1}{1+\left(\frac{x}{\alpha}\right)^2}$	$\begin{cases} \frac{2R_0}{\pi}\arctan\left(\frac{L}{2\alpha}\right), & \text{if } 0 \le c \le L/2, \\ \frac{R_0}{\pi}\left[\arctan\left(\frac{L-c}{\alpha}\right)+\arctan\left(\frac{c}{\alpha}\right)\right], & \text{if } c \ge L/2 \end{cases}$	$\frac{R_0}{\pi}\left[\arctan\left(\frac{L+c}{\alpha}\right)-\arctan\left(\frac{c}{\alpha}\right)\right]$

Amplification and attenuation measure population size changes in the first time step, but they do not give information about future time steps. To bridge the gap between first-step and asymptotic behavior, researchers define amplification and attenuation *envelopes*, which extend the metrics to multiple time steps [164, 218, 227]. They are, respectively, the maximum and minimum possible growth rates over t time steps. For matrix model (3.1), the amplification envelope $\bar{\rho}_t$ and attenuation envelope $\underline{\rho}_t$ are

$$\bar{\rho}_t \equiv \max_{\mathbf{n}_0 \neq 0} \frac{||\mathbf{n}_t||}{||\mathbf{n}_0||} = \max_{\mathbf{n}_0 \neq 0} \frac{||\mathbf{A}^t \mathbf{n}_0||}{||\mathbf{n}_0||} = ||\mathbf{A}^t||, \tag{3.19}$$

$$\underline{\rho}_t \equiv \min_{\mathbf{n}_0 \neq 0} \frac{||\mathbf{n}_t||}{||\mathbf{n}_0||} = \min_{\mathbf{n}_0 \neq 0} \frac{||\mathbf{A}^t \mathbf{n}_0||}{||\mathbf{n}_0||} = \text{minCS}(\mathbf{A}^t). \tag{3.20}$$

These metrics are the maximum and minimum column sums of $\mathbf{A}^t$ rather than simply $\mathbf{A}$. Plotted as functions of t, $\bar{\rho}_t$ and $\underline{\rho}_t$ provide upper and lower bounds on the population relative to its initial size, forming envelopes on the dynamics.

The easiest way to translate amplification and attenuation envelopes to the MHM is to discretize space using approximation (3.8), which yields a familiar matrix recursion (3.9) with matrix $\mathbf{K}$. Then, by analogy,

$$\bar{\rho}_t \approx ||\mathbf{K}^t||, \tag{3.21}$$

$$\underline{\rho}_t \approx \text{minCS}(\mathbf{K}^t). \tag{3.22}$$

These metrics converge (to their respective values) as the number of subintervals N in discretization (3.8) increases.

So far I have only discussed ways to measure the *possibility* for transient dynamics. It is the initial population distribution $n_0(x)$ that determines what transient dynamics will actually occur. To make these techniques less hypothetical and more practical, I now consider which initial conditions lead to short-term growth or decline. I also determine the initial conditions that maximize or minimize the short-term change in population size.

The set of initial distributions $n_0(x)$ includes every integrable function on the interval $[-L/2, L/2]$, which is an uncountably infinite set. Rather than sort through such a complicated set to see which elements cause amplification or attenuation, I consider a subset of initial conditions that still captures some ecological meaning. Namely, I use the set of populations distributed normally over the habitat,

$$\{n_0(x) \sim N(\mu, \sigma) \mid \mu \in [-1/2, 1/2],\ \sigma > 0\}. \tag{3.23}$$

The normal distribution is a flexible model for population abundance that is appropriate in many cases, although there are exceptions [see, e.g., 27, 91]. Other distributions, such as the beta distribution, may be more appropriate, depending on the species. To map out the effect of initial conditions, I simply draw numerous initial distributions from set (3.23) and, for each distribution, run the system forward one time step. Since set (3.23) contains only two parameters, I can plot the distributions that amplify or attenuate as a function of those parameters.

3.4 Case study: Fender's blue butterfly

To show transient dynamics in model (3.5), I use Fender's blue butterfly (*I. icarioides fenderi*), a subspecies restricted to prairie landscapes in western Oregon's Willamette Valley [71]. The subspecies is listed as endangered [71], but conservation efforts have increased population levels recently [200]. Climate-induced changes in fire regimes [159] and invasive weed species [205] may worsen threats to Fender's blue habitat. While the butterfly is a habitat specialist and exhibits complex dispersal [199], it does meet other criteria for use in the moving-habitat model (3.5).

Mathematical models of Fender's blue include difference equations [198], population viability analyses (PVAs) [201], and IDEs [252]. These approaches focus on population survival over decades or longer. However, transient behavior (over less than a decade) may be more salient for Fender's blue. As with many insects, short-term population size is highly variable,

due partly to extreme weather events [200]. Although PVAs generally assume that current conditions will persist over long timescales such as a century [201], climate change is likely to break that assumption through increased temperature and weather variability in the region [160], disruption of fire regimes [244], and weed invasion [188].

Fender's blue butterflies inhabit prairie fragments containing their main larval food source, Kincaid's lupine (*Lupinus sulphureus kincaidii*). Habitat patches range from less than 2 ha to over 50 ha [201]. To best illustrate transient dynamics, I will consider patches on the upper end of the size spectrum and above (25–100 ha). In keeping with Zhou and Kot [252], I assume patches are square in shape and consider one side to be the habitat length.

Fenders' blue dispersal has been described as a biased, correlated random walk [199], which violates the assumption of isotropic movement in model (3.5). Nevertheless, for the sake of comparing long- and short-term dynamics, I follow Zhou and Kot [252] by using the exponential power distribution,

$$k(x) = \frac{\beta}{2\alpha\Gamma(1/\beta)} \exp\left[-\left(\frac{|x-y|}{\alpha}\right)^{\beta}\right], \tag{3.24}$$

where α is a scale parameter and β controls the distribution's kurtosis. For $\beta < 2$, the distribution is leptokurtic; for $\beta > 2$, platykurtic. Leptokurtosis can arise from rare, long-distance dispersal [49] or individual variation in dispersal [28]. With β fixed, α can be estimated from the mean absolute deviation,

$$\delta_1 = \frac{\alpha\Gamma(2/\beta)}{\Gamma(1/\beta)}. \tag{3.25}$$

Mirroring Zhou and Kot [252], I set $\delta_1 = 0.4$ km, based on field measurements in Schultz [197].

Population growth rates ranged from 0.99/yr to 2.66/yr in one study [201]. Growth rate was only weakly related to population size, which indicates only weak density-dependence and justifies using the linear model (3.5). Zhou and Kot [252] found that populations would

need high reproductive rates (> 2.5/yr, depending on parameter choices) to withstand even small velocities of climate change.

While range shifts have not yet been observed for Fender's blue butterflies, the Pacific Northwest is expected to experience a climate velocity of around 0.1 km/yr [61, 160]. For prairie habitat, some estimates of climate velocity are even higher, reaching 1 km/yr [140]. The integrodifference model of Zhou and Kot [252] predicts that, even with high net reproductive rates, Fender's blue populations may be unable to track their habitats long-term. What kinds of transients can we expect from this subspecies?

3.5 Results

After parameterizing model (3.5) for Fender's blue butterfly, simulations show that both amplification and attenuation can occur (Fig. 3.1). Transients arise from either changes in biological and environmental parameters (Fig. 3.1a–b) or changes in initial population distribution (Fig. 3.1c–d). Note that parameter changes affect both transient and asymptotic dynamics (Fig. 3.1a–b), but changes in initial distribution only affect transient dynamics. I assume no Allee [5] effect, so long-term dynamics are determined only by the parameters in operator K (3.7). Transients can result in a mismatch between short- and long-term trends, as well as large differences between trajectories with similar long-term behavior.

I now take a more systematic look at how transient and asymptotic dynamics compare in model (3.5). Whereas amplification and attenuation describe transients, the dominant eigenvalue λ_1 of operator K determines long-term behavior. If $\lambda_1 < 1$, the population collapses eventually; if $\lambda_1 > 1$, the population persists long-term. The dispersal kernels I consider guarantee that operator K has a unique, positive dominant eigenvalue.

How does the speed of climate change c affect transients? If c is above a certain value—the critical speed—the population cannot persist [252]. The critical speed also separates the types of transients that can occur in the MHM. For low speeds of climate change (Fig. 3.2, region I), $\ln \underline{\rho}_1 > 0$ and $\ln \lambda_1 > 0$, so all initial populations grow in the first step and persist long-term. Transient and asymptotic dynamics match. For higher c-values, $\ln \underline{\rho}_1 < 0$ (Fig.

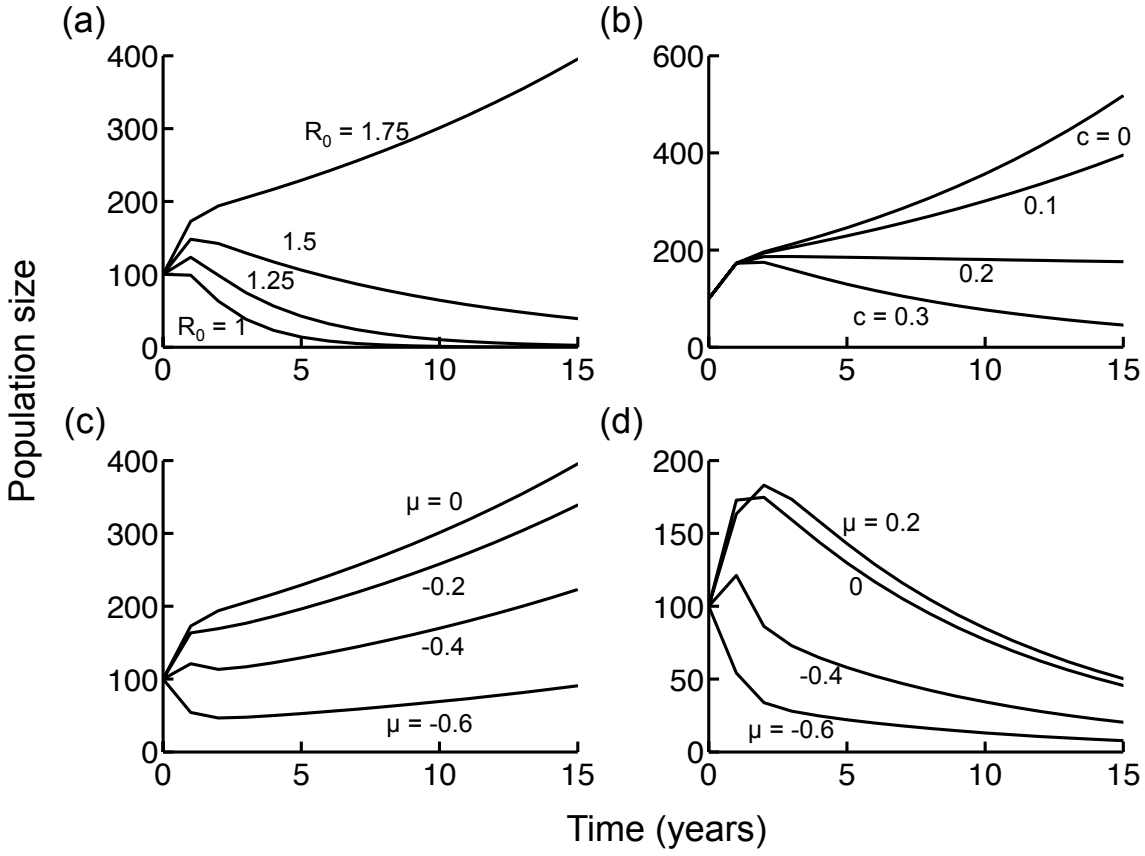

Figure 3.1: Transients (such as amplification or attenuation) can arise from changes in parameters such as (a) the net reproductive rate and (b) the speed of climate change, or (c–d) from changes in the initial population distribution in the habitat. In (c–d), μ (measured in km) is the mean of a normally-distributed initial population with respect to the middle of the habitat. $\mu < 0$ indicates an initial distribution toward the trailing edge of the moving habitat; $\mu > 0$, toward the leading edge. I varied parameters from a baseline of $R_0 = 1.75$/yr, $L = 1$ km, $c = 0.1$ km/yr, $\beta = 2$, and an initial population distribution of $n_0(x) \sim \mathrm{N}(\mu = 0, \sigma = 0.2)$.

3.2, region II), meaning some initial populations decline even though they persist long-term.

Once c exceeds the critical speed (Fig. 3.2, boundary between regions II and III), $\ln \lambda_1 < 0$, so all initial populations collapse eventually. However, if c is not too high, the population may grow before collapsing (Fig. 2, region III). Some populations with the right initial conditions will appear, initially, to do better than those with worse initial conditions, even if long-term behavior is similar. If c is too high, so that $\ln \bar{\rho}_1 < 0$, all initial populations decrease monotonically toward zero (Fig. 3.2, region IV).

For Fender's blue butterfly, Fig. 3.2 suggests that persistence is likely for low c-values, but that short-term decline may still occur (region II). There is a wide range of higher c-values for which populations may decline long-term but grow short-term (region III). Thus, high rates of climate change can mask the population's risk of collapse.

In general, the signs of $\ln \underline{\rho}_1$, $\ln \lambda_1$, and $\ln \bar{\rho}_1$ determine what types of transient dynamics can occur (Fig. 3.3). Each region (I)–(IV) corresponds to a unique set of possible dynamics. Transients that mismatch long-term dynamics are only possible in regions (II) and (III). The parameters in operator K determine the region, and initial population distribution determines whether transients occur.

Changes in net reproductive rate R_0 have an opposite effect on transients than changes in c (Fig. 3.4). For low R_0-values, all trajectories decrease in both the short- and long-term (region IV). At intermediate R_0-values, amplification (region III) or attenuation (region II) can occur. The width of region III compared to region II has predictive power: given an observation of short-term population increase (assuming R_0 is unknown), it is more likely that the population will survive long-term (region II or I) than collapse (region III).

Not all combinations of transient/asymptotic dynamics are possible as the habitat length L changes (Fig. 3.5). Since $\ln \underline{\rho}_1$ is always negative, an observation of initial population decline is not necessarily alarming if the habitat is sufficiently large (region II). However, for Fender's blue butterfly, many patches are small ($L < 1$ km), in which case initial decrease likely foretells collapse (regions IV and III). Model (3.5) may, however, overestimate mortality from flux through habitat boundaries since it does not account for edge effects.

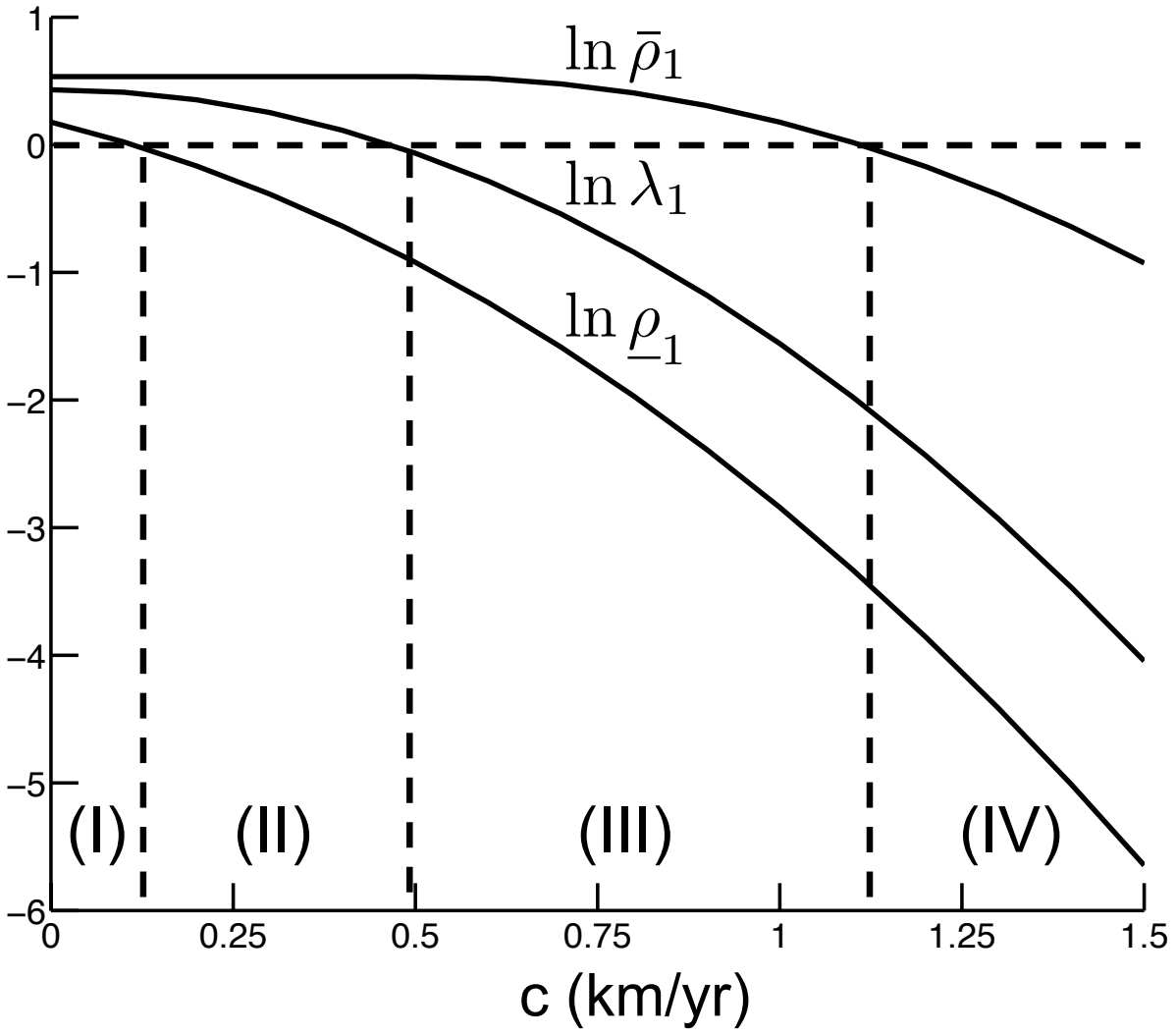

Figure 3.2: Plot of the logarithms of amplification $\bar{\rho}_1$, attenuation $\underline{\rho}_1$, and the dominant eigenvalue λ_1 as functions of the speed of climate change c. The sign of each of the three values determines what kinds of dynamics can occur. In region (I), all population increase; in (II), some populations may decrease before increasing; in (III), some may increase before decreasing; and in (IV), all populations decrease toward extinction (compare with Fig. 3). I used $R_0 = 2.5$/yr, $L = 1$ km, and $\beta = 2$.

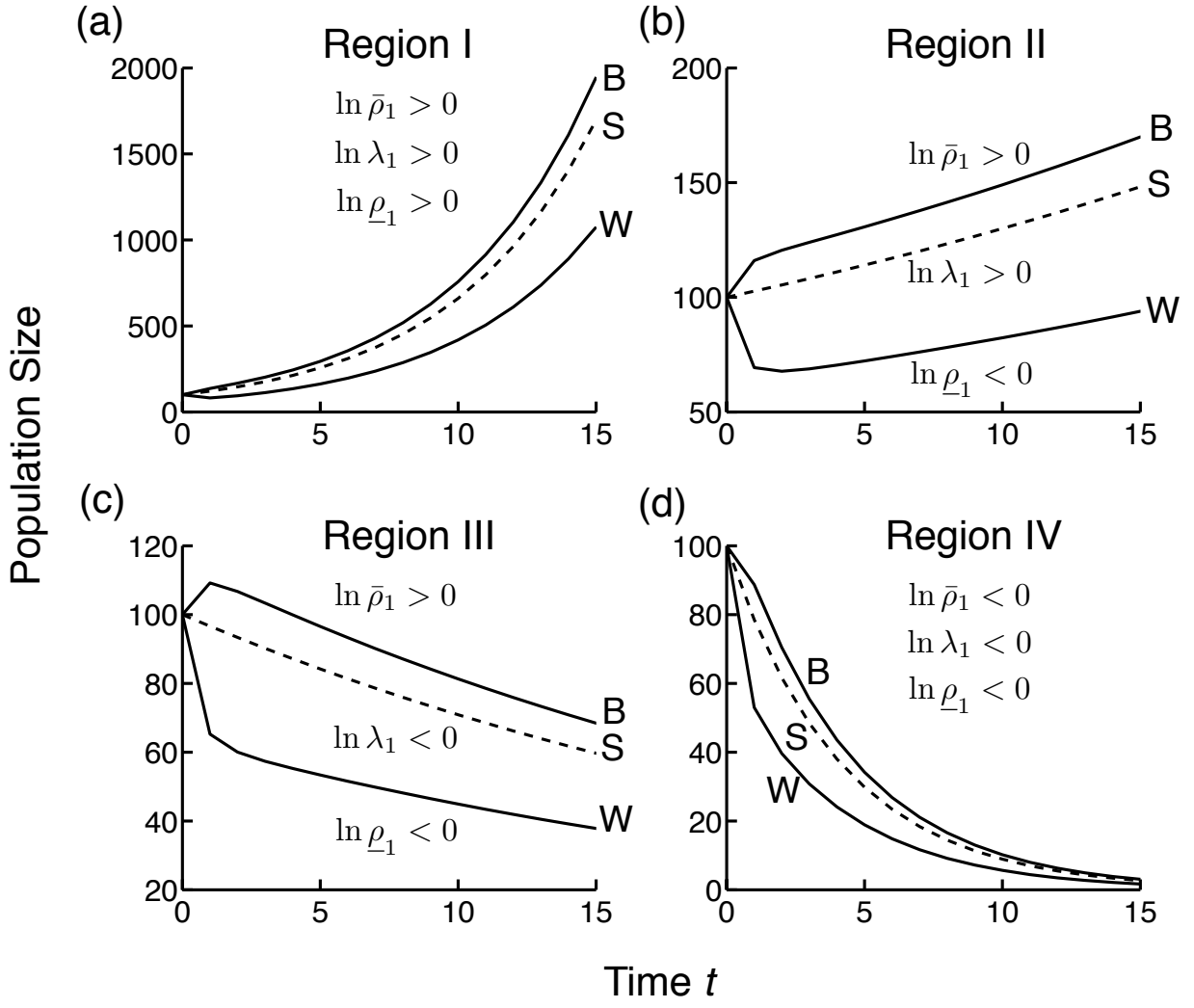

Figure 3.3: Depending on the amplification $\bar{\rho}_1$, attenuation $\underline{\rho}_1$, and dominant eigenvalue λ_1 of operator K, the dynamics of MHM (3.5) can behave one of four ways (Regions I–IV). Within each region, I have chosen three different initial population distributions, which represent the best (B) initial distribution for growth, the worst (W), and a stable (S) initial distribution that is the dominant eigenvector of operator K ("stable" indicates the population is already set at the spatially stable distribution). (a) In region I, all trajectories increase; (b) in region II, some trajectories (such as W) decline before growing; (c) in region III, some (such as B) increase before decreasing; and (d) in region IV, all trajectories decrease. The parameters of operator K determine which region the system is in (see Figs. 3.2, 3.4–3.6). Please note the differences in the vertical axes for each region.

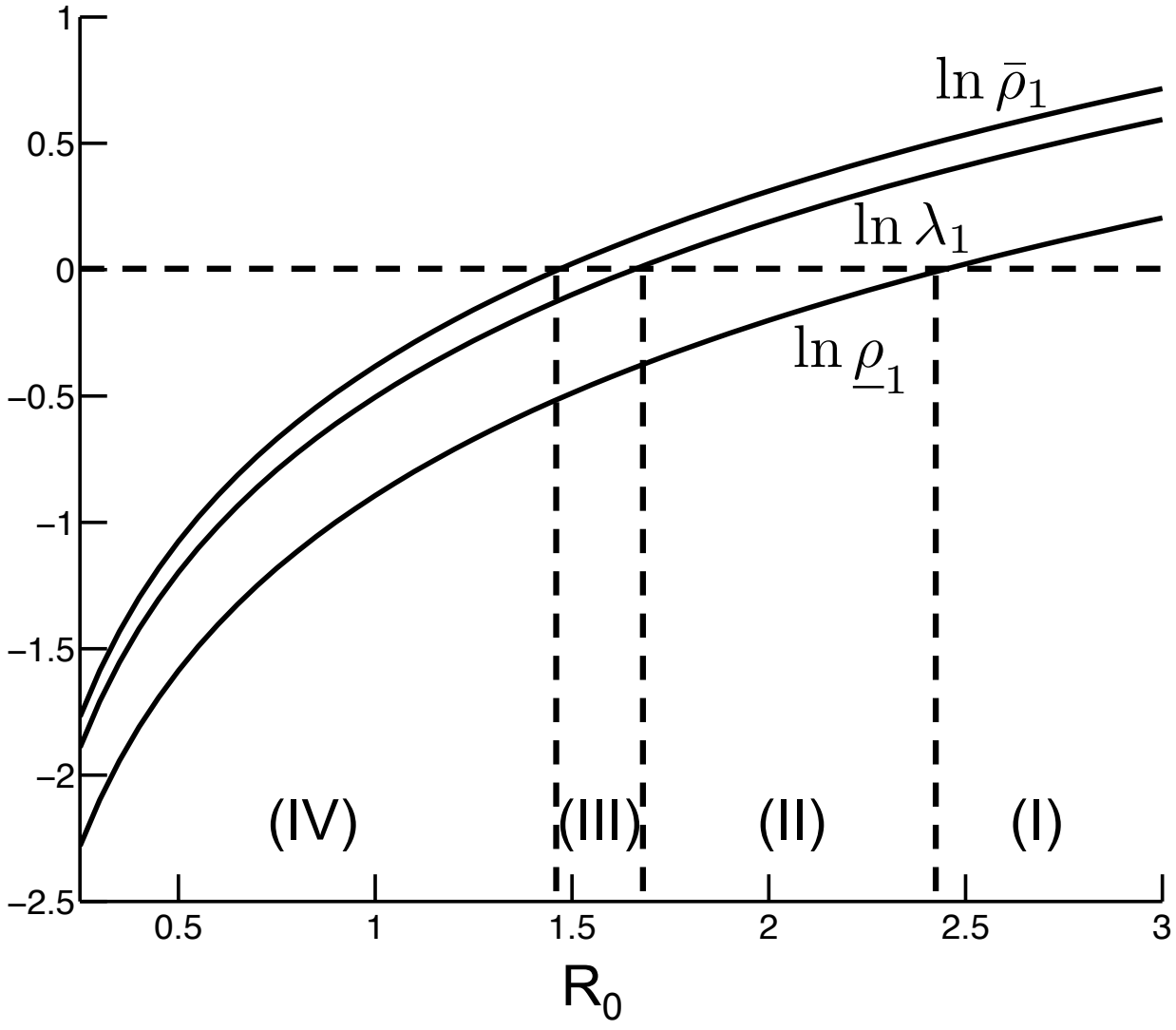

Figure 3.4: Plot of the logarithms of amplification $\bar{\rho}_1$, attenuation $\underline{\rho}_1$, and the dominant eigenvalue λ_1 as functions of the net reproductive rate R_0. As R_0 increases, the dynamics transition from region (IV) to region (I) (see Fig. 3). The region around $R_0 = 0$ was excluded, as the ordinate approaches negative infinity. I used $L = 1$ km, $c = 0.1$ km/yr, and $\beta = 2$.

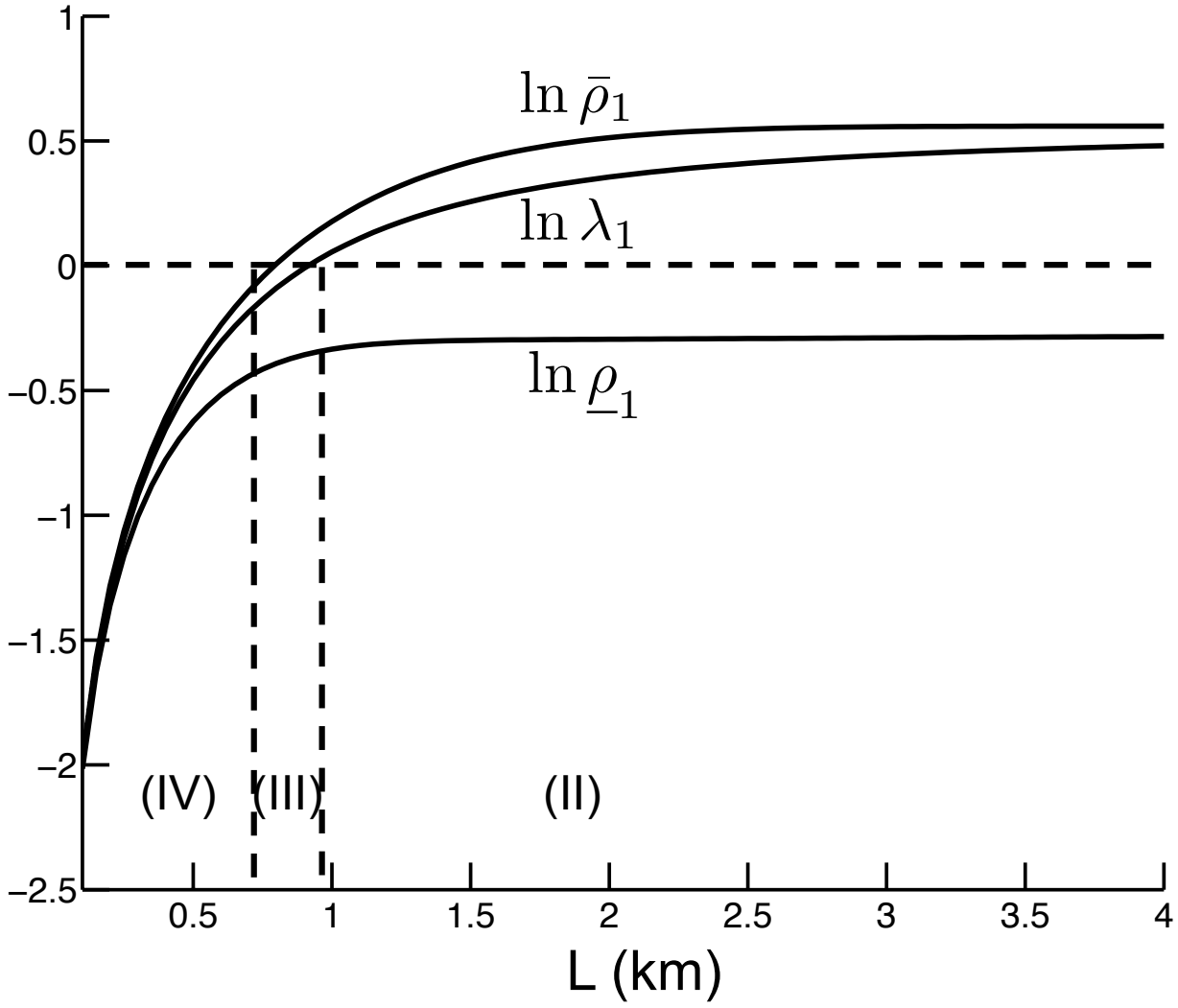

Figure 3.5: Plot of the logarithms of amplification $\bar{\rho}_1$, attenuation $\underline{\rho}_1$, and the dominant eigenvalue λ_1 as functions of the habitat length L. As L increases, the dynamics transition from region (IV) to region (II) (see Fig. 3.3). Since region (I) is excluded for these parameter choices, attenuation is possible even for large habitat sizes. The region around $L_0 = 0$ was excluded, as the ordinate approaches negative infinity. I used $R_0 = 1.75$/yr, $c = 0.1$ km/yr, and $\beta = 2$.

The shape of the dispersal kernel also affects transients (Fig. 6). Recall from definition (3.24) that $\beta > 2$ corresponds to platykurtic kernels with broad shoulders and thin tails, while $\beta < 2$ corresponds to leptokurtic kernels with sharp peaks and heavy tails. For platykurtic kernels, all population trajectories increase in the short- and long-term (region I). In contrast, very leptokurtic kernels make attenuation possible (region II). Since leptokurtic kernels such as the exponential distribution are common models of butterfly dispersal [216], the shape of the dispersal kernel is more likely to cause attenuation for Fender's blue.

Amplification and attenuation envelopes show how system (3.5) can behave as it transitions from short-term to long-term dynamics (Fig. 3.7). $\bar{\rho}_t$ and $\underline{\rho}_t$ are upper and lower bounds on population size, relative to initial size, as functions of time t. Both envelopes either increase (when $\ln \lambda_1 > 0$, Fig. 3.7a) or decrease (when $\ln \lambda_1 < 0$, Fig. 3.7b) with time. The logarithms of the envelopes are approximately linear with slope $\ln \lambda_1$ (see Appendix for discussion). If $\ln \lambda_1 > 0$, there is a period of time (or transient window TW) when the population may be below the initial size even though it persists long-term (Fig. 3.7a, region TW). Past the window, all populations are larger than the initial population. For the parameter values used, Fender's blue populations may take at most eight generations to recover to initial size after attenuation (Fig. 3.7a).

Similarly, if $\ln \lambda_1 < 0$, there is a transient window when population can exceed the initial size, even though the population crashes long-term (Fig. 3.7b, region TW). Past the window, all populations are smaller than the initial size. In this example, a doomed Fender's blue population may maintain above its initial population size for as many as twelve generations (Fig. 3.7b). While twelve generations is minute on an eco-evolutionary timescale, it could easily take up an entire conservation planning period.

The length of the transient window depends on the dominant eigenvalue λ_1. When λ_1 approaches 1, the slope of the middle lines in Fig. 3.7 approaches zero, which lengthens the transient window. Thus, system (3.5) has the longest-lasting transients when the stability of equilibrium $n(x) \equiv 0$ is weak. Transients dominate for precisely the unstable populations that are of management concern. A similar result, known as critical slowing-down, holds for

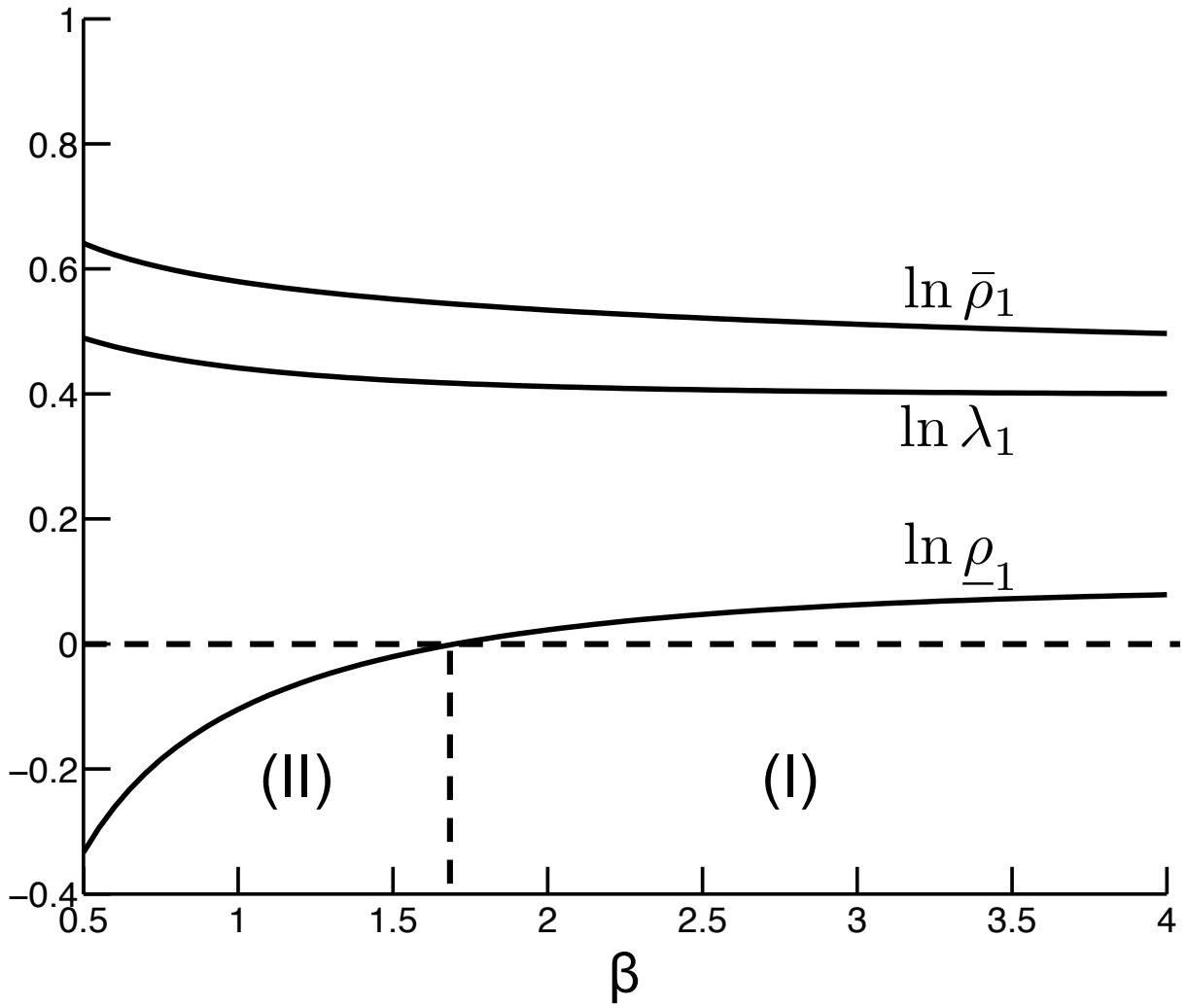

Figure 3.6: Plot of the logarithms of amplification $\bar{\rho}_1$, attenuation $\underline{\rho}_1$, and the dominant eigenvalue λ_1 as functions of the dispersal kernel shape parameter β. As β increases, the dispersal kernel becomes more platykurtic (normally distributed at $\beta = 2$), and the dynamics transition from region (II) to region (I) (see Fig. 3.3). For these parameter choices, the population always persists and attenuation is possible for some leptokurtic kernels (region II). Note that the three curves do not move in the same direction as β increases. I used $R_0 = 1.75$/yr, $c = 0.1$ km/yr, and $L = 1$ km.

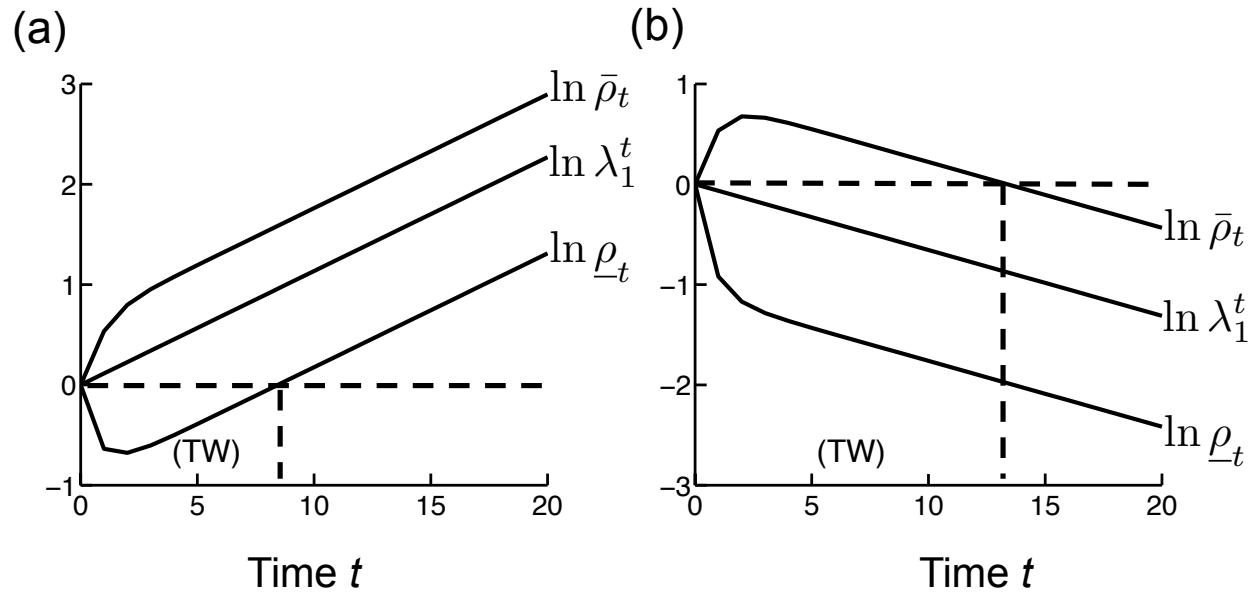

Figure 3.7: Plot of the logarithms of the amplification envelope $\bar{\rho}_t$ and attenuation envelope $\underline{\rho}_t$, along with a line with slope $\ln \lambda_1$. All possible trajectories must fall within the two envelopes, which are roughly linear with slope $\ln \lambda_1$ for large t. (a) When $\ln \lambda_1 > 0$ (persistence), the size of the transient window (TW) is how long a population can decline before recovering to its initial size. (b) When $\ln \lambda_1 < 0$ (extinction), the size of the transient window (TW) is how long a population can increase before decreasing back to its initial size.

a wide variety of other systems and has been studied extensively [56, 192, 245].

Amplification and attenuation envelopes only give best- and worst-case scenarios; the population's initial distribution determines whether transients occur and for how long. To test the effect of initial population distribution on transients, I consider Gaussian initial distributions. Plotting the logarithm of the first-step population growth rate, as a function of μ and σ, shows which initial conditions cause an initial increase or decrease in size (Fig. 3.8). Positive values mean the population size will grow in the first step; negative values mean it will shrink in the first step.

Initial Fender's blue populations with high μ and low σ show the greatest amplification, while those with low μ and low σ show the greatest attenuation (Fig. 3.8). Populations that start with a narrow distribution toward the leading edge of the moving habitat get the greatest short-term boost. There is an optimal initial distribution near $\mu = 0.15$, $\sigma = 0$ that best balances the losses out the leading and trailing edges of the habitat. Populations with a narrow distribution at the trailing edge of the moving habitat lose more propagules into unsuitable area as the habitat moves.

To find the initial distributions $n_0(x)$ that maximize (or minimize) the first-step growth rate, consider the definitions of amplification (3.16) and attenuation (3.17). They involve the values $y \in [-L/2, L/2]$ that maximize (or minimize) the integral

$$z(y) \equiv R_0 \int_{-L/2}^{L/2} k(x + c - y)\, dx. \tag{3.26}$$

Expression (3.26) is the total population size after a population concentrated entirely at source location y, $n_0(x) = \delta(x - y)$, has grown and dispersed. As a result, the extrema of $z(y)$ give the locations where a population pulse will experience the highest or lowest first-step growth rate. Plotting $z(y)$ (or its logarithm, Fig. 3.9) for various dispersal kernels suggests that, if $k(x)$ is unimodal with a peak at $x = 0$, then $z(y)$ will be unimodal with a maximum at $y = c$ and a minimum at $y = -L/2$, for $c > 0$. That is, the initial distribution

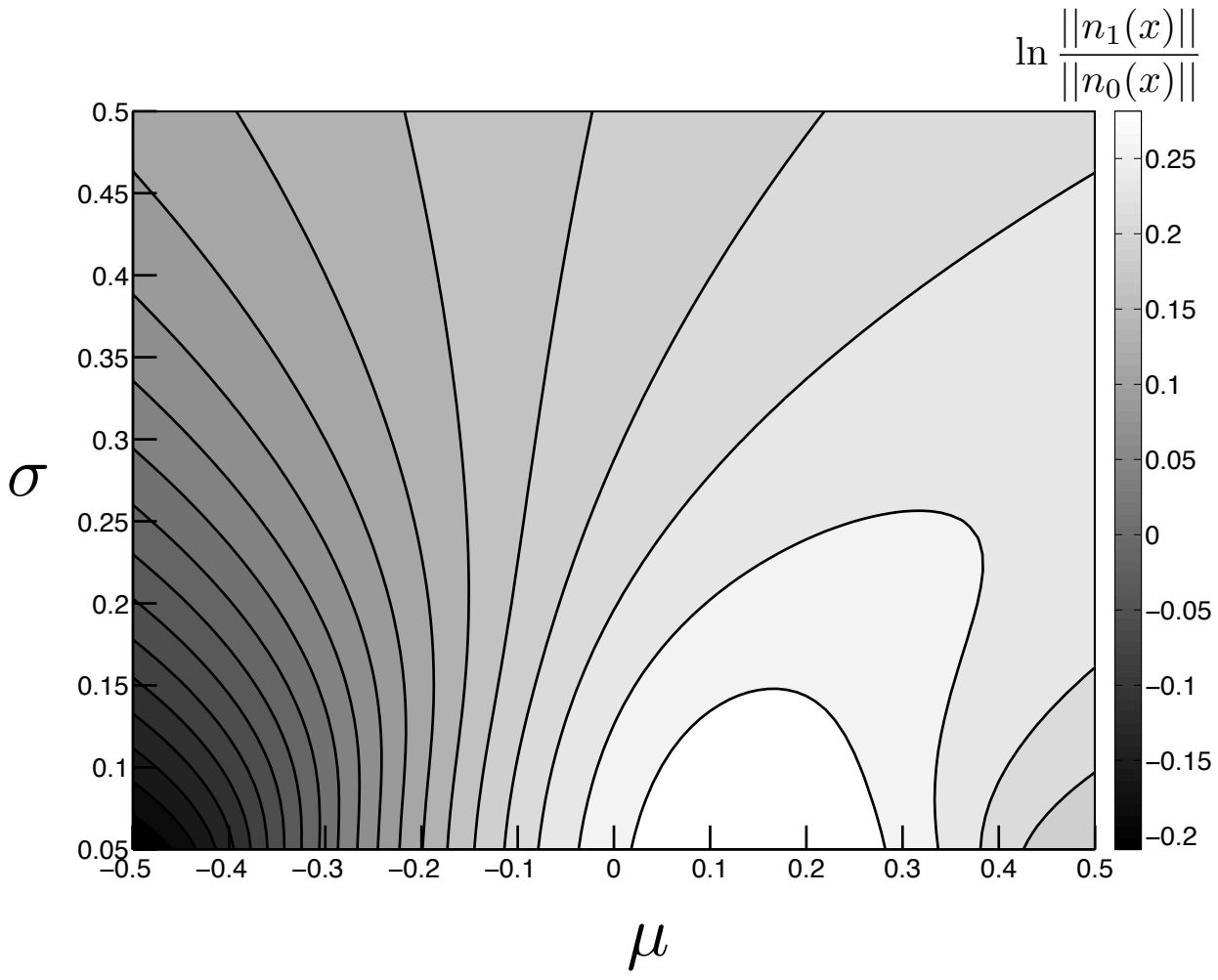

Figure 3.8: Each point (μ, σ) indicates a Gaussian initial distribution, $n_0(x) \sim \mathrm{N}(\mu, \sigma)$, in the habitat. $x = 0$ is the center of the habitat, and positive x-values indicate a mean toward the leading edge of the moving habitat. Contour values above zero indicate amplification, and values below zero indicate attenuation. I used $R_0 = 2$/yr, $L = 1$ km, $c = 0.15$ km/yr, and $\beta = 2$.

that grows the most in one generation is a pulse of individuals located c units from the middle of the habitat. The initial distribution that grows least is a pulse located at the very back edge of the moving habitat.

3.6 Case study: Stage-structured plant populations

The methods described above are not limited to simple unstructured models. Metrics of transients exist for any discrete-time system that can be approximated by matrix recursion (3.9). This includes stage-structured integrodifference models [e.g., 165]. Recently, [96] modeled four stage-structured plant species on moving habitats with the IDE

$$\mathbf{n}_{t+1}(x) = \int_{-L/2+ct}^{L/2+ct} [\mathbf{K}(x-y) \circ \mathbf{A}]\mathbf{n}_t(y)\, dy, \tag{3.27}$$

where $\mathbf{n}_t(x)$ is a vector of population densities in each stage at time t. Element a_{ij} of demographic matrix $\mathbf{A}$ describes the per-capita production of stage-i individuals by stage-j individuals. Each element $k_{ij}(x-y)$ of $\mathbf{K}(x-y)$ is a dispersal kernel describing movement from location y to x associated with the transition from stage j to i. Here, the symbol "$\circ$" denotes element-by-element matrix multiplication.

Harsch et al. [96] used IDE (3.27) to study the long-term persistence of their focal plant species, as well as how climate change impacts the success of different life-history strategies. They found that rapid growth, high fecundity, and long-distance dispersal benefit species' long-term persistence in moving habitats.

By shifting spatial coordinates and discretizing space similarly to approximation (3.8), one can write a matrix recursion approximation for IDE (3.27). For a population with p stages, discretizing the moving habitat $[-L/2, L/2]$ with q spatial grid points gives the approximation

$$\mathbf{n}_{t+1} \approx (\mathbf{K} \circ \mathbf{A})\mathbf{n}_t, \tag{3.28}$$

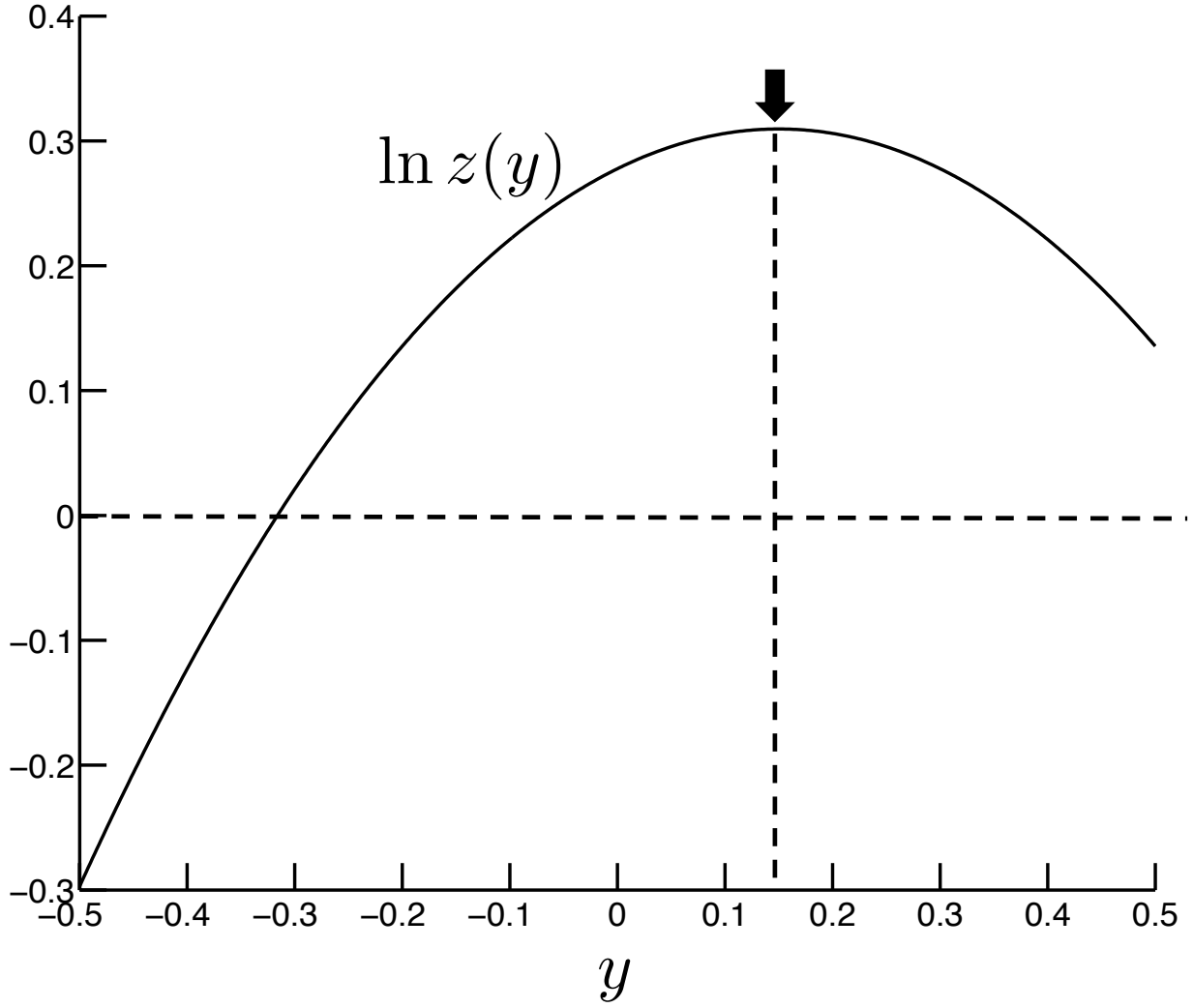

Figure 3.9: It describes whether a pulse of individuals at location y will grow or shrink in one time step. The extrema of $z(y)$ are $\bar{\rho}_1$ and $\underline{\rho}_1$. A population pulse c units from the middle of the habitat toward the front (arrow) will grow the most in one time step. Any pulse located at y where $\ln z(y) > 0$ will grow initially. I used $R_0 = 2$/yr, $L = 1$ km, $c = 0.15$ km/yr, and $\beta = 2$. This plot is essentially the $\sigma = 0$ slice of Fig. 3.8 (note the maximum at $\mu = 0.15 = c$).

where $\mathbf{n}_t$ is a $pq \times 1$ vector of densities and $\mathbf{K}$ is a $pq \times pq$ block matrix,

$$\mathbf{K} = \begin{bmatrix} \mathbf{K}_{11} & \cdots & \mathbf{K}_{1p} \\ \vdots & \ddots & \vdots \\ \mathbf{K}_{p1} & \cdots & \mathbf{K}_{pp} \end{bmatrix}. \tag{3.29}$$

Each submatrix $\mathbf{K}_{ij}$ (where $i, j = 1, \ldots, p$) has elements k_{mn} (where $m, n = 1, \ldots, q$) written in terms of the original dispersal kernels $k_{ij}(x - y)$, such that

$$k_{mn} = k_{ij}(x_m + c - y_n)\Delta x. \tag{3.30}$$

From approximation (3.28), amplification and attenuation are, as before,

$$\bar{\rho}_1 \approx ||\mathbf{K} \circ \mathbf{A}||_1, \tag{3.31}$$

$$\underline{\rho}_1 \approx \text{minCS}(\mathbf{K} \circ \mathbf{A}). \tag{3.32}$$

Any population modeled by equation (3.27) that includes a non-dispersing stage will have an attenuation of zero, since a pulse of individuals in that stage, placed at the trailing edge of the habitat, will be wiped out in one time step. In contrast, some stage-structured models include a very fecund stage; a pulse of individuals in that stage, placed at the right location, will grow tremendously in one generation.

I used parameter values from Harsch et al. [96] to plot amplification, as a function of climate velocity, for four plant species on moving habitats (Fig. 3.10). The species—primrose (*Primula vulgaris*), wild teasel (*Dipsacus sylvestris*), European black pine (*Pinus nigra*), and longleaf pine (*Pinus palustris*)—span very different life histories. The dominant eigenvalues associated with the four species fall within the range $\lambda_1 \in [0, 2.13]$ as c increases from 0 m/yr to 1 m/yr [see Table 1 in 96]. In contrast, the amplification values $\bar{\rho}_1$ span three

orders of magnitude. Because each population contains a non-dispersing stage, each has an attenuation of zero when $c > 0$ (hence, I did not plot attenuation).

The size of $\bar{\rho}_1$ and its sensitivity to climate speed vary across the four species. *P. vulgaris* and *P. palustris* populations can only grow by a factor of one or two in the first generation (Fig. 3.10a,d), whereas *D. sylvestris* and *P. nigra* populations can grow by a factor of tens or hundreds in one step (Fig. 3.10b,c). For the two pine species, $\bar{\rho}_1$ is robust to changes in climate speed, whereas $\bar{\rho}_1$ declines sharply after a threshold c-value for *P. vulgaris* and *D. sylvestris*.

Differences in the size of $\bar{\rho}_1$ and its sensitivity to c depend on both dispersal and demography. The species with higher mean dispersal distances (*P. nigra* and *P. palustris*) have $\bar{\rho}_1$-values that are robust to climate velocity [see Appendix B of 96, for dispersal parameters]. Populations with high mean dispersal distances (relative to habitat length) spread propagules nearly evenly over the habitat, lessening the effect of habitat movement on growth rate.

The largest column sum of the demographic matrix, $||\mathbf{A}||_1$, only partially predicts of the amplification of the corresponding spatial system [for the species' demographic matrices, see Appendix A of 96]. Since dispersal only adds mortality to stage transitions in model (3.27), $||\mathbf{A}||_1$ is an upper bound on $||\mathbf{K} \circ \mathbf{A}||_1$. However, if dispersal causes a large number of propagules to be lost outside suitable habitat, $||\mathbf{A}||_1$ may be a very loose upper bound. The demographic matrix of *P. nigra* has the largest column sum out of the four, but due to its wide dispersal kernel, many propagules land outside suitable habitat and $\bar{\rho}_1$ is smaller that expected.

This quick example shows that structured populations with similar long-term behavior can differ in their short-term dynamics by many orders of magnitude. I leave it to later work to show more rigorously how spatial and demographic structure interact to produce transients.

3.7 Discussion

Environmental changes are moving species' habitats, endangering populations that cannot track their habitats [32, 52, 194]. Spatial models that describe population dynamics are

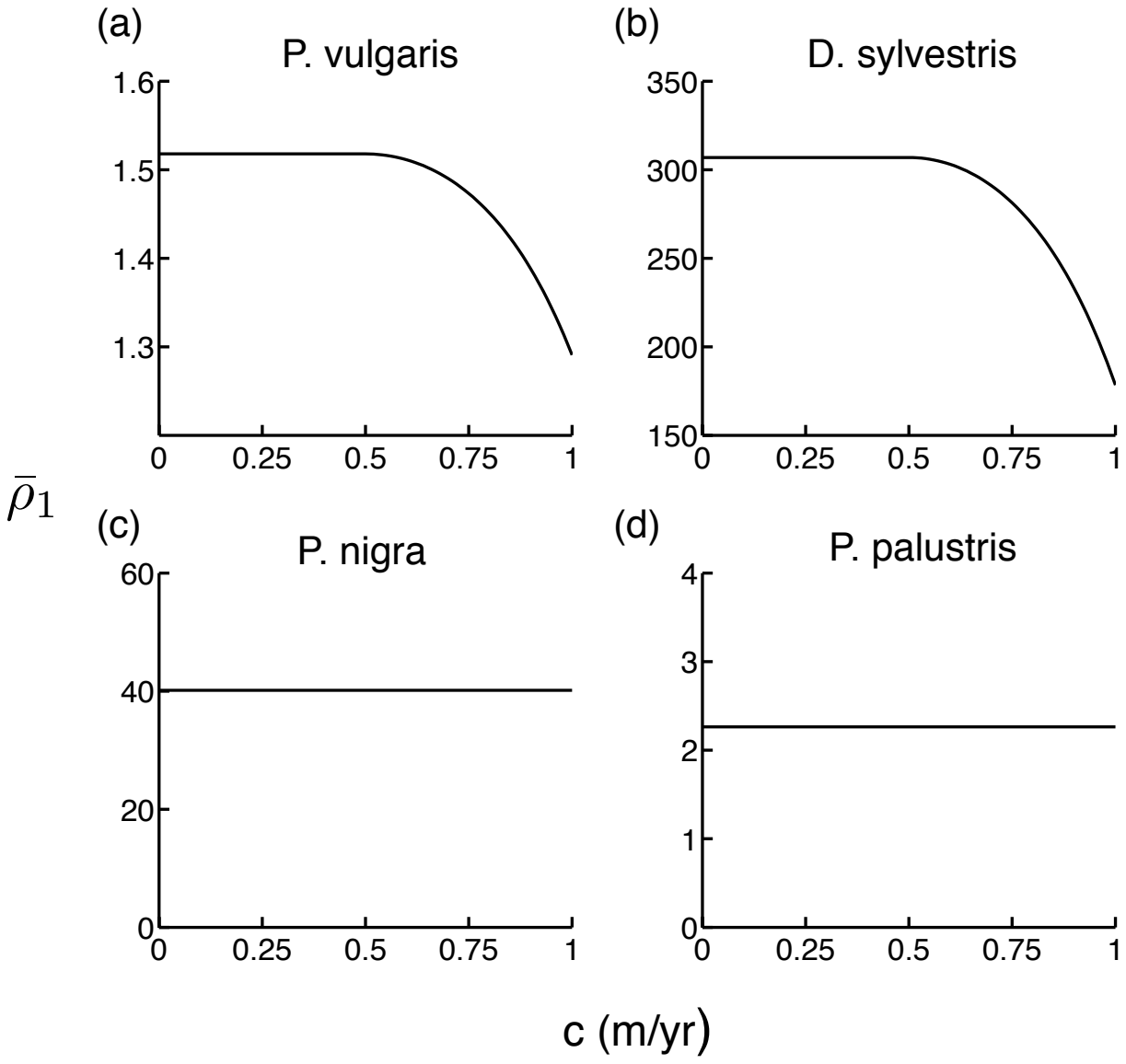

Figure 3.10: Note the difference in scale between $\bar{\rho}_1$, which spans three orders of magnitude. For some species, (a–b) amplification declines sharply as climate speed increases; for others, (c–d) amplification is robust to high climate speeds. Attenuation was not included since it was zero for $c > 0$ in all species. I used parameter values matching those in **(author?)** [96] (see their Table 1 and Appendices).

more important than ever. However, long-term and short-term population dynamics may not match. Since most management decisions involve making short-term plans for populations, spatial models need to account for both transient and asymptotic dynamics. Basing management on only one timescale may lead to inaccurate risk assessment or ineffective use of resources.

The moving-habitat model (3.3) describes a single, unstructured population tracking its moving habitat. Researchers have explored the asymptotic dynamics of a similar model [252, 253]. To quantify transients in the MHM, I borrowed from ideas in non-spatial, structured population models, which are similar mathematically. I calculated metrics such as amplification, attenuation, and their envelopes by either discretizing the model spatially (3.8) or by extending the idea of matrix column sums to the integral operator K (3.7).

Simulating model (3.3) shows that transients arise from both the initial population distribution over space and from biological and environmental parameters (the net reproductive rate, dispersal kernel shape, habitat length, and velocity of climate change). System parameters determine whether transients *can* happen; the initial distribution determines whether they *do* happen. Using Fender's blue butterfly as a case study, I tested the effect of parameters and initial distribution on transients, starting with the speed of climate change, c.

For a range of c-values below the critical speed of climate change, populations can attenuate despite long-term persistence (Fig. 3.2, region II). Transient dynamics create a "trap door" through which population size can fall even if the model predicts long-term growth. Though populations in model (3.3) never reach a density of zero, in reality, populations below a threshold size are at extinction risk from demographic or environmental stochasticity. Monitoring populations is therefore important even when all indicators predict growth.

For a range of c-values above the critical speed, populations can amplify despite long-term extinction (Fig. 3.2, region III). Even if a population cannot track its habitat long-term, transient dynamics temporarily boosts the population if it has a favorable initial distribution. If appropriate management action is taken during the window of transient growth, the

population may survive long-term.

Changes in the net reproductive rate, habitat length, and dispersal kernel shape also affect transients. In general, populations with higher reproductive rates and larger habitats will have higher amplification values. The shape of the dispersal kernel has complex effects on amplification and attenuation. For Fender's blue butterfly, measured parameter values suggest that the reproductive rate may cause a mismatch between short- and long-term dynamics (Fig. 3.4, regions II and III). The species' habitat sizes are likely too small to cause a mismatch (Fig. 3.5, region IV), although model (3.3) likely overestimates mortality through the habitat edges. Leptokurtic dispersal kernels, which describe many butterfly species, may result in attenuation for Fender's blue butterfly (Fig. 3.6, region II). Although complete and accurate parameter information is seldom the case, model (3.3) helps determine which ranges of parameter values could result in transients.

Amplification and attenuation envelopes, which give the maximum and minimum possible population growth rates over time, show that transient dynamics can persist for many generations (Fig. 3.7). The zeros of functions $\ln \bar{\rho}_t$ and $\ln \underline{\rho}_t$ give the maximum possible time period when population size can be larger or smaller, respectively, than the initial size. The closer the system is to losing stability (as $\lambda_1 \to 1$), the longer the window of potential amplification or attenuation. Thus, the MHM predicts that as climate change destabilizes populations, some at-risk populations will show no signs of decline for a long period, akin to extinction debt [112].

Transients ultimately depend on the population's initial spatial distribution. Distributions with a mean close to the leading edge of the moving habitat and low variance have the highest first-step growth rate, whereas those with a mean close to the trailing edge and low variance have the lowest first-step growth rate (Fig 3.8). Concentrating individuals close to the leading edge assures that most offspring will land in habitable territory once the habitat moves, whereas concentrating the population close to the trailing edge forces most offspring to land outside suitable habitat. If a population's initial distribution within its habitat is known, the MHM suggest how to gauge the population's potential for transients.

The initial conditions that maximize or minimize the first-step growth rate are population pulses located at either the best or worst single locations in the moving habitat. If the dispersal kernel is symmetric and unimodal, the location that gives the highest amplification is c units from the center of the moving habitat, toward the leading edge (as long as $c < L/2$).

Although debate surrounding population augmentation and assisted migration continues [41, 101, 183], the MHM suggests the best location to transplant individuals for a short-term population boost. Even if a population cannot persist long-term, periodically placing individuals at the optimal location within the moving habitat may keep the population afloat by repeated amplification.

The similarity between models (3.1) and (3.3) suggest that transient dynamics in the MHM mirror the effects of population momentum in human [120] and wildlife [124] populations. Curbing population size may take a long time if the population has a young age structure with high momentum [70]. Similarly, populations in the MHM with a "young" spatial distribution—weighted toward the leading edge of the habitat—may grow for a long time before declining. An "old" spatial distribution—weighted toward the trailing edge—may decline initially before building up momentum and growing. The MHM highlights the potential for comparing concepts between population models of multiple interacting states.

In the end, do transient spatial dynamics associated with climate change help or hurt populations? Some populations will do better than expected (due to amplification), while others will do worse (due to attenuation). The moving-habitat model (3.3) I have discussed is a simple way to delineate which is which, based on a population's biology, environment, and distribution.

The MHM rests on a number of assumptions that could be loosened. First, model (3.3) assumes that growth is density-independent. While compensatory growth does not affect asymptotic survival or extinction in moving-habitat models, it should have a strong effect on transient behavior, such that the magnitude of amplification or attenuation may be dampened by density-dependence. One approach is to view model (3.3) as the linearization of a nonlinear model around the $n(x) = 0$ equilibrium, in which case metrics $\bar{\rho}_1$ and $\underline{\rho}_1$ should

still give a good indication of first-step growth.

Second, this study touched only briefly on stage-structured populations in moving habitats (Section 6). Structured model (3.27) opens up the potential for modeling a much wider variety of species. When transients can arise from either spatial or demographic effects, it is unclear when the two sources of transient dynamics cancel or combine. Similar analysis would apply to spatially explicit multispecies models. Given that biotic interactions are projected to constrain many species' climate responses [10, 102], understanding the role of transient effects due to species interaction should become increasingly important. The above work supports the increased attention paid to transient dynamics as a way of aligning modeling and management timescales for more effective conservation.

Chapter 4

INCORPORATING ACCLIMATION INTO CONSERVATION DURING CLIMATE CHANGE

4.1 Introduction

Species now face many environmental changes that affect survival. Habitat loss, overexploitation, pollution, and invasive species threaten many populations [33, 68, 104]. In addition, changes in temperature, precipitation, and other climate variables are moving the locations of species' suitable habitats [171, 170, 42]. To avoid local extinction, organisms can track suitable conditions by dispersing, acclimate by changing their phenotypes, or adapt by evolving [4, 44, 107]. Constraints on these three responses vary and may prove deadly for many populations [29, 43, 109, 182, 193, 194, 238].

Environmental changes also affect humans' ability to conserve species. Formerly suitable habitat inside reserves may become inhabitable. Populations may shift outside current reserve boundaries into unprotected territory, spurring interest in whether current protected areas are adequate [83, 122, 222]. There is an growing push for conservationists to account for species' ability to disperse, acclimate, or adapt to novel conditions [11, 84, 100, 103, 107, 206, 217]. Adding to the ecological complexity are uncertainties around future climate stemming from economic, technological, and geophysical sources. These issues have immediate consequences for conservation planning. How have land managers adapted their strategies to the challenges climate change presents?

Most modern management approaches seek the extrema (or near-extrema) of some objective function using linear programming, simulated annealing, and other techniques. The goal is to determine which sites or reserves to select for protection so as to maximize (or minimize) the objective. Approaches differ mainly in their objective functions and the extent

to which they incorporate biological and environmental information. Recent objectives include connecting reserves in a way that minimizes the spatial gradient of temperature along corridors [167], maximizing conservation over a range of different climate and economic scenarios [134, 143, 237], and maximizing conservation under best- and worst-case scenarios of dispersal, adaptation, and acclimation [92, 119, 161].

The above approaches are promising, but they have three main drawbacks. First, dynamics such as growth and dispersal often do not play an explicit role; rather, future distributions are projected based on current realized niches. Without a mechanistic representation of population processes, it is difficult to determine the effects of, for example, density-dependent growth or long-distance dispersal.

Second, models that do incorporate population processes explicitly often assume a limited number of scenarios for species' ability to disperse, acclimate, or adapt. For example, a model may include "no dispersal" and "infinite dispersal" scenarios, or "no acclimation" and "perfect acclimation" scenarios, with little gradation in between.

Third, reserve selection or optimization often occurs after—rather than alongside—simulation of population processes [but see, e.g., 20, 106, 105]. In such cases, there is not a dynamic feedback over time between conservation actions and population distribution, despite the fact that current management decisions affect future distributions, which affect future management decisions, and so on.

I propose a new reserve selection framework that incorporates population dynamics (growth, dispersal, and the ability to acclimate), sequential reserve selection (the ability to make conservation decisions at each time step), and feedback between selection decisions and population dynamics (so that selection affects population density in real time). Thus, population processes and reserve selection are intertwined over time through a nonlinear feedback loop. Certainly, population dynamics [36], sequential reserve selection [53, 219, 158], and feedback effects [20, 106, 105, 157] in selection models are not new. My goal is to extend and combine such techniques, along with the potential for acclimation, in the context of climate change.

Climate change presents the "triple challenge" that (a) species can respond in multiple ways, (b) populations will likely be moving conservation targets as their ranges shift, and (c) future management decisions and population levels affect each other over time. The proposed model will address all three challenges.

The rest of the paper is structured as follows. I start in Section 4.2 with a formal, mathematical description of the site selection model. In Section 4.3, I illustrate the usage and benefits of the model by applying it to a particular species, the Apollo butterfly *Parnassius apollo*. In section 4.4, I discuss how population dynamics, climate change and management decisions shape the conservation outcome. Finally, in Section 4.5, I overview limitations and extensions of the model.

4.2 Model formulation

A mixed integer linear program (MILP) is a convenient way to integrate population dynamics and management decisions. Consider a single population that can inhabit sites or patches indexed $i \in \{1, 2, \ldots, N\}$ at points in time $t \in \{1, 2, \ldots, T\}$. Suppose that each site may be selected for some conservation action. The objective is to determine which sites to select at each point in time so that some proxy for conservation is largest. "Conservation action" applies loosely: it could range from formally setting aside a reserve to performing a management action such as grazing or prescribed burning. Decision variables $X_{i,t}$ describe site selection, where

$$X_{i,t} = \begin{cases} 1 & \text{if site } i \text{ is selected at time } t, \\ 0 & \text{otherwise.} \end{cases} \tag{4.1}$$

Dynamics occur in four stages: dispersal, reproduction, mortality due to site selection or unselection, and mortality due to environmental conditions. The ability of individuals to acclimate is calculated before the program starts (in preprocessing) based on projected environmental conditions and estimated acclimation ability.

I assume each of the four stages occurs roughly synchronously in the population. $D_{i,t}$ is the population size in site i following the t-th dispersal event (it will be important later that these variables are in units of population size, not density). $N_{i,t}$ is the population size in site i after the population has grown according to some growth function. $S_{i,t}$ is the population size in site i after the effects of selecting or not selecting i at time t have occurred ("S" standing for "selection effects"). Populations in selected sites incur less mortality than those in unselected sites. Finally, $M_{i,t}$ is the population size after the mortality effects due to the environment. For example, a population may occupy a site where the average temperature differs from the optimal temperature for performance, and mortality occurs as a function of the temperature difference. Mortality is due to both environmental variables and the ability of incoming individuals to acclimate to new conditions.

The population begins with some initial population size $M_{i,0}$ over the set of sites and proceeds

$$M_{i,0} \to D_{i,1} \to N_{i,1} \to S_{i,1} \to M_{i,1} \to D_{i,2} \tag{4.2}$$

and so on. At each stage, I assume population density cannot exceed some carrying capacity K_i set by the size of the patch i.

The objective is to maximize the total sum of population size over the planning period.

$$\text{Maximize} \quad \sum_{i=1}^{N} \sum_{t=1}^{T} M_{i,t}. \tag{4.3}$$

One way to justify objective (4.3) is the goal is to allow individuals to produce some ecological benefit over the timesteps they are alive. So the units in sum (4.3) are individual–years, much like worker–hours. If each individual–year contributes a certain ecological benefit, the objective *should* be to maximize the total individual–years.

However, many different objective functions are possible, depending on the biological emphasis. Adding weights to sum (4.3) can emphasize short-term or long-term conservation [20].

Alternatively, retaining population levels above a minimum viable level may be necessary to maintain genetic diversity. I will use objective (4.3) for demonstrative purposes.

During the dispersal stage, individuals disseminate among the sites. In the most general case, there is some probability p_{ij} of moving from site j to site i. Then

$$D_{i,t} \leq \sum_{j=1}^{N} p_{ij}\, M_{j,t-1}, \qquad \forall i, t. \tag{4.4}$$

I use an inequality in constraint (4.4) because the objective function will force $D_{i,t}$ to be as large as possible. The probabilities $\{p_{ij}\}$ depend on the distance between sites and, potentially, the presence of dispersal barriers and other topographic features. As a simple first approximation, I obtain the p_{ij} values by calculating the matrix of distances between pairs of sites, evaluating those distances according to a measured distribution of dispersal distances for the population, and normalizing the probabilities within columns so that

$$\sum_{i=1}^{N} p_{ij} = 1, \qquad \forall j. \tag{4.5}$$

That is, all dispersers land in a site. For populations that lose significant numbers of individuals outside the set of sites, assumption (4.5) may not be appropriate. In such cases, one can account for loss outside the set of sites by integrating the dispersal kernel numerically over a destination site area, relative to the center of the source site [20].

Density-dependent population growth is often nonlinear, making it unsuitable for a linear program. To capture nonlinear growth in a MILP, in begin with a growth curve, such as the Beverton–Holt stock-recruitment curve [21], and construct a piecewise function that produces the same dynamics (in this case, logistic growth) [213].

Logistic growth occurs as follows. If $D_{i,t}$ is below a threshold β, the population size is small and exponential growth occurs. If $D_{i,t}$ exceeds β, the population size tapers toward the site's carrying capacity, K_i. A binary variable $y_{i,t}$ produces the switch in growth.

$$y_{i,t} = \begin{cases} 0 & \text{if} \quad D_{i,t} < \beta, \\ 1 & \text{if} \quad D_{i,t} \geq \beta. \end{cases} \tag{4.6}$$

The indicator variable $y_{i,t}$ turns on and off with the constraints

$$D_{i,t} - \beta \leq K_i \, y_{i,t} \qquad \forall i, t, \tag{4.7}$$

$$D_{i,t} \geq \beta \, y_{i,t} \qquad \forall i, t. \tag{4.8}$$

Limiting the disperser population below the carrying capacity for each patch,

$$D_{i,t} \leq K_i, \qquad \forall i, t. \tag{4.9}$$

Then the growth function is captured in the constraints

$$N_{i,t} - K_i \, y_{i,t} \leq (1 + \gamma_1) D_{i,t} \qquad \forall i, t, \tag{4.10}$$

$$N_{i,t} - K_i (1 - y_{i,t}) \leq (1 - \gamma_2) D_{i,t} + K_i \, \gamma_2 \qquad \forall i, t. \tag{4.11}$$

When the population is below the threshold and $y_{i,t} = 0$, it grows exponentially according to constraint (4.10), and constraint (4.11) is non-binding. Above the threshold, the population tapers toward the carrying capacity according to (4.11), and constraint (4.10) is non-binding. Please see St. John [213] for details. To make sure the population does not exceed the carrying capacity, constrain

$$N_{i,t} \leq K_i \qquad \forall i, t. \tag{4.12}$$

The above method of capturing nonlinear growth may be extended to more complicated density-dependence, such as the Allee effect, by using more than one threshold in the piecewise-defined function.

After growth, mortality occurs in two stages, subdivided into $S_{i,t}$ and $M_{i,t}$. First, mortality occurs based on whether a site is selected. In unselected sites, only a fraction $0 \leq \eta \leq 1$ of $N_{i,t}$ survive.

$$S_{i,t} - K_i X_{i,t} \leq \eta \, N_{i,t} \qquad \forall i, t. \tag{4.13}$$

Again, the population cannot exceed carrying capacity.

$$S_{i,t} \leq K_i \qquad \forall i, t. \tag{4.14}$$

A second round of mortality occurs at each site based on the mismatch between the population's average phenotype and the optimal phenotype. In this study, I use the body temperature of larvae as the relevant phenotype, and the optimal body temperature for growth as the optimal phenotype. I assume that the population has a reaction norm that relates the mean temperature of a site at a given time, $E_{i,t}$, to the body temperature of larvae at that site and time, $Z_{i,t}$. I assume further that all individuals at a particular site and time have the same body temperature.

To relate environmental conditions to phenotypes, I use a linear reaction norm that includes a term for acclimation.

$$Z_{i,t} = \kappa \, Z_{\text{opt}} + (1 - \kappa)(a + bE_{i,t}) \tag{4.15}$$

for some constant $0 \leq \kappa \leq 1$ and constants a and b. Here, κ represents the population's ability to acclimate, and parameters a and b represent the pre-acclimation effect of ambient temperature on larval body temperature (i.e., the effect of temperature in the case where

larvae have no ability to seek out suitable microhabitats). Z_{opt} is the optimal temperature for performance, which I base on the mean temperature across occupied sites at the beginning of the model simulation.

In populations with no ability to acclimate ($\kappa = 0$), the phenotype is completely controlled by the environment (via a and b) and there is no tendency toward Z_{opt}. In populations with perfect acclimation ability ($\kappa = 1$), the phenotype is always at the optimal value. The motivation behind equation (4.15) is that, when larvae hatch, the ambient temperature of their immediate surroundings affects their body temperature via $(a + bE_{i,t})$. Depending on their ability to thermoregulate by seeking microhabitats, larval body temperature can get closer to the optimal temperature for fitness, Z_{opt}.

To relate body temperature to performance, I use a Gaussian fitness curve [see, e.g., 8, 46]. Assume that there is an optimum phenotype Z_{opt} that maximizes fitness. The Gaussian function is a common choice for the fitness curve, since it has stabilizing selection toward the optimal phenotype [46, 45].

$$M_{i,t} \leq \exp\left[-\frac{(Z_{i,t} - Z_{\text{opt}})^2}{2\sigma^2}\right] S_{i,t} \qquad \forall i, t, \tag{4.16}$$

The parameter σ represents the breadth of the fitness curve, or the breadth of tolerance. In the case where multiple traits affect performance (a more realistic scenario), a multivariate Gaussian on the right-hand side of (4.16).

Using equation (4.15) to model acclimation has some advantages and disadvantages. The parameters a and b are conversion factors between the environmental variable and individual phenotype, since $E_{i,t}$ and $Z_{i,t}$ may have different units. As a result, $\kappa \in [0, 1]$ is dimensionless and can be compared across populations. Moreover, in equation (4.15), $Z_{i,t}$ is not density-dependent, so one can use climate projections to estimate $E_{i,t}$ and then calculate $Z_{i,t}$ values before actually running the model.

One drawback of equation (4.15) is that it is over-parameterized. Many studies measure the environmental variable and phenotype directly, without the intermediate step of calcu-

lating $a + bE_{i,t}$. If $E_{i,t}$ has a direct correlation with $Z_{i,t}$, then setting $a = 0$, $b = 1$ may be a fair assumption. Another disadvantage is that equation (4.15) is memoryless with respect to phenotypes. That is, the new average phenotype at a site is not the weighted sum of immigrating phenotypes, and there is no information on genotype or recombination. Thus, the model does not address heritable variations, and it assumes that acclimation ability is equal for the whole population.

I have arranged the sequence of biological and conservation effects in a certain order (dispersal, growth, and mortality). Care should be taken that the ordering is valid for the system of interest. The life-history of the species I consider below matches the sequence, but other species may not.

The most important part of the model is the space of management decisions on which population dynamics play out. Economic and political factors set constraints on how management can occur, and there is often uncertainty around future land prices, availability, and budget [226, 143]. For now, I assume the cost of selecting sites is known, keeping in mind that managers can easily incorporate more sophisticated assumptions. Let the cost of selecting site i during period t be $C_{i,t}$. With a budget over the planning period of B,

$$\sum_{i=1}^{N} \sum_{t=1}^{T} C_{i,t} X_{i,t} \leq B. \tag{4.17}$$

Many variations on constraint (4.17) are possible, depending on the economic situation. I assume here that $C_{i,t}$ is proportional to the size of the site i in hectares, but that need not be the case. It is also common to model budget annually, so that there is a constraint involving B_t for $t \in \{1, 2, \ldots, T\}$.

4.3 Case study: Parnassius apollo

4.3.1 Description

To test model (4.4)-(4.17) , I consider the Apollo butterfly *Parnassius apollo* (Linnaeus 1758). The species inhabits open, rocky, subalpine and montane habitats throughout Europe

and Asia [225]. Numerous subspecies exist as a result of isolation after the most recent colonization of its range in the late Pleistocene [88]. They are often considered a flagship species for the entire montane environment. *P. apollo* is of high conservation concern: it is listed as near threatened by the IUCN, and is included in the Habitats Directive Annex 4, Bern Convention Annex 2, and CITES Appendix II [232]. The species is declining in areas of low altitude, and modeling studies place the species at high risk due to future habitat loss [243].

First, I briefly review the species' life-history, response to climate change, and recommended conservation actions. *P. apollo* does not fit all model assumptions perfectly, but it is a suitable species for demonstration.

P. apollo is univoltine. It has a single annual flight period in mid-summer, after which females deposit eggs that overwinter [12]. Adults feed on a limited range of nectar sources [16, 2]. After hatching, larvae feed on host plants of the *Sedum* genus [162]. Females do not oviposit on the host plant, often placing eggs randomly [76]. Larvae locate hosts through searching randomly [75]. The life span of the adult butterfly is around one month [2].

Population densities of *P. apollo* are often low. Density can show periods of stability, as well as large fluctuations from year to year, likely due to habitat differences [73, 87, 142]. There is a strong correlation between female abundance in one year and larval abundance in the next year [76].

The species is a good flyer, although movement over meadow patches is constrained by the location of nectar and host plant sources [24]. Adults appear most frequently on large host plant patches that are close to nectar plant patches [76]. Using mark-release-recapture data, distributions of dispersal distance have been fit with negative exponential functions [24, 76]. Successful reproduction can only occur on host plant patches [24]. Surrounding forest likely acts as a dispersal barrier and deceases habitat connectivity, as it does in other *Parnassius* species [195].

P. apollo shows both local adaptation and the ability to acclimate using phenotypic plasticity. Males change their mate searching behavior in response to weather conditions

[2]. Larvae use behavioral thermoregulation to find microhabitats with an intermediate temperature. Individuals maintain metabolism across a wide temperature range, indicating adaptation to high daily and seasonal temperature fluctuations [162]. Here, I will focus on behavioral thermoregulation in larvae as the mechanism of acclimation. That is, I focus on the ability of larvae to locate microhabitats with ambient temperatures optimal for growth. Microhabitat selection is only one component of plasticity for this species, and I leave it to future studies to incorporate more life-history events that affect fitness. Since *P. apollo* has a high thermal breadth, I will use the mean temperature during the time of larval growth as an environmental covariate.

The species has already responded to climate change, and will likely continue. Historically, *P. apollo* was a glacial invader, expanding southward within glacial periods and contracting into fragmented montane habitats during interglacials [225]. Recently, increasing temperatures have caused a rise in the lower range limit [12, 203] and an advancement of the onset of flight. In addition, afforestation and the loss of host plant due to competing plant species are pushing ranges upslope [234, 195]. Temperature variability through events such as false springs has let to high larval mortality in certain years [12]. Although few insect species went extinct through Pleistocene glacial cycles, *P. apollo* is at risk because it is a specialist [187] and because its fragmented habitat may prevent it from colonizing new suitable areas [243].

Despite having legal protection, the butterfly seldom receives attention to habitat management. The formulation and implementation of management plants is an urgent need [232]. Conservation recommendations include grazing to prevent shrubland succession [12, 62, 232], maintaining suitable types and densities of host plants [73, 12, 75, 232, 87], maintaining nectar plant density and proximity to host plants [16, 76, 232], maintaining a mosaic of microhabitats with different temperatures [12, 87], protecting suitable habitat even where butterflies are absent [73, 12], supporting the population with semi-natural rearing in the case of weather anomalies [142], and stimulating gene flow in populations with more generalist characteristics [88].

4.3.2 Model parameterization

I obtained data on meadow sites in Switzerland spanning a mountainside, for which past observations of *P. apollo* exist. I relied on colleagues who used ArcGIS to obtain a set of sites that include suitable habitat for *P. apollo* (Fig. 4.1). The study area includes 157 sites, with elevations ranging from 629 m to 2544 m. A complete set of parameter values specific to this site was not available, so I estimated parameters from an ensemble of published research on the species. Some data rely on studies on *P. apollo* in other regions. Other parameter values are speculative, if data were unavailable, for the purpose of demonstrating the model. I have divided the parameters into biological, environmental, and managerial (Table 4.1).

Data on growth, dispersal, and temperature sensitivity came from studies on *P. apollo* elsewhere in Europe. I used *P. apollo* counts from observations at the study site to set the initial population size at each site. The effect of management (η) is harder to quantify for since it depends on the specific management action. I chose $\eta = 0.50$ for the baseline model [i.e., an unselected site loses 50% of its population in stage (4.13)].

Environmental data for the site is more readily available, including the the size, elevation, and distance between sites. Temperature measurements at the sites were taken at the same time as the population size measurements. I used projections for Swiss climate to derive seven warming scenarios: a no-change model, and models for the upper and lower projected warming rates for each of the A1B, A2, and B1 scenarios.

Since this study was not coordinated with an actual management plan at the site, the economic parameters are entirely speculative. As a way of turning the uncertainty into something useful, I conduct a brief bioeconomic analysis that determines when it would be profitable to take management action. I will relate the cost of management, the rate of climate change, and the ecosystem service value above which it is financially beneficial to take management action.

I used IBM's ILOG CPLEX software to solve the baseline model (with parameters given by Table 4.1), as well as seven other models with different parameters (Table 4.2).

Table 4.1: Parameters used in the baseline MILP for *P. apollo*. GIS analysis was performed by a colleague, Kornel Czimber. For parameters with no estimates, I made efforts

Parameter	Value	Equation	Source
Biology:			
Dispersal kernel	$p_{ij} = \alpha \exp(\alpha d_{ij}), \quad \alpha = 0.002/\text{m}$	4.4, 4.5	[76, 24] (kernel type)
Carrying capacities	$K_i = 12.5$ individuals/ha $\cdot \text{Area}_i$, $i = 1, 2, \ldots, 157$	4.7–4.9	[3]
Growth threshold	$\beta_i = 0.5K_i$, $i = 1, 2, \ldots, 157$	4.6–4.8	[no estimates]
Performance curve	$Z_{\text{opt}} = 2°\text{C}$, $\sigma = 2°\text{C}$	4.16	[no estimates]
Reaction norm	$a = 0$, $b = 1$	4.15	[12]
Acclimation ability	$\kappa = 0.5$	4.15	[12]
Initial population size	$\{M_{i,0}\}$, $i = 1, 2, \ldots, 157$	4.5	[GIS analysis]
Effect of no management	$\eta = 0.50$	4.13	[no estimates]
Environment			
Initial temperatures	$\{E_{i,0}\}$, $i = 1, 2, \ldots, 157$	4.15	[GIS analysis]
Rate(s) of climate change	$\{c_i\}$, $i = 1, \ldots, 7$	[not shown explicitly]	[69]
Site area	$\{\text{Area}_i\}$, $i = 1, 2, \ldots, 157$	[not shown explicitly]	[GIS analysis]
Distance between sites	$\{d_{ij}\}$, $i, j = 1, 2, \ldots, 157$ (see supplement)	[not shown explicitly]	[GIS analysis]
Site elevations	$\{\text{Elev}_i\}$, $i = 1, 2, \ldots, 157$	[not shown explicitly]	[GIS analysis]
Management			
Total budget	$B = 0.25 \sum_{i=1}^{N} \sum_{t=1}^{T} C_{i,t}$	4.17	[No estimates]
Cost of selection	\$100/ha/yr	[not shown explicitly]	[154] (but varies)
Planning period	$T = 10$ years	[throughout]	[No estimates]

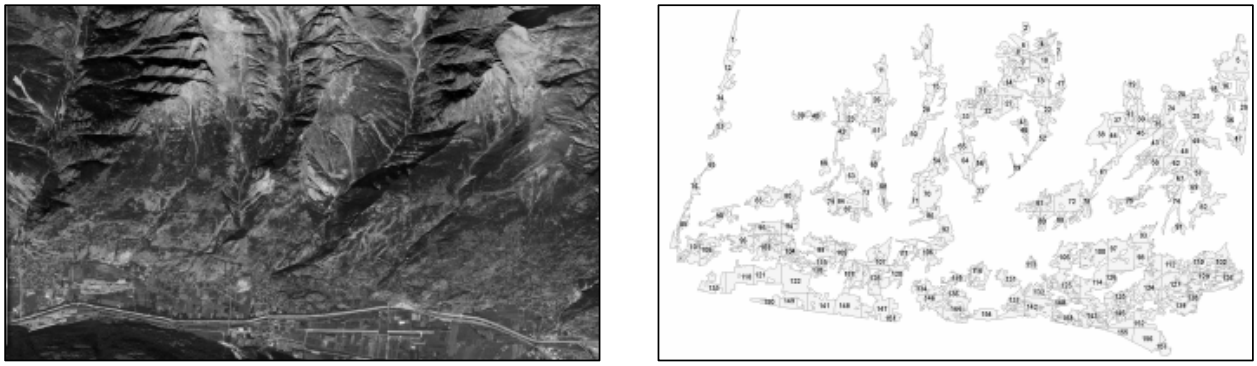

Figure 4.1: Location of case study (left) and site GIS layer (right) showing the 157 meadow sites used in the analysis.

Table 4.2: Parameters used in variations on the baseline model for *P. apollo*. Values are identical to the baseline except for the changes given in the "Parameter values" column.

	Scenario	Parameter values
1	Baseline	[Table 4.1]
2	Low acclimation	$\kappa = 0.25$
3	No acclimation	$\kappa = 0$
4	Low thermal breadth	$\sigma = 0.5°\text{C}$
5	Medium thermal breadth	$\sigma = 1°\text{C}$
6	Low dispersal	$\alpha = 0.023/\text{m}$
7	Low budget	$B = 0.10 \sum_{i=1}^{N} \sum_{t=1}^{T} C_{it}$
8	High budget	$B = 0.50 \sum_{i=1}^{N} \sum_{t=1}^{T} C_{it}$

4.4 Results

The MILP outlined above has too many parameters to explore the full parameter space of how it behaves. In this case study, I focus on the interplay between acclimation, climate change, and management decisions. First, how does acclimation ability affect where and when to optimally select sites? Second, under what conditions is it profitable to take management action, given the ecosystem services the population provides? Third, under what conditions is it necessary to take management action to maintain the population size above a certain critical level? Fourth, how much better does a model taking acclimation into account do than one that ignores acclimation ability?

Climate change has a negative effect on the ecological benefit achieved from management (Fig. 4.2). The temperature effect on the population worsens as the warming rate increases, so there is more mortality due to the environment. However, for populations that can acclimate, conservation can attain a much higher objective value. The relatively shallow slope (on the scale used in Fig. 4.2) means that a small increase in κ can "cover for" a large increase in climate rate, when management action is taken. Moreover, the objective function does not increase linearly with acclimation ability, since the difference between $\kappa = 0.5$ and $\kappa = 0.25$ is much greater than the difference between $\kappa = 0.25$ and $\kappa = 0$. This result suggests that targeting species with moderate acclimation ability is especially effective, and that it is important to measure a population's acclimation ability as closely as possible.

One way to visualize the resulting management plan is to plot the selected sites, along with population sizes, over time (Fig. 4.3). I chose a single climate scenario, the lower-range estimate for the A1B emission scenario ($c = 0.0355°\text{C/yr}$). The initial population includes a number of high-density sites at lower elevation, as well as a single upslope site with high population size. The optimal solution quickly narrows the area of focus from the entire mountainside to the upslope population, allowing it to expand to adjacent sites.

Another way to visualize the optimal management plan described by solving the MILP is to plot the average selected site elevation (SSE), as well as the highest and lowest selected

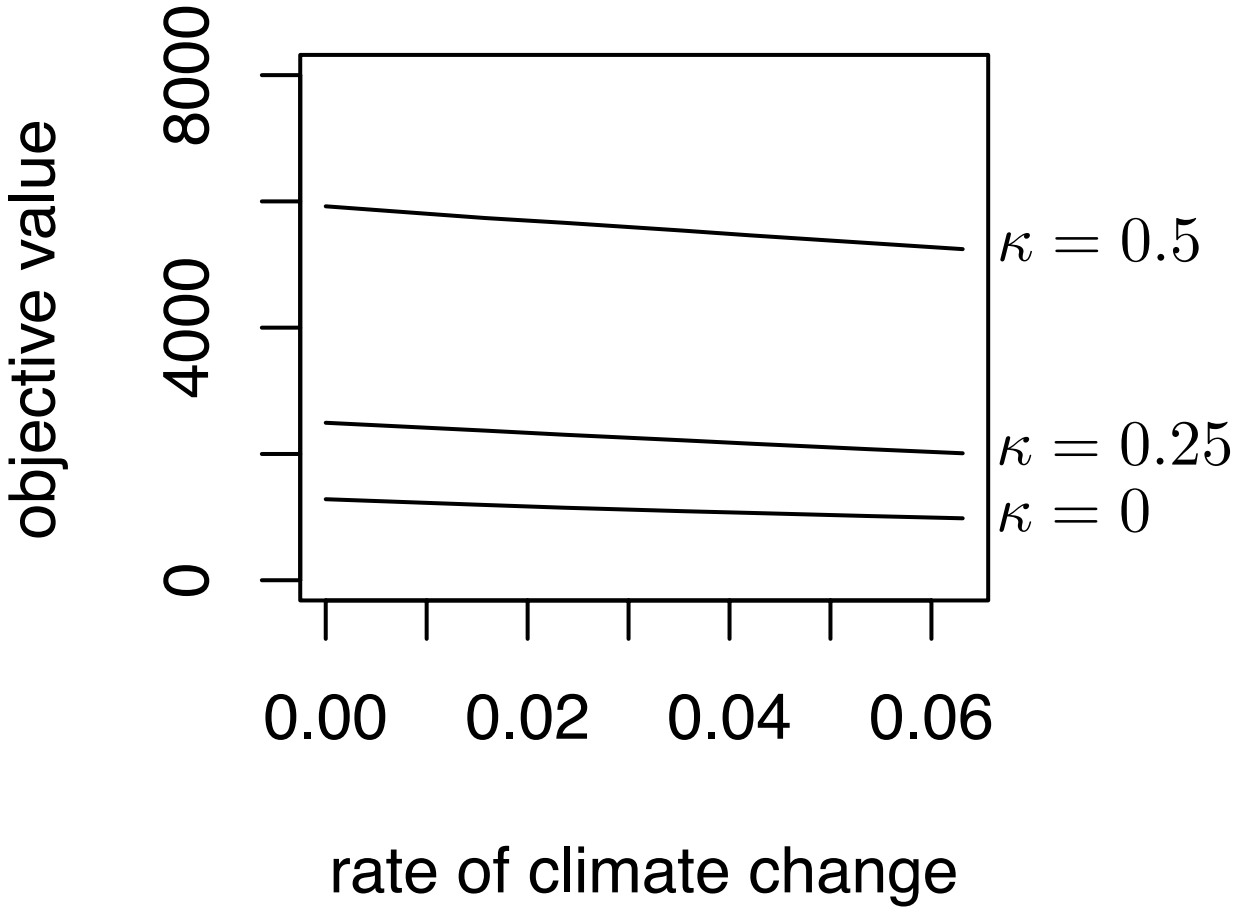

Figure 4.2: As the rate of climate change increases, the optimal conservation value possible decreases. For a given climate rate, the objective value increases with acclimation ability. Acclimation augments conservation efforts. I used baseline scenario parameters.

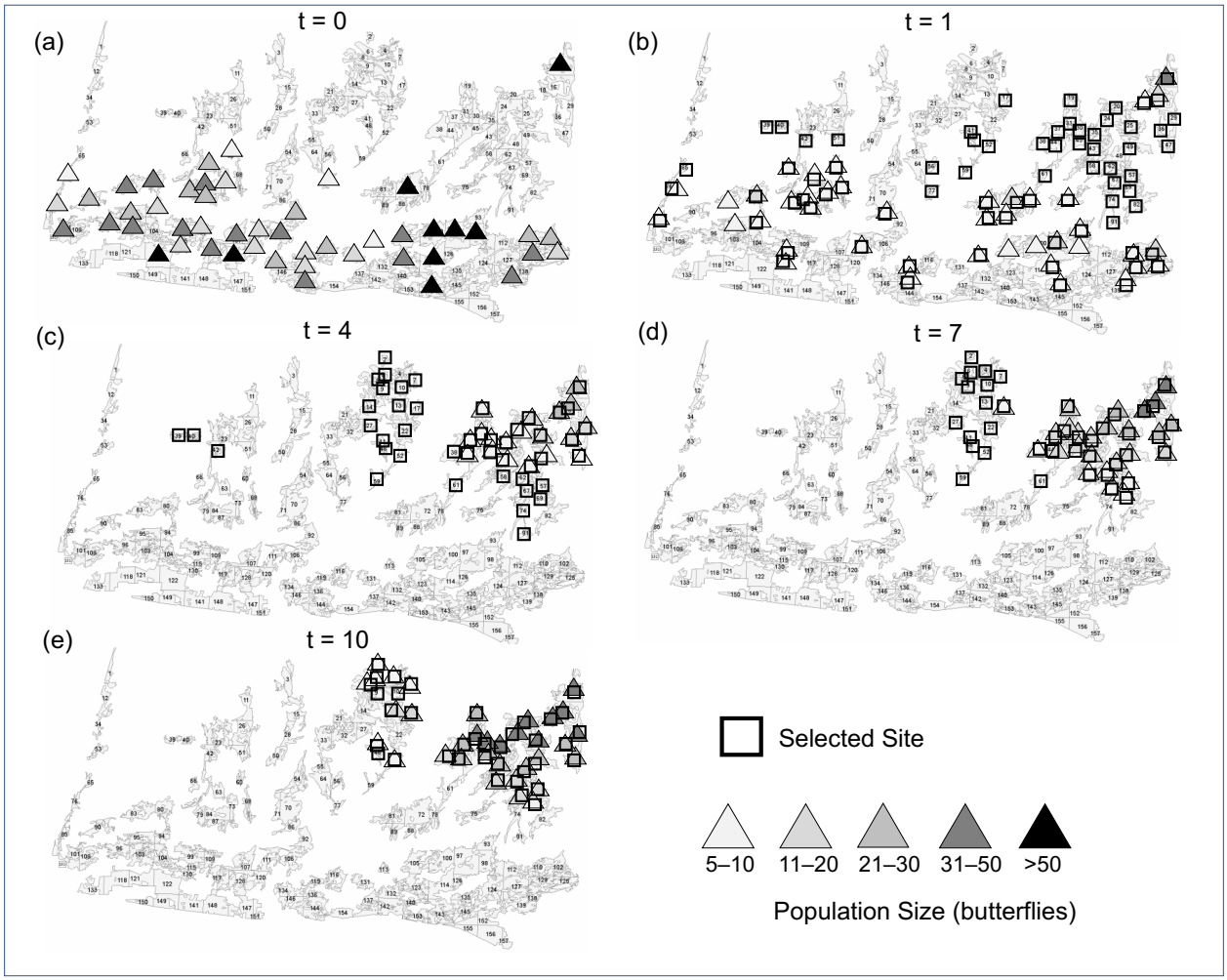

Figure 4.3: Maps of baseline model solution for different time steps. I used an intermediate climate scenario with the baseline parameter values and plotted population size and selected sites $\{X_{i,t} = 1\}$ for $t = 1, 4, 7, 10$.

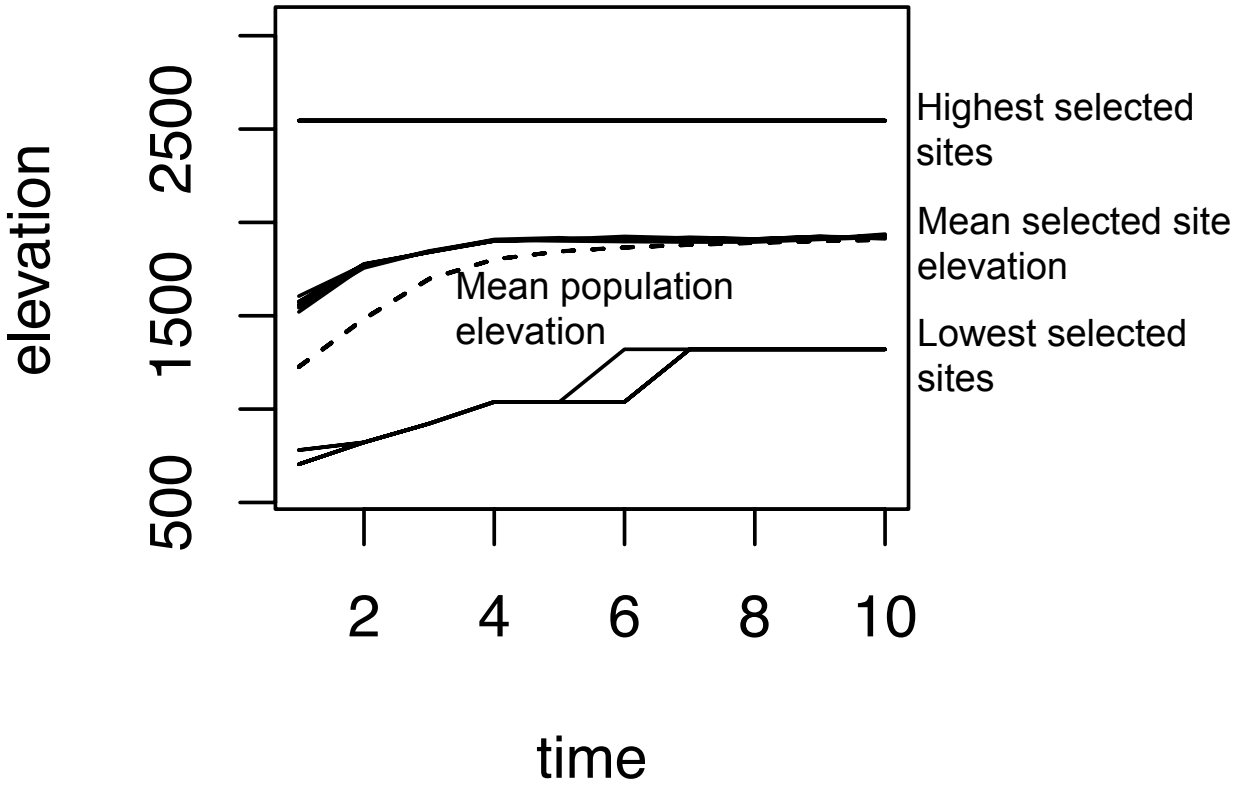

Figure 4.4: The upper and lower sets of curves show the highest and lowest elevations of selected sites over time, plotted for seven different climate speeds. The middle set of solid curves is the weighted mean of the elevation of selected sights. For this scenario, site selection facilitates the average elevation of populated sites (dotted curve) to increase. I used baseline scenario parameters.

site elevation, over time (Figure 4.4). For the baseline parameter scenario, the average (arithmetic mean) of SSEs increases by about 400m in four years before leveling out. The lowest SSE increases by about 500m over seven years, while the highest stays the same. For higher rates of climate change, the lowest SSE increases sooner. Importantly, the mean SSE is closely related to the mean elevation of the population. Management decisions track the population as it expands upslope.

To test the effect of dispersal distance on management, I used a much smaller mean

dispersal distance in Scenario 2 (see Table 4.2). Plotting the mean and min/max SSEs shows a different management strategy (Fig. 4.5). The selected sites are static until a threshold period, around 5 years, when the model suggests to increase SSEs. The low-dispersal model is more sensitive to climate change, especially at the lower and average SSE, since each set of trajectories has more variation. The value of the model is especially clear here, since there is no obvious reason to switch strategies starting at 5 years just by looking at the population trajectory.

The rate of climate change affects the objective function (Fig. 4.2), but its affect on management choices in this study can be minimal (Fig. 4.4). How does climate change affect the total population size over time? I measured population size over time for Scenarios 1–4 (see Table 4.2). Specifically, these include a baseline case (Fig. 4.5a), a low-acclimation case ($\kappa = 0.25$, Fig. 4.6b), a no-acclimation case ($\kappa = 0$, Fig. 4.6c) and a low thermal breadth ($\sigma = 0.5°$C, Fig. 4.6d).

In many cases, total population is similar across a broad range of climate scenarios. After a number of years, some population trajectories begin to diverge based on the rate of warming (Fig. 4.6b,c). Such populations are on the edge between persistence and extinction, so differences in the warming rate cause large differences in population size over time. Other populations show little difference in size across a wide range of climate scenarios (Fig. 4.6a,d).

Fig. 4.6 shows that even with optimal management, small changes in acclimation ability can mean the difference between population persistence and collapse. Since many species can acclimate in multiple ways (affecting multiple components of fitness), accurately measuring acclimation ability is vital to conservation.

When the population either strongly persists (Fig. 4.6a) or quickly collapses (Fig. 4.6d), there is little difference between different climate scenarios. However, when the population has weak stability, it is much more sensitive to the rate of climate change (Fig. 4.6b,c). That is, populations for which conservation can do the most to "turn around" are the most sensitive to climate change.

Population trajectories for *P. apollo* show transient dynamics such as attenuation (Fig.

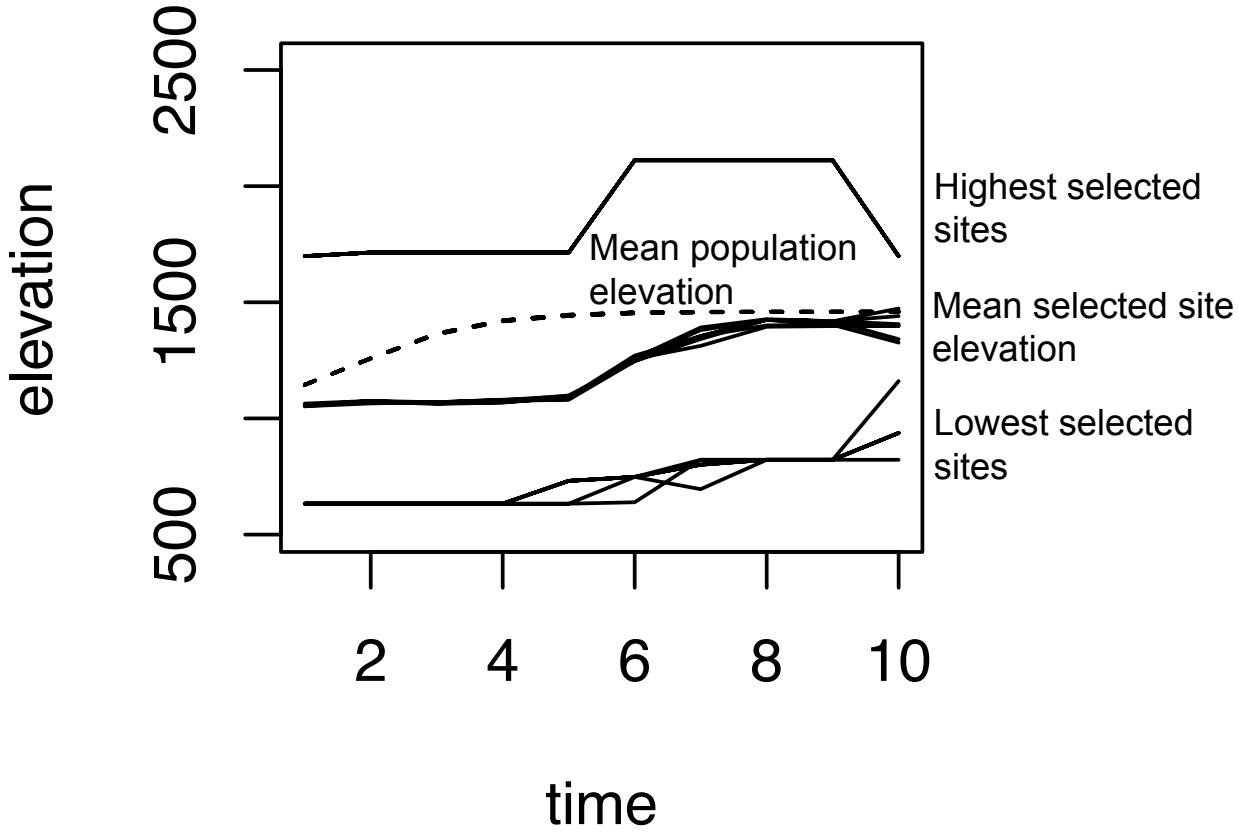

Figure 4.5: Effect of low dispersal on which sites are selected. I used the baseline parameters except low dispersal to test the effect on the average and extreme elevations of selected sites. While the population increases in elevation over time, the optimal management strategy includes sudden shift of sites selected around 5 years of stasis. The different curves within each low, high, or middle cluster are solutions for different climate rates.

4.6a) and amplification (Fig. 4.6c). These transients may be due to the initial population distribution among sites, as well as biological and environmental parameters (confer with Chapter 3).

A goal of many conservation programs is to maintain the population size above a certain level [187]. Low populations may suffer from inbreeding depression, Allee effects, and other negative effects. Plotting the population trajectory under optimal management can inform whether management could maintain the population above some critical size (Fig. 4.7). If the critical size is above n^*, the location of the horizontal tangent to the population curve, then the population is at risk and management is advisable. This is not a novel use of modeling, but it is significant that for the baseline *P. apollo* case, the effect of different climate scenarios is indistinguishable for many years. Thus, a manager could assess whether maintaining critical size is feasible without precise climate projections.

When economic parameters are unavailable, as is the case in this study, it is helpful to explore the effect of the total budget on the objective value. To incorporate the effect of climate change, I plotted the objective function vs. warming rate for four different budgets (Fig. 4.8). As a reference, I plotted the maximum budget (upper line), which corresponds to selecting every site at every time period. The "High Budget" allotted 50% of the maximum budget (Table 4.2, Scenario 8); the "Medium Budget" allotted 25% of the maximum (Scenario 1), and the "Low Budget" allotted 10% of the maximum.

One noticeable effect is the sharp diminishing returns on the objective value. The objective value gain between 50% and 100% of the maximum budget is around 200 butterfly–years, or less than 3% of the objective value. In contrast, the gain from 10% to 25% of maximum budget produces about a 60% increase in objective value. Moreover, climate change has a negative effect on the objective, regardless of the budget level. Depending on the budget level, each additional 0.01°C/yr of warming corresponds to a loss of between 61–106 butterfly–years in the objective function.

Another way to understand the economics of a management problem with limited information is to determine when it is financially profitable to take management action. Some

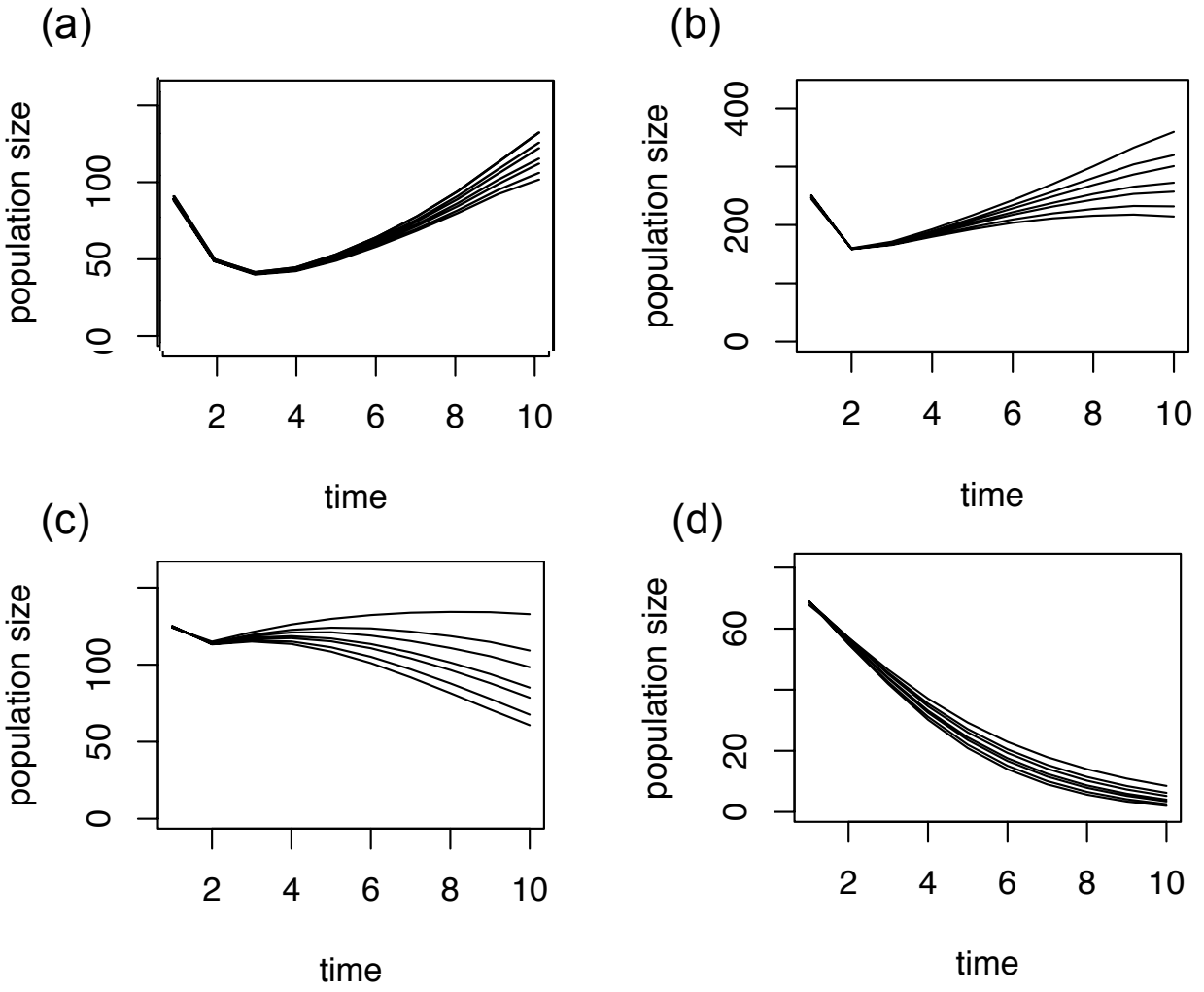

Figure 4.6: Scenarios include (a) the baseline, (b) lower acclimation ability, (c) no acclimation ability, and (d) the baseline with narrower thermal performance breadth. Even when managed optimally, the population size can either (a)-(b) decrease before regaining, or (c) increase before falling. Each curve within a plot corresponds to a climate speed scenario, ranging from zero to the highest projected rae.

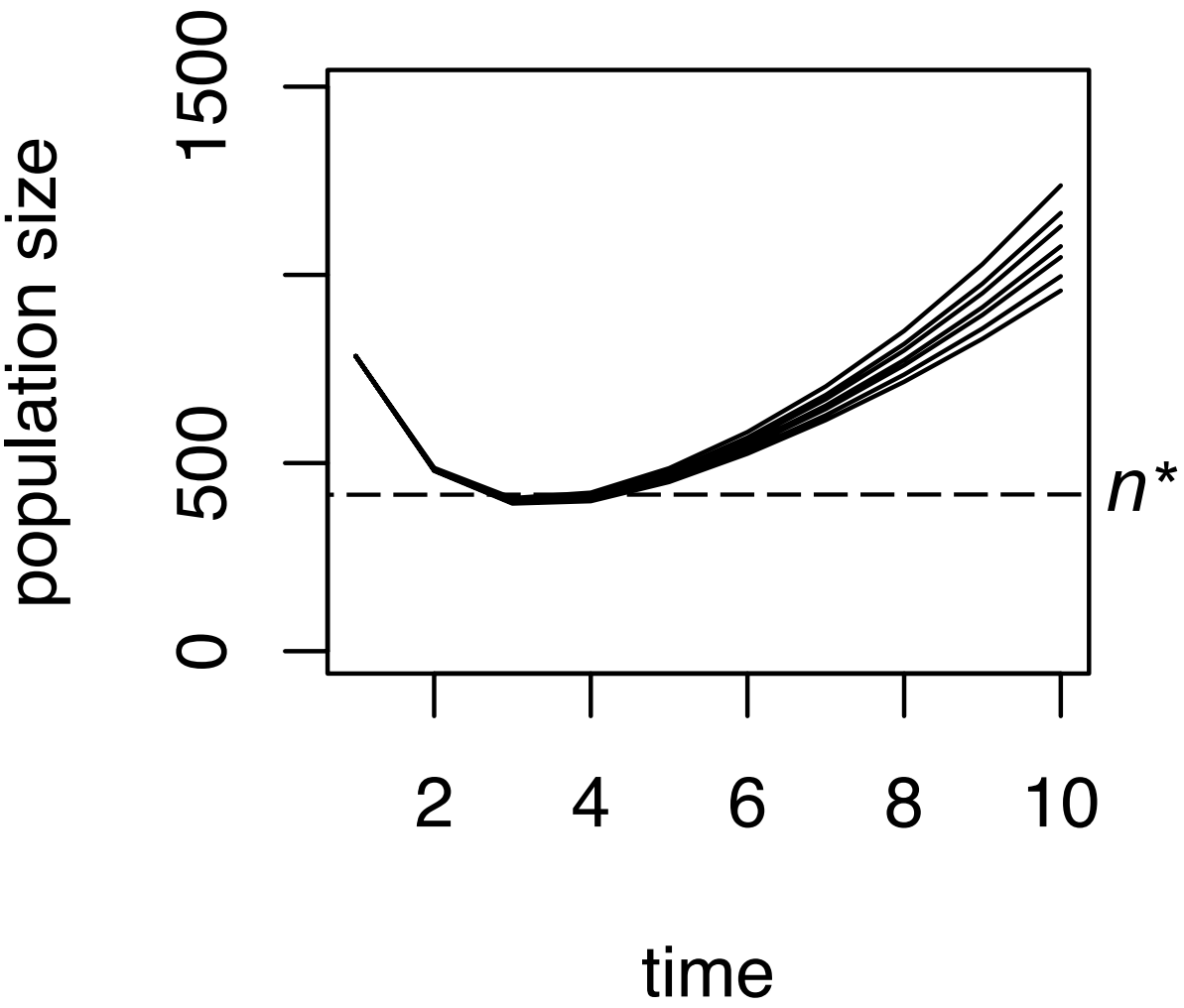

Figure 4.7: If the horizontal tangent to the highest curve is larger than a critical value n^*, then management is necessary to maintain the population above n^*.

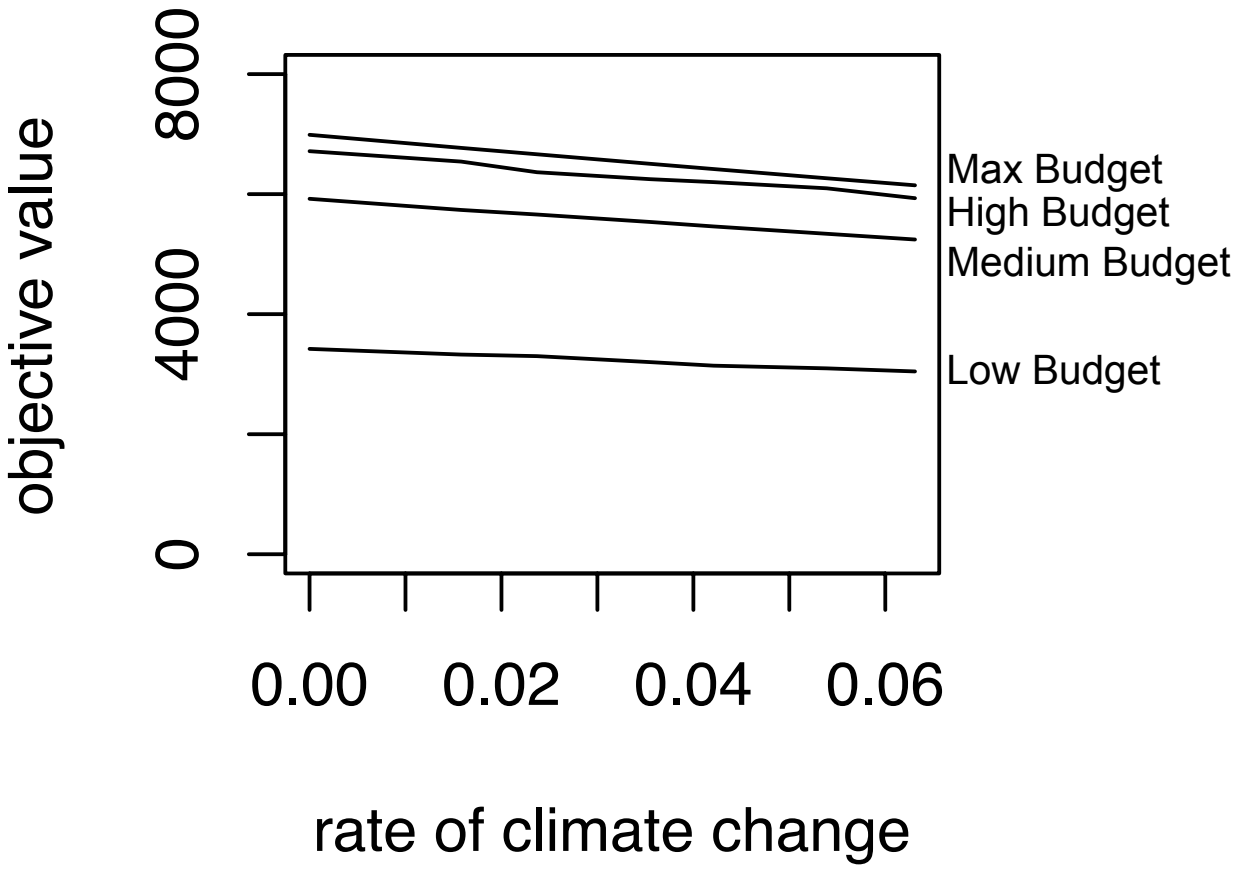

Figure 4.8: The maximum budget is associated with the cost of selecting all sites at all times. As the budget increases from zero to the maximum budget, the curve relating climate rate and objective increases toward the envelope of the max budget. That is, the max budget sets the limit on how much ecological benefit can be achieved under a given climate scenario.

conservationists advocate trying to place instrumental value on ecosystem services as an incentive for investors to support conservation action. If the value of the ecosystem services provided by conserved species is greater than the management budget, the management plan is advisable from an economic viewpoint.

To compare monetary value, I need to make sure units match. As is, the objective function value

$$M_{\text{obj}} = \sum_{i=1}^{N} \sum_{t=1}^{T} M_{i,t} \tag{4.18}$$

is in units of individuals–years (similar to worker–hours), which I abbreviate ind–yr. To express the objective value in terms of dollars of ecosystem service, suppose there is a conversion factor v, with units \$/(ind–yr), so that the monetary value of the objective function $M_{\$}$ can be expressed as

$$M_{\$} = v \cdot M_{\text{obj}}. \tag{4.19}$$

I make the assumption that the budget in constraint (4.17) is proportional to the area of sites selected, so that the cost of selecting sites is some fixed cost C_{fixed} (\$/hectare) times the total area conserved,

$$B = C_{\text{fixed}} \cdot \sum_{i=1}^{N} \sum_{t=1}^{T} A_i X_{i,t} \tag{4.20}$$

where A_i is the area (in hectares) of site i.

For simplicity, I will ignore discount rates and assume there is a net profit if

$$M_{\$} > B, \tag{4.21}$$

$$v \cdot M_{\text{obj}} > C_{\text{fixed}} \cdot \sum_{i,t} A_i X_{i,t}, \tag{4.22}$$

or

$$\frac{v}{C_{\text{fixed}}} > \frac{\sum_{i,t} A_i X_{i,t}}{M_{\text{obj}}}. \tag{4.23}$$

Relationship (4.23) is helpful since the right-hand side is known from the MILP model output. So even if the value of ecosystem services and the cost of site management are difficult to estimate, their ratio must be greater than a certain constant to be financially profitable.

As an example, I plotted the critical ratio on the left-hand side of (4.23) as a function of the climate rate, for the baseline budget (Fig. 4.9). The utility of quantifying the critical ratio is that it makes the decision to manage or not more robust to parameter uncertainty. The values of C_{fixed} and especially v may be unknown. If one of the two values is estimable, Fig. 4.9 gives a sense of what the other would need to be to generate profit.

Generally, weed removal operations such as those recommended for *P. apollo* cost in the range of a few hundred dollars per hectare [154]. For an intermediate rate of climate warming (0.04°C/yr), the ecosystem service value would need to be on the order of $10,000 per butterfly–year to be profitable. That amount is likely too high a figure for *P. apollo*, but for others that are critically endangered or provide essential agricultural services, high values may be typical.

Regardless of ecosystem service value, the positive slope in Figure 4.9 means that climate change inflicts a financial cost. This result matches the expectation that there is a tradeoff between investing to minimize the rate of climate change and investing to repair the damage from climate change.

One of the primary contributions of the model I have discussed is the ability to include acclimation into population dynamics and management. To quantify how important it is to account for acclimation, I compared the results of the baseline MILP run to a scenario where acclimation does not appear in the decision framework.

To create a scenario where the population can acclimate but the model does not account for it, I performed an iterative process that alternates between two steps. First, I solved the MILP with baseline parameter values, except setting $\kappa = 0$ (no acclimation). The outcome

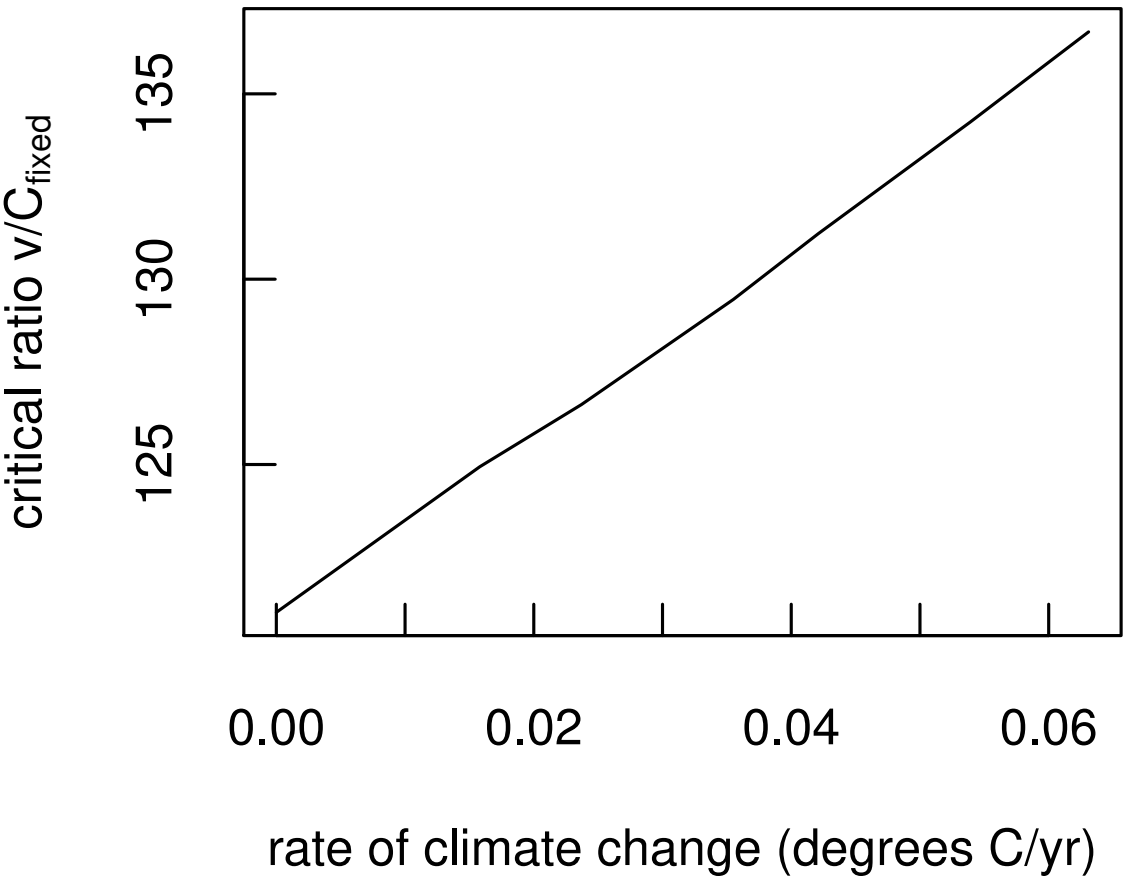

Figure 4.9: The critical ratio v/C_{fixed} that determines profitability. If, for a certain rate of climate change, the ratio of ecosystem service value v to the cost per hectare of management C_{fixed} is above the curve, optimal management will result in a net profit.

includes $\{X_{i,1}\}$, the set of site selection decisions for the first year. I then substituted those decision variables into the cycle of population dynamics to simulate what would *actually* happen if the population could acclimate, using $\kappa = 0.5$. The result is the set of actual population sizes $M_{i,1}$ after the first year. Next, I reran the MILP including the "hard-coded" $M_{i,1}$, again using $\kappa = 0$, to get $X_{i,2}$, substituted those decision values into the simulation, and repeated the process for 10 time steps.

The result of the iterative process is that the population size (and consequently, objective value) for the no-acclimation scenario is less than the population size for the baseline model that includes acclimation (Fig. 4.10)

4.5 Discussion

The ideal conservation scenario is, in a sense, to find a balance between biodiversity and human impact. Climate change offsets that balance in a variety of ways. Many species have already used dispersal or acclimation (i.e., phenotypic plasticity) to adjust to environmental changes. Management tools such as reserve design algorithms–and, in general, any method of allocating finite resources–need to respond to species accordingly.

In this study, I developed a mixed-integer linear program that can be used to make the best use of conservation resources during climate change. The model contributes to the growing literature on accounting for multiple climate responses at once. I chose not to model adaptation, another possible climate response, since it involves the preservation of information across time steps. I modeled acclimation (along with growth and dispersal) in a way that is memoryless and easy to incorporate into a mathematical program.

I chose a MILP for multiple reasons. First, it provides truly optimal management recommendations, in contrast to heuristic methods that may find feasible but suboptimal solutions. Second, the MILP can incorporate population dynamics and management decisions in a feedback loop over time, in contrast to approaches that project future species abundance before selecting sites for management. Third, the MILP is flexible, since incorporating more realistic information (such as economic constraints) can be included as additional constraints,

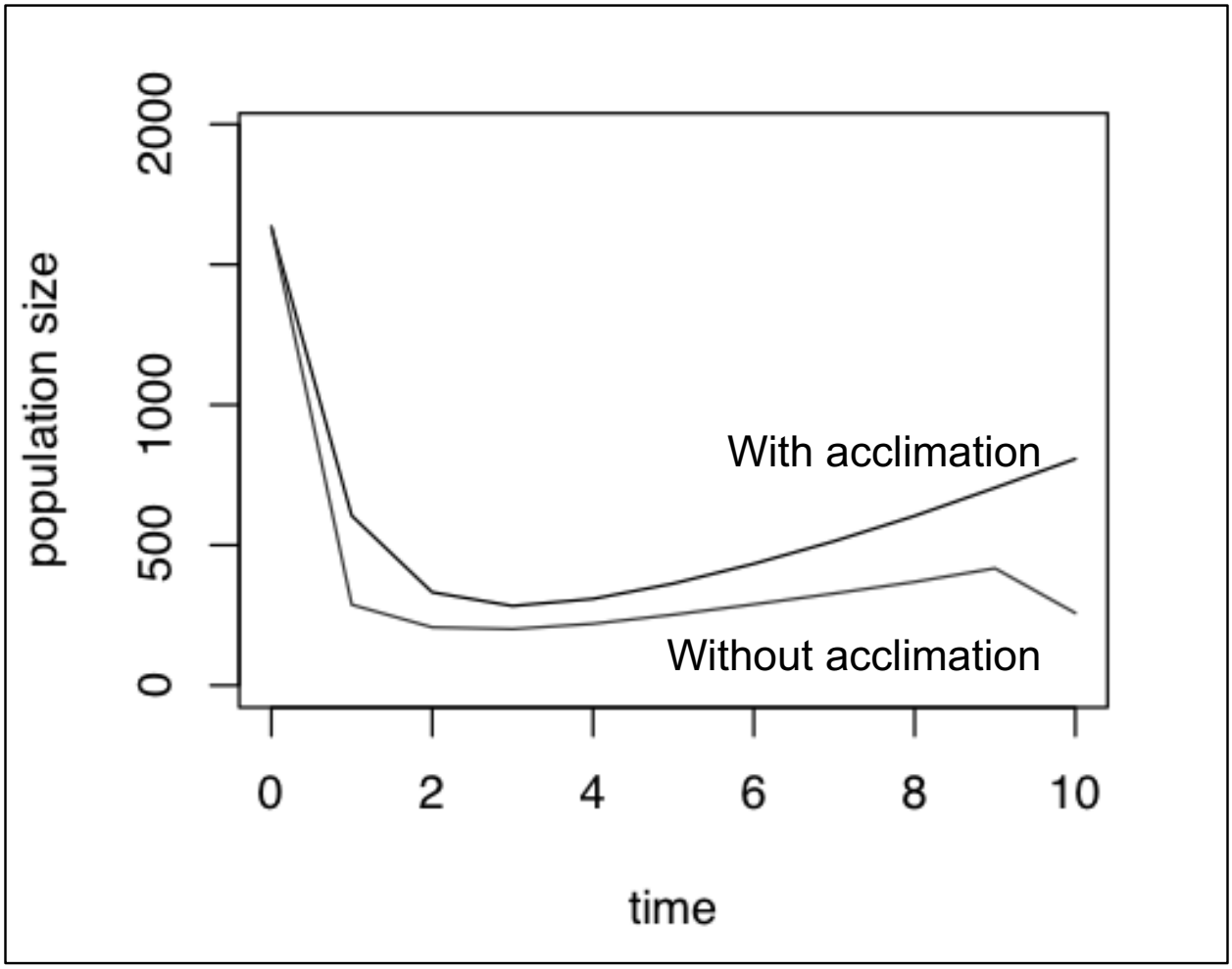

Figure 4.10: Difference between acclimation and no-acclimation modeling frameworks. The no-acclimation model performs worse than the model taking acclimation into account in terms of producing a lower population size over time.

without affecting the entire problem structure. That is, managers can shape the model to their specific situations without remaking the entire model.

The case study I have chosen at alpine meadow sites in Switzerland did not include a pre-existing management plan or a full study of *P. apollo* characteristics at the sites. As a result, I synthesized *P. apollo* across different sites in Europe to parameterize the model. I conducted sensitivity analysis on the model by solving the MILP under multiple scenarios (Table 4.2). By varying biological, environmental, and management parameters, I explored the range of conservation goals and population dynamics the model can produce.

The ability of individuals to acclimate (as measured here by κ) has a large effect on outcome of the model (Fig. 4.2). Although *P. apollo* may be able to acclimate in multiple ways, I focused on behavioral thermoregulation in larvae as they seek out shade or sun to achieve optimal body temperature. As expected, populations with higher acclimation ability result in a higher objective function value. Recall that I chose an objective function that sums the total number of "butterfly–years" over the planning horizon, the idea being that a manager may wish to maximize the total ecosystem service value of the population.

Acclimation and climate change interact to determine the conservation outcome. I used the rate of warming (°C/year) as a metric of climate change. As the severity of climate warming increases, the objective value goes down, regardless of acclimation ability. Thus, even managed species with a relatively high acclimation ability will see a considerable loss due to climate warming.

A key question for land managers is whether existing spatial conservation programs should change as species' ranges shift. In this model, I found that the answer is generally "yes," but that the specifics depend heavily on the population's dispersal ability.

For *P. apollo* populations with a high dispersal distance, the model recommends selecting sites that track the population upslope over time (Fig. 4.4). Since I constructed the model so that management and population dynamics are intertwined, it is difficult to say which direction the causality goes (i.e., whether the selected sites track the population, or whether they facilitate the population's elevation shift). It is notable that the mean population

elevation levels out after a certain period (around six years). This is possibly due to the scarcity of meadow sites further upslope compared to lower elevations (see Figure 4.1).

The low-dispersal case results in a very different management plan that includes maintaining selected sites for around five years before tracking the populations upslope (Fig. 4.5). Again, it is hard to tease out whether this is an effect of site availability upslope, or due to some other factor. The sudden shift in management strategy occurs at the upper, lower, and mean elevation levels in synchrony. Here, an advantage of using a MILP comes through: the model finds optimal strategies that may not be obvious or intuitive.

Most management plans occur on the timescale when transient dynamics may dominate, and this case study is no exception (Fig. 4.6). Depending on the model parameters, the total population size can either decrease before increase or vice versa. I also found that some management scenarios are more robust to the rate of climate change than others. In particular, populations that are on the border between long-term persistence and collapse are the most sensitive to the warming rate. The variation in population size over time underscores that measuring acclimation ability (when there is reason to expect it) should be a standard part of management planning.

Plotting the population size over time gives insight into whether the population may dip below a critical level that increases the risk of collapse. Since *P. apollo* population sizes are often small, there is the potential danger of inbreeding depression, for example [88]. If maintaining a certain size is the more salient management goal, the objective function (4.3) could be easily altered to meet the goal. Instead of a maximization problem, one could create a max-min objective function that maximizes the minimum total population size over time. For example,

$$\max : \qquad \min \sum_{i=1}^{N} M_{i,t} \qquad \forall t. \tag{4.24}$$

Objective (4.24) would be geared toward maintaining model population levels over time rather than producing the largest overall population size.

Since little to no economic information was available for the site of the case study, I performed sensitivity analysis on the total budget (Fig. 4.8). There is a maximum possible conservation value achievable, corresponding to the maximum budget, where all sites are selected at all times. As the budget approaches the maximum budget, there are diminishing returns on the objective function. As a result, it only takes a moderate percentage of the maximum budget to attain most of the possible conservation value.

Figure 4.8 shows that climate change comes with a financial cost. Specifically, suppose that, for a given budget and rate of warming, the model shows that a certain objective value can be achieved. If the rate of warming is actually higher, one could find the budget at which (given the higher warming rate) that same objective could be achieved. The increase in budget would be the cost of that increment of warming rate. As managers continue to assess how to incorporate climate change into models, it will be increasingly helpful to place a monetary value on environmental changes.

Finally, I examined how the potential valuation of ecosystem services could help determine the net profit or loss of management. Since the model calculates the objective value and total area of sites selected, one can constrain the relationship (4.23) between ecosystem value and management cost in a break-even scenario. The high ratio of value to cost found in this model (Fig. 4.9) indicates that a conservation project at the site of interest is not likely to be profitable, financially. However, that conclusion should not be taken as motivation against taking action, since the instrumental value of biodiversity itself is hard to quantify.

Perhaps the greatest drawback of the MILP I have described is that it has many "moving parts" and parameters, all of which have some level of uncertainty. Thus, my main goal has been to explore the parameter space to see which patterns are robust and which are sensitive. In future work, I plan to apply the model to a case study where site-specific biological, environmental, and budgetary data are available.

Chapter 5

CONCLUSIONS AND PROSPECTS

Climate change presents many challenges for future biodiversity, including the movement of species' suitable habitat. I have argued that spatial models offer powerful methods for dealing with habitat movement. In this work, I used integrodifference equations and an integer programming framework to model and manage species responding to moving habitats. The potential of these and similar models comes from their balance between theory and practice. That is, they can advance basic science and conservation applications at the same time. At their best, models fit into the scientific process by creating a feedback between theory, evidence, and application.

5.1 Conceptual advances

The models discussed in Chapters 2, 3, and 4 give some mechanistic understanding for the ecological processes associated with climate change. In Chapter 2, I analyzed a two-dimensional integrodifference equation (IDE) describing a population on a rectangular moving habitat (2.1). The model confirmed the destructive interactive effect between habitat movement and habitat fragmentation. When human or geographic features constrain a population's habitat from multiple directions, keeping pace with climate change becomes much more difficult. Furthermore, model (2.1) showed that a population's theoretical speed of invasion (given unlimited habitat) is not a reliable metric for climate risk. The critical speed of climate change that a species can tolerate approaches its invasion speed as the habitat size increases. However, limitations on habitat length or width greatly reduce the critical speed relative to the invasion speed.

Perhaps the more surprising result of model (2.1) is that the shape of the dispersal

kernel interacts with habitat shape in a very specific way to influence persistence. Previous work has shown that the tails of dispersal kernels influence spread and persistence, and in the case of moving-habitat model (2.1), kurtosis plays a large role. The kurtosis of the kernel—whether it has thin or fat tails—determines whether it is better for the population to have more habitat in the direction parallel or perpendicular to the direction of habitat movement. Quantifying the tails of dispersal kernels is notoriously difficult, but it plays an important role in understanding which species will persist during climate change.

In Chapter 3, in investigated a simple moving-habitat model (3.3), with a focus on short-term (transient) dynamics. I found a helpful conceptual link between model (3.3) and non-spatial, stage-structured models (3.1) that explains why transients occur in the moving-habitat model. Any dynamical system that includes two or more interacting states that can be approximated by a matrix recursion (3.9) can show transient dynamics. The equivalency between any such matrix-like models means that metrics for transients, such as attenuation and amplification, are easy to calculate by analogy.

I found that, since model (3.3) is linear, transient dynamics are the result of two "filters" on dynamics. The first filter is the operator K (3.7); its parameters determine whether transients *can* occur by dividing up phase space based on parameter values (see, e.g., Fig. 3.2). The second filter, initial conditions, determine whether transients *will* happen, as a function of the population's initial distribution over space (Fig. 3.8). Understanding these two filters separately makes it clearer when models should expect transients in moving-habitat models.

Another conceptual advantage of model (3.3) is that it provides an explanation for critical slowing-down, the phenomenon that systems exhibit long transients as they begin to destabilize. The length of the transient window (3.7), during which short- and long-term dynamics can mismatch, depends on the system's dominant eigenvalue. When the dominant eigenvalue is close to one, transients can, in theory, last arbitrarily long. Thus, model (3.3) affirms that critical slowing-down may be a general property of dynamical systems even with very different formulations.

5.2 Applicability

A good model should be applicable to the systems it describes. Ecological models, perhaps more than others in the sciences, must walk the line between realism and simplicity. The models I have discussed do a fairly good job at connecting to real populations without becoming overly complicated. I found data from multiple species to parameterize the moving-habitat models and the site selection model.

The literature on parameterizing integrodifference equations is fairly extensive, to the benefit of moving-habitat models (2.1) and (3.3). I used measured data on growth and dispersal to model two butterfly species, *Parnassius smintheus* and *Icaricia icarioides fenderi*, as well as four plant species (see Section 3.6). An important caveat for growth parameters is the absence of Allee effect, which holds true for the species I considered. Others have addressed how to deal with Allee effects in IDEs.

In some cases, fitting dispersal kernels for IDEs is difficult. Studies on the Rocky Mountain Apollo butterfly (*P. smintheus*) measured dispersal distances between meadow sites, whereas model (2.1) includes only one contained habitat. As such, results should be interpreted carefully.

Climate change introduces a new issue for fitting IDEs such as those above. The velocity of climate change measures how fast (and in what direction) a species' habitat is moving. The models I described give a good first approximation to habitat movement, but they do not capture nuances such as oscillating direction of movement and inter-annual differences in the speed.

The site selection model I discussed in Chapter 4 contains the most "moving parts" to parameterize. The biological components such as growth and dispersal are similar to those in the moving-habitat model, with the addition of acclimation. Although measurements of acclimation ability are becoming common, I only included one component of acclimation (behavioral thermoregulation). Many species, including the focal species *P. apollo*, can acclimate in other ways such as changes in phenology. Accounting for all types of acclimation

that could impact fitness is a data-intensive task that I did not attempt here.

I included very little economic consideration into fitting the site selection model. Estimating budgets and costs associated with conservation is very situation-specific. For example, land prices for acquiring sites may depend on local economic influences. The model I explored is easier to fit in cases where management includes a standardized action with a fixed cost for labor or materials.

Overall, these models rest midway between theory and data. They are not designed with a specific site or population in mind. To an extent, they cannot incorporate data as easily as statistical models such as species distribution models can. As a tradeoff, they arguably apply to a wider variety of situations and offer more explanatory power.

5.3 Hypothesis development

Falsifiability has long been a litmus test for models in science. But an issue comes up in climate change ecology: a hypothesis is not very useful if the only way to test it is to wait and see whether a population persists or collapses due to environmental change. The risk is too great. There are many ways around this issue, including laboratory experiments, common garden experiments, analysis of preexisting datasets, and paleontological reconstruction.

The models I have discussed generate testable hypotheses, many of which lend themselves to using preexisting data or laboratory experiments. For example, the two-dimensional MHM asserts that the "best" habitat shape for a population, given a constraint on area, depends on the species' dispersal kernel. One might test the hypothesis using insect populations in a controlled setting with an induced temperature gradient that moves as cycles of reproduction and dispersal proceed. By controlling the amount of hospitable area in front and to the sides of the population, one can alter the habitat shape. Higher dispersal kernel moments such as kurtosis are difficult to control, but proxies for kurtosis such as individual variation in dispersal might be helpful.

A similar moving-habitat lab setting could test for transient dynamics. Model (3.3) shows that there is an optimal initial population distribution that maximizes the first-step

growth rate. By manipulating the initial location of individuals and varying the rate of habitat movement, an experimenter could test whether the dynamics move through the regions in Figure 3.2, for example.

The site selection model is more difficult to validate other than by implementing it on an actual set of sites. At the very least, the results highlight that testing whether a population can acclimate (using any variety of laboratory techniques) should be a key step in the management process.

It is my hope that these studies inspire work along the entire gradient from theory, to computation, to implementation. In my estimation, there is only one way to counter the negative synergies involved in climate change: to rely on the positive synergy that comes from communication between theoretical and applied ecologists.

Appendix A

CHAPTER 2 APPENDIX

A.1 Nyström's method

A.1.1 Constructing matrix **A**

To discretize integral eigenvalue problem (2.7) using Nyström's method, first define grid points

$$x_i = -L/2 + i \cdot \Delta x, \qquad i = 0, 1, \ldots, n, \tag{A.1}$$

$$y_j = -W/2 + j \cdot \Delta y, \qquad j = 0, 1, \ldots, m, \tag{A.2}$$

where $\Delta x = L/n$ and $\Delta y = W/m$. Create identical grid points x'_k and y'_ℓ so that $\Delta x' = \Delta x$ and $\Delta y' = \Delta y$. Next, evaluate both sides of eigenvalue problem (2.7) only at grid points and approximate each integral on the right-hand side with a sum using, for example, the repeated trapezoidal rule. Because there are four sets of grid points, the resulting problem is, in a sense, four-dimensional. Additional indices are necessary to condense the system into a matrix eigenvalue problem with two dimensions. Define the indices

$$p(i, j) = i + 1 + (n + 1)j, \qquad q(k, \ell) = k + 1 + (n + 1)\ell. \tag{A.3}$$

The mapping from (i, j) pairs to p-values effectively reshapes a two-dimensional array into a one-dimensional vector (and similarly for the mapping from (k, ℓ) pairs to q-values), making the problem two-dimensional. Integral equation (2.7) becomes

$$\lambda u_p = R_0 \sum_{q=1}^{(n+1)(m+1)} A_{p,q} u_q, \tag{A.4}$$

where u_p is the p-th element of the reshaped vector u, and the element in row p, column q of matrix $\mathbf{A}$ is

$$A_{p,q} = \alpha_1 \, \alpha_2 \, k(x_i + c - x'_k, \, y_j - y'_\ell) \, \Delta y_1 \Delta y_2, \tag{A.5}$$

where

$$\alpha_1 = \begin{cases} \frac{1}{2} & \text{if} \quad k = 0 \text{ or } n, \\ \\ 1 & \text{otherwise;} \end{cases} \qquad \alpha_2 = \begin{cases} \frac{1}{2} & \text{if} \quad \ell = 0 \text{ or } m, \\ \\ 1 & \text{otherwise.} \end{cases} \tag{A.6}$$

System (A.4) is now a standard matrix eigenvalue problem.

A.1.2 Avoiding dispersal kernel singularities

If the dispersal kernel is singular at the origin, one way to avoid evaluating the singularity is to shift y' grid points onto the midpoints of y grid points,

$$y'_\ell = -W/2 + \Delta y/2 + \ell \cdot \Delta y', \qquad \ell = 0, 1, \ldots, m-1. \tag{A.7}$$

The action of the integral operator $\mathcal{K}$ in eigenvalue problem (2.7) is now the composition of two operators, $\mathcal{K}_1$ and $\mathcal{K}_2$. The first calculates values at (x, y) grid points, stored in some vector u. The second calculates values at (x', y') grid points stored in another vector, v. Applying Nyström's method to $\mathcal{K}_1$ and $\mathcal{K}_2$ as above yields a pair of matrices, $\mathbf{A}_1$ and $\mathbf{A}_2$, satisfying

$$u_{t+1} = \mathbf{A}_1\, v_t, \qquad v_{t+1} = \mathbf{A}_2\, u_t. \tag{A.8}$$

Since $u_{t+2} = \mathbf{A}_1\mathbf{A}_2\, u_t$, the critical speed occurs when $\rho(\mathbf{A}_1\mathbf{A}_2) = 1$.

A.2 Legendre expansion

A.2.1 Constructing matrix $\mathbf{B}$

To construct matrix $\mathbf{B}$ in eigenvalue problem (2.15), first recover the Legendre expansion coefficients $b_{ijk\ell}$. Multiplying both sides of kernel expansion (2.14) by Legendre polynomials in each variable, integrating over the domain, and using orthogonality properties (2.11)–(2.12) gives

$$b_{ijk\ell} = \left[\frac{(2i+1)(2j+1)(2k+1)(2\ell+1)}{L^2W^2}\right] \times$$

$$\int_{-L/2}^{L/2}\int_{-L/2}^{L/2}\int_{-W/2}^{W/2}\int_{-W/2}^{W/2} k(x+c-x', y-y')X_i(x)X_j(x')Y_k(y)Y_\ell(y')\,dy'\,dy\,dx'\,dx. \tag{A.9}$$

To obtain a matrix eigenvalue problem, substitute kernel expansion (2.14) into integral eigenvalue problem (2.15).

$$\lambda u(x,y) = R_0 \int_{-L/2}^{L/2} \int_{-W/2}^{W/2} \sum_{i,j,k,\ell=0}^{N} b_{ijk\ell}\, X_i(x) X_j(x') Y_k(y) Y_\ell(y')\, u(x',y')\; dy'\; dx' \tag{A.10}$$

$$= R_0 \sum_{i,j,k,\ell=0}^{N} b_{ijk\ell}\, X_i(x) Y_k(y) \left(\int_{-L/2}^{L/2} \int_{-W/2}^{W/2} X_j(x') Y_\ell(y')\; u(x',y')\, dy'\, dx' \right) \tag{A.11}$$

$$= R_0 \sum_{i,j,k,\ell=0}^{N} b_{ijk\ell}\, X_i(x) Y_k(y)\, u_{j\ell}, \tag{A.12}$$

where

$$u_{j\ell} \equiv \int_{-L/2}^{L/2} \int_{-W/2}^{W/2} X_j(x') Y_\ell(y')\; u(x',y')\, dy'\, dx'. \tag{A.13}$$

Multiplying both sides of equation (A.12) by Legendre polynomials $X_r(x)Y_s(y)$ and integrating,

$$\lambda \int_{-L/2}^{L/2} \int_{-W/2}^{W/2} u(x,y) X_r(x) Y_s(y)\, dx\, dy$$

$$= R_0 \sum_{i,j,k,\ell=0}^{N} b_{ijk\ell}\; u_{j\ell} \int_{-L/2}^{L/2} \int_{-W/2}^{W/2} X_i(x) X_r(x) Y_k(y) Y_s(y)\, dy\, dx.$$

Using definition (A.13) and orthogonality,

$$\lambda u_{ik} = R_0 LW \sum_{j=0}^{N} \sum_{\ell=0}^{N} \frac{b_{ijk\ell}\; u_{ik}}{(2i+1)(2k+1)}. \tag{A.14}$$

I have reverted to indices (i,k) rather than (r,s).

System (A.14) has four sets of indices and is, in a sense, four dimensional. Additional indices are needed to condense the system into a matrix eigenvalue problem with two dimensions. Let

$$p(i,k) = i + 1 + (N+1)k, \qquad q(j,\ell) = j + 1 + (N+1)\ell, \tag{A.15}$$

where $i, j, k, \ell \in \{0, 1, \ldots, N\}$. The mapping from (i,k) pairs to p-values effectively reshapes a two-dimensional array into a one-dimensional vector (and similarly for the mapping from (j,ℓ) pairs to q-values), making the problem two-dimensional. System (A.14) becomes

$$\lambda u_p = R_0 LW \sum_{q=1}^{(N+1)^2} B_{p,q} u_q, \tag{A.16}$$

where u_p is the p-th entry of the reshaped vector u. The element in row p, column q of matrix $\mathbf{B}$ is

$$B_{p,q} = \frac{b_{ijk\ell}}{(2i+1)(2k+1)}. \tag{A.17}$$

A.2.2 Taylor expansion method coefficients

The coefficients in approximation (2.20) found by expanding the kernel in a Taylor series are

$$\alpha \equiv \int_{-L/2}^{L/2} \int_{-W/2}^{W/2} k(x,y)\, dy\, dx, \tag{A.18}$$

$$\beta \equiv \int_{-W/2}^{W/2} [k(L/2,y) - k(-L/2,y)]\, dy, \tag{A.19}$$

$$\gamma \equiv \int_{-W/2}^{W/2} \left[\frac{\partial k}{\partial x}(L/2,y) - \frac{\partial k}{\partial x}(-L/2,y)\right] dy, \tag{A.20}$$

$$\delta \equiv \int_{-L/2}^{L/2} \left[\frac{\partial k}{\partial y}(x,W/2) - \frac{\partial k}{\partial y}(x,-W/2)\right] dx. \tag{A.21}$$

A.3 Optimal aspect ratio for the symmetrized Gaussian kernel

Conjectures 1a and 1b are unproven, but one can show a special case of Conjecture 1b, that $\theta_{\text{opt}} = 1$ for Gaussian dispersal kernels. Begin by approximating the spectral radius $\rho(\theta)$ using geometric symmetrization and the eigenfunction-one Rayleigh quotient (2.22). Symmetrization does not give an exact value for $\rho(\theta)$, but it does give a tight lower bound and is analytically tractable. It may not be surprising that, should a maximal $\rho(\theta)$ exist for a symmetrical kernel, it might occur at $\theta = 1$, when $L = W$. What is less obvious (and what I will prove) is that a maximum does exist, and that it is unique.

Given a Gaussian kernel,

$$k(x + c - x', y - y') = \frac{1}{2\pi\sigma^2} \exp\left[\frac{-(x + c - x')^2}{2\sigma^2}\right] \exp\left[\frac{-(y - y')^2}{2\sigma^2}\right], \tag{A.22}$$

the symmetrized kernel, using formula (2.21), is

$$k_G(x+c-x', y-y') = \frac{1}{2\pi\sigma^2}\exp\left[\frac{-c^2}{2\sigma^2}\right]\exp\left[\frac{-(x-x')^2}{2\sigma^2}\right]\exp\left[\frac{-(y-y')^2}{2\sigma^2}\right]. \quad \text{(A.23)}$$

The Rayleigh quotient approximation for the spectral radius with constant eigenfunction, as a function of L and W, is

$$\rho(L,W) = \frac{\int_{-L/2}^{L/2}\int_{-L/2}^{L/2}\int_{-W/2}^{W/2}\int_{-W/2}^{W/2} k_G(x+c-x', y-y')\,dy'\,dy\,dx'\,dx}{LW}. \quad \text{(A.24)}$$

The numerator of approximation (A.24) is separable, so that the spectral radius can be written as

$$\rho(L,W) = CI(L)I(W), \quad \text{(A.25)}$$

where

$$C = \frac{1}{2\pi\sigma^2}\exp\left(\frac{-c^2}{2\sigma^2}\right), \quad \text{(A.26)}$$

and

$$I(L) = \sqrt{2\pi}\sigma\,\mathrm{erf}\left(\frac{L}{\sqrt{2}\sigma}\right) - \frac{2\sigma^2}{L} + \frac{2\sigma^2}{L}\exp\left(\frac{-L^2}{2\sigma^2}\right). \quad \text{(A.27)}$$

$I(W)$ is identical to $I(L)$ with W replacing L. (I have not absorbed the constant C into $I(L)$ and $I(W)$ to make future calculations easier.)

This is now a constrained optimization problem: to maximize $\rho(L,W)$ subject to the constraint $LW = A$. Before using the method of Lagrange multipliers, I need to describe a few properties of the function $I(L)$ necessary for the proof. Then, I construct a Lagrangian

function and find the unique critical point of the associated system. Finally, using the associated bordered Hessian matrix shows that the critical point gives a maximum.

The first two derivatives of $I(L)$ are

$$I'(L) = \frac{2\sigma^2 - 2\sigma^2 \exp\left(\frac{-L^2}{2\sigma^2}\right)}{L^2} > 0 \quad \text{for} \quad L > 0, \tag{A.28}$$

and

$$I''(L) = \frac{2L^2 \exp\left(\frac{-L^2}{2\sigma^2}\right) - 4\sigma^2 + 4\sigma^2 \exp\left(\frac{-L^2}{2\sigma^2}\right)}{L^3} \tag{A.29}$$

$$= \frac{2\exp\left(\frac{-L^2}{2\sigma^2}\right) - 2I'(L)}{L}. \tag{A.30}$$

The above derivatives help prove the following useful lemma.

Lemma 1:

$$I'(L) < \frac{I(L)}{L} < 1, \qquad \text{for} \quad L > 0. \tag{A.31}$$

Proof:

It is sufficient to show that $I(L)$ is concave down and that $\lim_{L\to 0^+} I'(L) = 1$. That is, if $I'(L)$ is decreasing and bound from above by one, $I(L)$ must satisfy the lemma.

First, I show that $I''(L)$ is negative. From expression (A.29),

$$I''(L) = \frac{1}{L^3} \exp\left(\frac{-L^2}{2\sigma^2}\right) \left[2L^2 - 4\sigma^2 \exp\left(\frac{L^2}{2\sigma^2}\right) + 4\sigma^2\right]. \tag{A.32}$$

Since $\exp(L) > L + 1$ when $L \neq 0$,

$$I''(L) < \frac{1}{L^3} \exp\left(\frac{-L^2}{2\sigma^2}\right) \left[2L^2 - 4\sigma^2 \left(\frac{L^2}{2\sigma^2} + 1\right) + 4\sigma^2\right] \tag{A.33}$$

$$= 0. \tag{A.34}$$

Then, using L'Hôpital's rule twice on expression (A.28), the desired limit quickly follows. ■

With the above lemma available, I now construct the Lagrangian function with objective function $\rho(L, W)$ and constraint $g(L, W) = LW - A = 0$.

$$\Lambda(L, W, \lambda) = \rho(L, W) - \lambda g(L, W). \tag{A.35}$$

The necessary first-order conditions for critical points are

$$\Lambda_L = CI'(L)I(W) - \lambda W \qquad = 0, \tag{A.36}$$

$$\Lambda_W = CI(L)I'(W) - \lambda L \qquad = 0, \tag{A.37}$$

$$\Lambda_\lambda = LW - A \qquad = 0. \tag{A.38}$$

Here, subscripts indicate partial differentiation. From (A.36) and (A.37),

$$\lambda = \frac{CI'(L)I(L)}{W} = \frac{CI(L)I'(W)}{L}. \tag{A.39}$$

Rearranging the last equation,

$$\frac{I'(L)L}{I(L)} = \frac{I'(W)W}{I(W)}. \tag{A.40}$$

If the function

$$J(L) \equiv \frac{I'(L)L}{I(L)} \tag{A.41}$$

is one-to-one for $L > 0$, then equation (A.40) implies $L = W$, and with the constraint $LW = A$, the only critical point is $(L, W) = (\sqrt{A}, \sqrt{A})$. It is sufficient to show $J(L)$ is one-to-one by showing it is monotone decreasing.

From expressions (A.28) and (A.29) for $I'(L)$ and $I''(L)$,

$$J'(L) = \frac{1}{L}\left[II'' + \frac{II'}{L} - (I')^2\right]. \tag{A.42}$$

(I assume differentiation is with respect to L on the right-hand side.) Substituting expression (A.30) for I'',

$$J'(L) = \frac{1}{L}\left[I\left(\frac{2}{L}\exp\left(\frac{-L^2}{2\sigma^2}\right) - \frac{2}{L}I'\right) + \frac{II'}{L} - (I')^2\right] \tag{A.43}$$

$$= \frac{1}{L}\left[\frac{2I}{L}\exp\left(\frac{-L^2}{2\sigma^2}\right) - \frac{II'}{L} - (I')^2\right]. \tag{A.44}$$

The first and second inequalities in Lemma 1 now give, one after the other,

$$J'(L) < \frac{1}{L}\left[2\exp\left(\frac{-L^2}{2\sigma^2}\right) - \frac{II'}{L} - (I')^2\right] \tag{A.45}$$

$$< \frac{1}{L}\left[2\exp\left(\frac{-L^2}{2\sigma^2}\right) - 2(I')^2\right] \tag{A.46}$$

$$= \frac{2}{L}\left[\exp\left(\frac{-L^2}{4\sigma^2}\right) + I'\right]\left[\exp\left(\frac{-L^2}{4\sigma^2}\right) - I'\right] \tag{A.47}$$

$$= \frac{2}{L^3}\left[\exp\left(\frac{-L^2}{4\sigma^2}\right) + I'\right]\left[L^2\exp\left(\frac{-L^2}{4\sigma^2}\right) + 2\sigma^2\exp\left(\frac{-L^2}{4\sigma^2}\right) - 2\sigma^2\right]. \tag{A.48}$$

Since $I'(L) > 0$, it is enough to show that

$$M(L) \equiv L^2\exp\left(\frac{-L^2}{4\sigma^2}\right) + 2\sigma^2\exp\left(\frac{-L^2}{4\sigma^2}\right) - 2\sigma^2 < 0 \tag{A.49}$$

when $L > 0$ to prove $J(L)$ is monotone decreasing. Note that $M(0) = 0$, and

$$M'(L) = -\frac{L^3}{2\sigma^2}\exp\left(\frac{-L^2}{4\sigma^2}\right) + 2L\exp\left(\frac{-L^2}{4\sigma^2}\right) - 2L\exp\left(\frac{-L^2}{2\sigma^2}\right) \tag{A.50}$$

$$= L\exp\left(\frac{-L^2}{4\sigma^2}\right)\left[-\frac{L^2}{2\sigma^2} + 2 - 2\exp\left(\frac{-L^2}{4\sigma^2}\right)\right] \tag{A.51}$$

$$< L\exp\left(\frac{-L^2}{4\sigma^2}\right)\left[-\frac{L^2}{2\sigma^2} + 2 - 2\left(-\frac{L^2}{4\sigma^2} + 1\right)\right] = 0. \tag{A.52}$$

Thus, $M(L) < 0$, which makes $J(L)$ monotone decreasing and one-to-one, which makes $L = W$ the only solution of equation (A.40). Together with the area constraint, the unique critical point is $(L, W) = (\sqrt{A}, \sqrt{A})$.

To show that the critical point maximizes the spectral radius, I will use the bordered Hessian matrix

$$H = \begin{pmatrix} 0 & -g_L & -g_W \\ -g_L & \Lambda_{LL} & \Lambda_{LW} \\ -g_W & \Lambda_{WL} & \Lambda_{WW} \end{pmatrix} \tag{A.53}$$

$$= \begin{pmatrix} 0 & -W & -L \\ -W & CI''(L)I(W) & CI'(L)I'(W) - \lambda \\ -L & CI'(L)I'(W) - \lambda & CI(L)I''(W) \end{pmatrix}. \tag{A.54}$$

(Recall that C is a constant.) For 3×3 matrix H, a sufficient condition for the critical point to be a maximum is $|H| > 0$, where the matrix is evaluated at the critical point [146]. $|\cdot|$ denotes the determinant.

$$|H| = -CW^2 I(L)I''(W) - CL^2 I''(L)I(W) + 2CLWI'(L)I'(W) - 2C\lambda LW. \tag{A.55}$$

At the critical point, $L = W$, so I will use L to represent both quantities.

$$|H| = -2CL^2 I''(L)I(L) + 2CL^2[I'(L)]^2 - 2CL^2\lambda \tag{A.56}$$

$$= 2CL^2 \left(-I''(L)I(L) + [I'(L)]^2 - \frac{I'(L)I(L)}{L} \right). \tag{A.57}$$

However, steps (A.42)–(A.52) already showed that

$$I''(L)I(L) - [I'(L)]^2 + \frac{I'(L)I(L)}{L} < 0 \tag{A.58}$$

when $L > 0$. The opposite quantity must be positive. Therefore, from expression (A.57), $|H| > 0$ and the unique critical point $(L, W) = (\sqrt{A}, \sqrt{A})$ maximizes the spectral radius. $\theta_{\text{opt}} = 1$ for the symmetrized Gaussian kernel.

A.4 Effect of switching length and width for the symmetrized generalized Gaussian kernel

One way to illustrate Conjecture 1 is to plot the level curves of shifted kernels with different kurtosis values. If the level curves are stretched along the x-axis (the dimension of habitat length), a habitat with larger length than width is better because it captures more of the kernel's probability mass (and, thus, more propagules). If level curves are stretched along the y-axis (the dimension of width), a habitat with larger width is preferable. I use the geometric symmetrization approximation (2.21) on the generalized Gaussian kernel (2.26) and show kurtosis determines the direction the level curves are stretched. The result provides evidence that, for the broad class of generalized Gaussian kernels, Conjecture 1 is true.

To simplify our approach, I will consider the square of the geometrically symmetrized kernel,

$$k_G^2(x + c - x', y - y') = k(x + c - x', y - y')\, k(x' + c - x, y - y'). \tag{A.59}$$

Evaluating (A.59) for the generalized Gaussian kernel (2.26) gives a distribution of the form

$$k_G^2(x + c - x', y - y') = \gamma \exp\left\{-\frac{1}{2}\left[(x + c - x')^2 + (y - y')^2\right]^\beta\right\} \exp\left\{-\frac{1}{2}\left[(x' + c - x)^2 + (y' - y)^2\right]^\beta\right\}, \tag{A.60}$$

where γ is a normalizing constant. Since x' and y' simply shift the kernel, I evaluate approximation (A.60) at $(x', y') = 0$ without loss of generality.

$$k_G^2(x+c, y) = \gamma \exp\left\{-\frac{1}{2}\left[(x+c)^2 + y^2\right]^\beta\right\} \exp\left\{-\frac{1}{2}\left[(x-c)^2 + y^2\right]^\beta\right\}. \tag{A.61}$$

As the speed of climate change c increases from zero, the level curves of kernel (A.61) stretch along one axis or the other when $\beta \neq 1$ (Fig. 6). To measure the effect of the stretch, slice kernel (A.61) along each axis and compare the corresponding functions.

$$f_1(x) \equiv k_G^2(x+c, 0) = \gamma \exp\left\{-\frac{1}{2}\left[(x+c)^2\right]^\beta - \frac{1}{2}\left[(x-c)^2\right]^\beta\right\}, \tag{A.62}$$

$$f_2(y) \equiv k_G^2(0+c, y) = \gamma \exp\left[-(c^2 + y^2)^\beta\right]. \tag{A.63}$$

Functions (A.62) and (A.63) are the cross sections of kernel (A.61) along the x- and y-axis, respectively. To compare the functions, set f_2 as a function of x, for example.

$$f_2(x) \equiv \gamma \exp\left[-(c^2 + x^2)^\beta\right]. \tag{A.64}$$

I now look for the conditions under which, for example, $f_1(x) > f_2(x)$, leading to a stretch along the x-axis.

$$\gamma \exp\left\{-\frac{1}{2}\left[(x+c)^2\right]^\beta - \frac{1}{2}\left[(x-c)^2\right]^\beta\right\} > \gamma \exp\left[-(c^2 + x^2)^\beta\right], \tag{A.65}$$

or

$$-\frac{1}{2}[(x+c)^2]^\beta - \frac{1}{2}[(x-c)^2]^\beta > -(c^2 + x^2)^\beta. \tag{A.66}$$

Switching sides,

$$(c^2 + x^2)^\beta \; > \; \frac{1}{2}[(x+c)^2]^\beta + \frac{1}{2}[(x-c)^2]^\beta. \tag{A.67}$$

The observation that

$$c^2 + x^2 = \frac{1}{2}(x+c)^2 + \frac{1}{2}(x-c)^2 \tag{A.68}$$

suggests using a convexity argument with the function $g(z) \equiv z^\beta$. In particular, Jensen's inequality states that if (and only if) $g(z)$ is concave down, then for any two values z_1 and z_2,

$$g\left(\frac{1}{2}z_1 + \frac{1}{2}z_2\right) > \frac{1}{2}g(z_1) + \frac{1}{2}g(z_2). \tag{A.69}$$

$g(z)$ is concave down only when $\beta < 1$. Setting

$$z_1 = (x+c)^2, \qquad\qquad z_2 = (x-c)^2, \tag{A.70}$$

inequality (A.67) is only true when $\beta < 1$. The same argument applies for $\beta > 1$, resulting in $f_1(x) < f_2(x)$. In general,

$$f_1(x) \begin{cases} > \; f_2(x) & \text{if} \quad \beta < 1, \\ = \; f_2(x) & \text{if} \quad \beta = 1, \\ < \; f_2(x) & \text{if} \quad \beta > 1. \end{cases} \tag{A.71}$$

The parameter β controls the kurtosis of the generalized Gaussian distribution. $\beta = 1$ gives a standard Gaussian. Increasing c has no effect on the Gaussian (Fig. A.1c–d), so there is no preference for habitat length or width. $\beta > 1$ gives platykurtic kernels, for which increasing c stretches the kernel along the y-axis (Fig. A.1a–b), favoring larger width. Finally, $\beta < 1$ gives leptokurtic kernels, for which increasing c stretches the kernel along the x-axis (Fig. A.1e–f), favoring larger length.

The use of convexity (A.69) above suggests a possible way to prove Conjecture 1. Recent definitions of kurtosis have centered around partial orderings of distributions that preserve certain ordering properties. One such ordering involves convexity [239]. If it can be shown that the partial ordering of two shifted kernels corresponds to an ordering of the importance of length and width (e.g., kernels with higher kurtosis favor habitat length over width), Conjecture 1 is proven. We will not attempt such a proof here, but convexity ordering provides a promising approach to our conjecture.

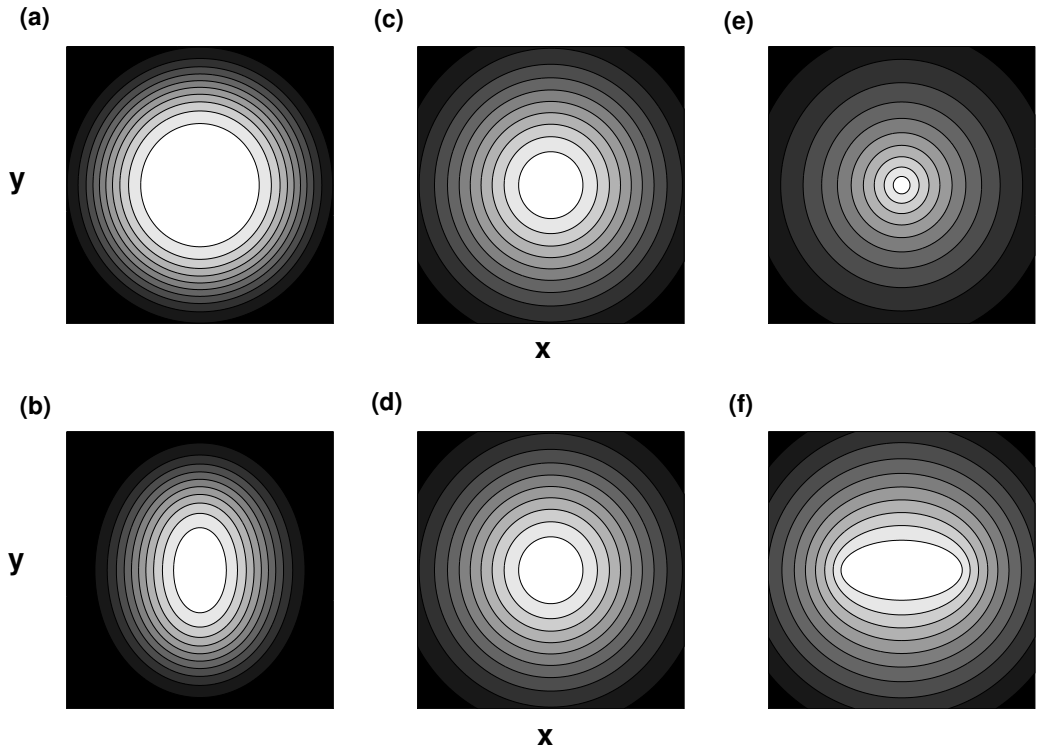

Figure A.1: Plots **(a)**, **(c)**, and **(e)** used $c = 0$. In plots **(b)**, **(d)**, and **(f)**, I increased c to 1 km/yr. I used $\beta = 2$ to obtain a platykurtic kernel for **(a)-(b)**, $\beta = 1$ to obtain a mesokurtic kernel for **(c)-(d)**, and $\beta = 1/2$ to obtain a leptokurtic kernel for **(e)-(f)**. The orientation of the level curves determines whether it is better to have a larger habitat length (for leptokurtic kernels) or larger width (for platykurtic kernels). For the Gaussian kernel, length and width have the same effect on persistence.

Appendix B

CHAPTER 3 APPENDIX

B.1 Linear approximations for envelopes

It is no coincidence that the amplification and attenuation envelopes in Fig. 7 look nearly linear with slope $\ln \lambda_1$. One explanation involves a set of approximations for the dominant eigenvalue of a matrix [251] [see also 129]. I begin with the amplification envelope. Consider the matrix approximation (3.8) for system (3.3). Denote $\mathrm{CS}_i(\mathbf{K})$ as the sum of the ith column of matrix $\mathbf{K}$, and $\mathrm{CS}_i(\mathbf{K}^t)$ as the sum of the ith column of matrix $\mathbf{K}^t$. [251] showed that, for any nonnegative matrix $\mathbf{K}$ with nonzero column sums,

$$\lambda_1(\mathbf{K}) \leq \max_i \left[\frac{\mathrm{CS}_i(\mathbf{K}^t)}{\mathrm{CS}_i(\mathbf{K}^{t-1})} \right] \leq \max_i \left[\frac{\mathrm{CS}_i(\mathbf{K}^{t-1})}{\mathrm{CS}_i(\mathbf{K}^{t-2})} \right] \leq \cdots \leq \max_i \left[\frac{\mathrm{CS}_i(\mathbf{K}^2)}{\mathrm{CS}_i(\mathbf{K})} \right]. \tag{B.1}$$

As t increases, the corresponding term in (B.1) is a tighter and tighter upper bound on the dominant eigenvalue λ_1.

The amplification envelope for matrix $\mathbf{K}$ is

$$\bar{\rho}_t = \max_i \mathrm{CS}_i(\mathbf{K}^t). \tag{B.2}$$

Rewriting definition (B.2) using a telescoping product,

$$\bar{\rho}_t = \max_i \left[\frac{\mathrm{CS}_i(\mathbf{K}^t)}{\mathrm{CS}_i(\mathbf{K}^{t-1})} \, \frac{\mathrm{CS}_i(\mathbf{K}^{t-1})}{\mathrm{CS}_i(\mathbf{K}^{t-2})} \, \cdots \, \frac{\mathrm{CS}_i(\mathbf{K}^2)}{\mathrm{CS}_i(\mathbf{K})} \, \mathrm{CS}_i(\mathbf{K}) \right]. \tag{B.3}$$

Distributing the maximum gives the inequality

$$\bar{\rho}_t \leq \max_i \left[\frac{\mathrm{CS}_i(\mathbf{K}^t)}{\mathrm{CS}_i(\mathbf{K}^{t-1})}\right] \cdot \max_i \left[\frac{\mathrm{CS}_i(\mathbf{K}^{t-1})}{\mathrm{CS}_i(\mathbf{K}^{t-2})}\right] \cdots \max_i \left[\frac{\mathrm{CS}_i(\mathbf{K}^2)}{\mathrm{CS}_i(\mathbf{K})}\right] \cdot ||\mathbf{K}||. \tag{B.4}$$

That is, an upper bound for the amplification envelope is the product of the successive approximations for the dominant eigenvalue. Similarly, for the attenuation envelope, a lower bound is

$$\underline{\rho}_t \geq \min_i \left[\frac{\mathrm{CS}_i(\mathbf{K}^t)}{\mathrm{CS}_i(\mathbf{K}^{t-1})}\right] \cdot \min_i \left[\frac{\mathrm{CS}_i(\mathbf{K}^{t-1})}{\mathrm{CS}_i(\mathbf{K}^{t-2})}\right] \cdots \min_i \left[\frac{\mathrm{CS}_i(\mathbf{K}^2)}{\mathrm{CS}_i(\mathbf{K})}\right] \cdot \mathrm{minCS}(\mathbf{K}). \tag{B.5}$$

In many cases, bounds (B.4) and (B.5) are very tight (data not shown). To account for the nearly linear form of the envelopes, note that, as t increases, the sequence of terms in inequality (B.1) gets closer to $\lambda_1(\mathbf{K})$. If the terms converge quickly, then the product of maximums in inequality (B.4) is approximately the product of multiple λ_1 values, so that

$$\bar{\rho}_t \approx [\lambda_1(\mathbf{K})]^{t-1} \cdot ||\mathbf{K}||_1. \tag{B.6}$$

Taking the logarithm of both sides gives the approximately linear form,

$$\ln \bar{\rho}_t \approx (t-1) \ln[\lambda_1(\mathbf{K})] + \ln ||\mathbf{K}||_1. \tag{B.7}$$

Similarly, for the attenuation envelope,

$$\ln \underline{\rho}_t \approx (t-1) \ln[\lambda_1(\mathbf{K})] + \ln[\mathrm{minCS}(\mathbf{K})]. \tag{B.8}$$

BIBLIOGRAPHY

[1] M. Abramowitz and I.A. Stegun. *Handbook of Mathematical Functions*. Dover, New York, 1970.

[2] P. Adamski and Z. Witkowski. Male patrolling modes in apollo butterfly parnassius apollo (l.): simulation of optimal choice (lepidoptera: Papilionidae). *Nature Conservation*, 62:27–36, 1999.

[3] P. Adamski and Z.J. Witkowski. Effectiveness of population recovery projects based on captive breeding. *Biological Conservation*, 140(1):1–7, 2007.

[4] S.N. Aitken, S. Yeaman, J.A .Holliday, T. Wang, and S. Curtis-McLane. Adaptation, migration or extirpation: climate change outcomes for tree populations. *Evolutionary Applications*, 1:95–111, 2008.

[5] WC Allee. *The Social Life of Animals*. Norton, New York, 1938.

[6] J.K. Alpin, Y.A .and Merikoski. A simple proof for the inequality between the perron root of a nonnegative matrix and that of its geometric symmetrization. *Lobachevskii Journal of Mathematics*, 31(3):222–223, 2010.

[7] A.W. Ando and M.L. Mallory. Optimal portfolio design to reduce climate-related conservation uncertainty in the Prairie Pothole Region. *Proceedings of the National Academy of Sciences*, 109:6484–6489, 2012.

[8] M.J. Angilletta. *Thermal Adaptation: A Theoretical and Empirical Synthesis*. Oxford University Press, 2009.

[9] M.B. Araújo, M. Cabeza, W. Thuiller, L. Hannah, and P.H. Williams. Would climate change drive species out of reserves? an assessment of existing reserve-selection methods. *Global Change Biology*, 10(9):1618–1626, 2004.

[10] M.B. Araújo and M. Luoto. The importance of biotic interactions for modelling species distributions under climate change. *Global Ecology and Biogeography*, 16:743–753, 2007.

[11] M.V. Ashley, M.F. Willson, O.R.W. Pergams, D.J. O'Dowd, S.M. Gende, and J.S. Brown. Evolutionarily enlightened management. *Biological Conservation*, 111:115–123, 2003.

[12] S. Ashton, D. Gutierrez, and R.J. Wilson. Effects of temperature and elevation on habitat use by a rare mountain butterfly: implications for species responses to climate change. *Ecological Entomology*, 34:437–446, 2009.

[13] M. Austin. Species distribution models and ecological theory: A critical assessment and some possible new approaches. *Ecological Modelling*, 200:1–19, 2007.

[14] N. Balakrishnan and C.-D. Lai. *Continuous bivariate distributions*. Springer, New York, 2009.

[15] I.R. Ball, H.P. Possingham, and M. Watts. Marxan and relatives: software for spatial conservation prioritisation. In *Spatial Conservation Prioritisation: Quantitative Methods and Computational Tools*, pages 185–195. Oxford University Press, Oxford, 2009.

[16] A. Baz. Nectar plant sources for the threatened Apollo butterfly (Parnassius apollo L. 1758) in populations of central Spain. *Biological Conservation*, 103:277–282, 2002.

[17] H. Berestycki, L. Desvillettes, and O. Diekmann. Can climate change lead to gap formation? *Ecological Complexity*, 20:264–270, 2014.

[18] H. Berestycki, O. Diekmann, C.J. Nagelkerke, and P.A. Zegeling. Can a species keep pace with a shifting climate? *Bulletin of Mathematical Biology*, 71:399–429, 2009.

[19] A.S. Best, K. Johst, T. Münkemüller, and J.M.J. Travis. Which species will successfully track climate change? The influence of intraspecific competition and density dependent dispersal on range shifting dynamics. *Oikos*, 116:1531–1539, 2007.

[20] M. Bevers, J. Hof, D.W. Uresk, and G.L. Schenbeck. Spatial optimization of prairie dog colonies for black-footed ferret recovery. *Operations Research*, 45:495–507, 1997.

[21] R.J.H. Beverton. *On The Dynamics Of Exploited Fish Populations*. Her Majesty's Stationery Office, London, 1957.

[22] G. Bocedi, D. Zurell, B. Reineking, and J.M.J. Travis. Mechanistic modelling of animal dispersal offers new insights into range expansion dynamics across fragmented landscapes. *Ecography*, 37:1240–1253, 2014.

[23] I. Boulangeat, D. Gravel, and W. Thuiller. Accounting for dispersal and biotic interactions to disentangle the drivers of species distributions and their abundances. *Ecology Letters*, 15:584–593, 2012.

[24] J. Brommer, M.S. Fred, et al. Movement of the Apollo butterfly Parnassius apollo related to host plant and nectar plant patches. *Ecological Entomology*, 24:125–131, 1999.

[25] B.W. Brook, N.S. Sodhi, and C.J.A. Bradshaw. Synergies among extinction drivers under global change. *Trends in Ecology and Evolution*, 23:453–460, 2008.

[26] R.W. Brooker, J.M.J. Travis, E.J. Clark, and C. Dytham. Modelling species' range shifts in a changing climate: the impacts of biotic interactions, dispersal distance and the rate of climate change. *Journal of Theoretical Biology*, 245:59–65, 2007.

[27] J.H. Brown. On the relationship between abundance and distribution of species. *American Naturalist*, 124:255–279, 1984.

[28] L.M. Brown and E.E. Crone. Individual variation changes dispersal distance and area requirements of a checkerspot butterfly. *Ecology*, 97:106–115, 2016.

[29] L.B. Buckley, J.J. Tewksbury, and C.A .Deutsch. Can terrestrial ectotherms escape the heat of climate change by moving? *Proceedings of the Royal Society B*, 280:1149, 2013.

[30] J.M. Bullock, S.M. White, C. Prudhomme, C. Tansey, R. Perea, and D.A.P. Hooftman. Modelling spread of british wind-dispersed plants under future wind speeds in a changing climate. *Journal of Ecology*, 100:104–115, 2012.

[31] M.T. Burrows, D.S. Schoeman, L.B. Buckley, P. Moore, E.S. Poloczanska, K.M. Brander, C. Brown, J.F. Bruno, C.M. Duarte, B.S. Halpern, J. Holding, C.V. Kappel, W. Kiessling, M.I. O'Connor, J.M. Pandolfi, C. Parmesan, F.B. Schwing, W.J. Sydeman, and A.J. Richardson. The pace of shifting climate in marine and terrestrial ecosystems. *Science*, 334:652–655, 2011.

[32] M.T. Burrows, D.S. Schoeman, A.J. Richardson, J.G. Molinos, A. Hoffman, L.B. Buckley, P.J. Moore, C.J. Brown, J.F. Bruno, C.M. Duarte, B.S. Halpern, O. Hoegh-Guldberg, C.V. Kappel, W. Kiessling, M.I. O'Connor, J.M. Pandolfi, C. Parmesan, W.J. Sydeman, S. Ferrier, K.J. Williams, and E.S. Poloczanska. Geographical limits to species-range shifts are suggested by climate velocity. *Nature*, 507:492–495, 2014.

[33] S.H.M. Butchart, M. Walpole, B. Collen, A. van Strien, J.P.W. Scharlemann, R.E.A. Almond, J.E.M. Baillie, B. Bomhard, C. Brown, J. Bruno, K.E. Carpenter, G.M. Carr, J. Chanson, A.M. Chenery, J. Csirke, N.C. Davidson, F. Dentener, M. Foster, A. Galli, J.N. Galloway, P. Genovesi, R.D. Gregory, M. Hockings, V. Kapos, J.-F. Lamarque, F. Leverington, J. Loh, M.A. McGeoch, L. McRae, A. Minasyan, M.H. Morcillo, T.E.E. Oldfield, D. Pauly, S. Quader, C. Revenga, J.R. Sauer, B. Skolnik, D. Spear, D. Stanwell-Smith, S.N. Stuart, A. Symes, M. Tierney, T.D. Tyrrell, and J.-C. Vié. Global biodiversity: indicators of recent declines. *Science*, 328:1164–1168, 2010.

[34] M. Cabeza, M.B. Araújo, R.J. Wilson, C.D. Thomas, M.J.R. Cowley, and A. Moilanen. Combining probabilities of occurrence with spatial reserve design. *Journal of Applied Ecology*, 41:252–262, 2004.

[35] M. Cabeza and A. Moilanen. Design of reserve networks and the persistence of biodiversity. *Trends in Ecology and Evolution*, 16:242–248, 2001.

[36] C. Carroll, R.F. Noss, P.C. Paquet, and N.H. Schumaker. Use of population viability analysis and reserve selection algorithms in regional conservation plans. *Ecological Applications*, 13:1773–1789, 2003.

[37] H. Caswell. *Matrix Population Models: Construction, Analysis, and Interpretation.* Sinauer, Sunderland, MA., 2001.

[38] H. Caswell, R. Lensink, and M.G. Neubert. Demography and dispersal: life table response experiments for invasion speed. *Ecology*, 84:1968–1978, 2003.

[39] H. Caswell and M.G. Neubert. Reactivity and transient dynamics of discrete-time ecological systems. *Journal of Difference Equations and Applications*, 11(4-5):295–310, 2005.

[40] H. Caswell, M.G. Neubert, and C.M. Hunter. Demography and dispersal: invasion speeds and sensitivity analysis in periodic and stochastic environments. *Theoretical Ecology*, 4:407–421, 2011.

[41] A.L.M. Chauvenet, J.G. Ewen, D. Armstrong, and N. Pettorelli. Saving the hihi under climate change: a case for assisted colonization. *Journal of Applied Ecology*, 50:1330–1340, 2013.

[42] I.-C. Chen, J.K. Hill, R. Ohlemüller, D.B. Roy, and C.D. Thomas. Rapid range shifts of species associated with high levels of climate warming. *Science*, 333(6045):1024–1026, 2011.

[43] L.-M. Chevin. Genetic constraints on adaptation to a changing environment. *Evolution*, 67:708–721, 2013.

[44] L.-M. Chevin and R. Lande. When do adaptive plasticity and genetic evolution prevent extinction of a density-regulated population? *Evolution*, 64(4):1143–1150, 2010.

[45] L.-M. Chevin and R. Lande. When do adaptive plasticity and genetic evolution prevent extinction of a density-regulation population? *Evolution*, 64:1143–1150, 2010.

[46] L.-M. Chevin, R. Lande, and G.M. Mace. Adaptation, plasticity, and extinction in a changing environment: towards a predictive theory. *PLoS Biology*, 8:e1000357, 2010.

[47] R. Church and C. ReVelle. The maximal covering location problem. In *Papers of the Regional Science Association*, volume 32, pages 101–118, 1974.

[48] R.L. Church, D.M. Stoms, and F.W. Davis. Reserve selection as a maximal covering location problem. *Biological Conservation*, 76:105–112, 1996.

[49] J.S. Clark. Why trees migrate so fast: confronting theory with dispersal biology and the paleorecord. *The American Naturalist*, 152(2):204–224, 1998.

[50] M.A. Clemens, C.S. ReVelle, and J.C. Williams. Reserve design for species preservation. *European Journal of Operational Research*, 112:273–283, 1999.

[51] L. Collatz. Einschließungssatz für die charakteristischen zahlen von matrizen. *Mathematische Zeitschrift*, 48:221–226, 1942.

[52] R.T. Corlett and D.A. Westcott. Will plant movements keep up with climate change? *Trends in Ecology & Evolution*, 28:482–488, 2013.

[53] C. Costello and S. Polasky. Dynamic reserve site selection. *Resource and Energy Economics*, 26(2):157–174, 2004.

[54] S.S. Coster, Veysey Powell J.S., and K.J. Babbit. Characterizing the width of amphibian movements during postbreeding migration. *Conservation Biology*, 28:756–762, 2014.

[55] R.D. Cousens and A.A. Rawlinson. When will plant morphology affect the shape of a seed dispersal "kernel"? *Journal fo Theoretical Biology*, 211(3):229–238, 2001.

[56] V. Dakos, M. Scheffer, E.H. Van Nes, V. Brovkin, V. Petoukhov, and H. Held. Slowing down as an early warning signal for abrupt climate change. *Proceedings of the National Academy of Sciences*, 105:14308–14312, 2008.

[57] E.G. DeChaine and A.P. Martin. Historic cycles of fragmentation and expansion in parnassius smintheus (papilionidae) inferred using mitochondrial dna. *Evolution*, 58(1):113–127, 2004.

[58] T. Delattre, J.-B. Pichancourt, F. Burel, and P. Kindlmann. Grassy field margins as potential corridors for butterflies in agricultural landscapes: a simulation study. *Ecological Modelling*, 221(2):370–377, 2010.

[59] L.M. Delves and J. Walsh. *Numerical Solution of Integral Equations*. Clarendon Press, Oxford, 1974.

[60] S. Dewhirst and F. Lutscher. Dispersal in heterogeneous habitats: thresholds, spatial scales, and approximate rates of spread. *Ecology*, 90:1338–1345, 2009.

[61] S.Z. Dobrowski, J. Abatzoglou, A.K. Swanson, J.A. Greenberg, A.R. Mynsberge, Z.A. Holden, and M.K. Schwartz. The climate velocity of the contiguous united states during the 20th century. *Global Change Biology*, 19:241–251, 2013.

[62] M. Dolek and A. Geyer. Conserving biodiversity on calcareous grasslands in the Franconian Jura by grazing: a comprehensive approach. *Biological Conservation*, 104:351–360, 2002.

[63] S. Dullinger, A. Gattringer, W. Thuiller, D. Moser, N.E. Zimmermann, A. Guisan, W. Willner, C. Plutzar, M. Leitner, T. Mang, et al. Extinction debt of high-mountain plants under twenty-first-century climate change. *Nature Climate Change*, 2:619–622, 2012.

[64] J. Elith and J.R. Leathwick. Species distribution models: ecological explanation and prediction across space and time. *Annual Review of Ecology, Evolution, and Systematics*, 40:677, 2009.

[65] M.M. Ellis and E.E. Crone. The role of transient dynamics in stochastic population growth for nine perennial plants. *Ecology*, 94:1681–1686, 2013.

[66] S.P. Ellner, D.Z. Childs, and M. Rees. *Data-driven Modelling of Structured Populations*. Springer, 2016.

[67] W.F. Fagan and F. Lutscher. Average dispersal success: linking home range, dispersal, and metapopulation dynamics to reserve design. *Ecological Applications*, 16:820–828, 2006.

[68] L. Fahrig. Effects of habitat fragmentation on biodiversity. *Annual Review of Ecology, Evolution, and Systematics*, 34:487–515, 2003.

[69] A.M. Fischer, A.P. Weigel, C.M. Buser, R. Knutti, H.R. Künsch, M.A. Liniger, C. Schär, and C. Appenzeller. Climate change projections for switzerland based on a bayesian multi-model approach. *International Journal of Climatology*, 32:2348–2371, 2012.

[70] G. Fischer and G.K. Heilig. Population momentum and the demand on land and water resources. *Philosophical Transactions of the Royal Society of London B: Biological Sciences*, 352:869–889, 1997.

[71] US Fish and Wildlife Service. Recovery plan for the prairie species of western Oregon and southwestern Washington. *US Fish and Wildlife Service, Portland, Oregon. xi*, 2010.

[72] J. Fort, J. Pérez-Losada, and N. Isern. Fronts from integrodifference equations and persistence effects on the neolithic transition. *Physical Review E*, 76:031913, 2007.

[73] M.S. Fred and J.E. Brommer. Influence of habitat quality and patch size on occupancy and persistence in two populations of the Apollo butterfly (Parnassius apollo). *Journal of Insect Conservation*, 7:85–98, 2003.

[74] M.S. Fred and J.E. Brommer. The decline and current distribution of Parnassius apollo (Linnaeus) in Finland; the role of Cd. In *Annales Zoologici Fennici*, pages 69–79. JSTOR, 2005.

[75] M.S. Fred and J.E. Brommer. Olfaction and vision in host plant location by Parnassius apollo larvae: consequences for survival and dynamics. *Animal Behaviour*, 79:313–320, 2010.

[76] M.S. Fred, R.B. O'Hara, and J.E. Brommer. Consequences of the spatial configuration of resources for the distribution and dynamics of the endangered Parnassius apollo butterfly. *Biological Conservation*, 130:183–192, 2006.

[77] B.G. Freeman and A.M.C. Freeman. Rapid upslope shifts in New Guinean birds illustrate strong distributional responses of tropical montane species to global warming. *Proceedings of the National Academy of Sciences*, 111:4490–4494, 2014.

[78] Z. Fric and M. Konvicka. Dispersal kernels of butterflies: power-law functions are invariant to marking frequency. *Basic and Applied Ecology*, 8:377–386, 2007.

[79] M. Fujiwara, K.E. Anderson, M.G. Neubert, and H. Caswell. On the estimation of dispersal kernels from individual mark-recapture data. *Environmental and Ecological Statistics*, 13:183, 2006.

[80] R.A. Garcia, M. Cabeza, C. Rahbek, and M.B. Araújo. Multiple dimensions of climate change and their implications for biodiversity. *Science*, 344:1247579, 2014.

[81] T.C. Giannini, D.S. Chapman, A.M. Saraiva, I. Alves-dos Santos, and J.C. Biesmeijer. Improving species distribution models using biotic interactions: a case study of parasites, pollinators and plants. *Ecography*, 36:649–656, 2013.

[82] L. Gilbert-Norton, R. Wilson, J.R. Stevens, and K.H. Beard. A meta-analytic review of corridor effectiveness. *Conservation Biology*, 24:660–668, 2010.

[83] P.K. Gillingham, J. Alison, D.B. Roy, R. Fox, and C.D. Thomas. High abundances of species in protected areas in parts of their geographic distributions colonized during a recent period of climatic change. *Conservation Letters*, 2014.

[84] L. Gillson, T.P. Dawson, S. Jack, and M.A. McGeoch. Accommodating climate change contingencies in conservation strategy. *Trends in Ecology & Evolution*, 28:135–142, 2013.

[85] K. Gotthard, D. Berger, and R. Walters. What keeps insects small? Time limitation during oviposition reduces the fecundity benefit of female size in a butterfly. *The American Naturalist*, 169:768–779, 2007.

[86] A. Guisan and W. Thuiller. Predicting species distribution: offering more than simple habitat models. *Ecology letters*, 8:993–1009, 2005.

[87] D. Gutiérrez, J. Harcourt, S.B. Díez, J.G. Illán, and R.J. Wilson. Models of presence–absence estimate abundance as well as (or even better than) models of abundance: the case of the butterfly Parnassius apollo. *Landscape Ecology*, 28:401–413, 2013.

[88] J.C. Habel, M. Reuter, C. Drees, and J. Pfaender. Does isolation affect phenotypic variability and fluctuating asymmetry in the endangered Red Apollo? *Journal of Insect Conservation*, 16:571–579, 2012.

[89] J.C. Habel and T. Schmitt. The burden of genetic diversity. *Biological Conservation*, 147:270–274, 2012.

[90] N.M. Haddad. Finding the corridor more traveled. *Proceedings of the National Academy of Sciences*, 105:19569–19570, 2008.

[91] C.A.S. Hall, J.A. Stanford, and F.R. Hauer. The distribution and abundance of organisms as a consequence of energy balances along multiple environmental gradients. *Oikos*, pages 377–390, 1992.

[92] A. Hamann and S.N. Aitken. Conservation planning under climate change: accounting for adaptive potential and migration capacity in species distribution models. *Diversity and Distributions*, 19:268–280, 2013.

[93] J.M. Hammersley and D.C. Handscomb. *Monte Carlo Methods*. John Wiley & Sons, Inc. New York, 1964.

[94] Lee Hannah. *Climate Change Biology*. Elsevier, Burlington, MA, 2014.

[95] M.A. Harsch, A. Phillips, Y. Zhou, M.-R. Leung, D.S. Rinnan, and M. Kot. Moving forward: Insights and applications of moving-habitat models for climate change ecology. *Journal of Ecology*, 2016.

[96] M.A. Harsch, Y. Zhou, J. HilleRisLambers, and M. Kot. Keeping pace with climate change: Stage-structured moving-habitat models. *The American Naturalist*, 184:25–37, 2014.

[97] A. Hastings. Transient dynamics and persistence of ecological systems. *Ecology Letters*, 4:215–220, 2001.

[98] A. Hastings. Transients: the key to long-term ecological understanding? *Trends in Ecology & Evolution*, 19:39–45, 2004.

[99] A. Hastings and K. Higgins. Persistence of transients in spatially structured ecological models. *Science*, 263:1133–1136, 1994.

[100] N.E. Heller and E.S. Zavaleta. Biodiversity management in the face of climate change: a review of 22 years of recommendations. *Biological Conservation*, 142:14–32, 2009.

[101] N. Hewitt, N. Klenk, A.L. Smith, D.R. Bazely, N. Yan, S. Wood, J.I. MacLellan, C. Lipsig-Mumme, and I. Henriques. Taking stock of the assisted migration debate. *Biological Conservation*, 144:2560–2572, 2011.

[102] J. HilleRisLambers, M.A. Harsch, A.K. Ettinger, K.R. Ford, and E.J. Theobald. How will biotic interactions influence climate change–induced range shifts? *Annals of the New York Academy of Sciences*, 1297:112–125, 2013.

[103] J.A. Hodgson, C.D. Thomas, B.A. Wintle, and A. Moilanen. Climate change, connectivity and conservation decision making: back to basics. *Journal of Applied Ecology*, 46:964–969, 2009.

[104] C. Hof, M.B. Araújo, W. Jetz, and C. Rahbek. Additive threats from pathogens, climate and land-use change for global amphibian diversity. *Nature*, 480:516–519, 2011.

[105] J. Hof, M. Bevers, D.W. Uresk, and G.L. Schenbeck. Optimizing habitat location for black-tailed prairie dogs in southwestern South Dakota. *Ecological Modelling*, 147:11–21, 2002.

[106] J. Hof, C.H. Sieg, and M. Bevers. Spatial and temporal optimization in habitat placement for a threatened plant: the case of the western prairie fringed orchid. *Ecological Modelling*, 115:61–75, 1999.

[107] A.A. Hoffmann and C.M. Sgrò. Climate change and evolutionary adaptation. *Nature*, 470:479–485, 2011.

[108] T. Horiguchi and Y. Fukui. A variation of the jentzsch theorem for a symmetric integral kernel and its application. *Interdisciplinary Information Sciences*, 2:139–144, 1996.

[109] R.B. Huey, M.R. Kearney, A. Krockenberger, J.A.M. Holtum, M. Jess, and S.E. Williams. Predicting organismal vulnerability to climate warming: roles of behaviour, physiology and adaptation. *Philosophical Transactions of the Royal Society B: Biological Sciences*, 367:1665–1679, 2012.

[110] V. Hutson, J. Pym, and M. Cloud. *Applications of Functional Analysis and Operator Theory*. Academic Press, London, 2005.

[111] IPCC. Climate change 2013: The physical science basis. contribution of working group i to the fifth assessment report of the intergovernmental panel on climate change. Cambridge University Press, Cambridge, United Kingdom, 2013.

[112] S.T. Jackson and D.F. Sax. Balancing biodiversity in a changing environment: extinction debt, immigration credit and species turnover. *Trends in Ecology & Evolution*, 25:153–160, 2010.

[113] R. Jentzsch. Über integralgleichungen mit positivem kern. *Journal für die reine und angewandte Mathematik*, 141:235–244, 1912.

[114] H.R. Joshi, S. Lenhart, and H. Gaff. Optimal harvesting in an integrodifference population model. *Optimal Control Applications and Methods*, 27:61–75, 2006.

[115] A.S. Jump and J. Peñuelas. Running to stand still: adaptation and the response of plants to rapid climate change. *Ecology Letters*, 8:1010–1020, 2005.

[116] L. Kanary, J. Musgrave, R.C. Tyson, A. Locke, and F. Lutscher. Modelling the dynamics of invasion and control of competing green crab genotypes. *Theoretical Ecology*, 7:391–406, 2014.

[117] S. Karlin. Positive operators. *Journal of Mathematics and Mechanics*, 8:907–937, 1959.

[118] S. Karlin. The existence of eigenvalues for integral operators. *Transactions of the American Mathematical Society*, pages 1–17, 1964.

[119] M. Kearney, W.P. Porter, C. Williams, S. Ritchie, and A.A. Hoffmann. Integrating biophysical models and evolutionary theory to predict climatic impacts on species' ranges: the dengue mosquito Aedes aegypti in Australia. *Functional Ecology*, 23:528–538, 2009.

[120] N. Keyfitz. On the momentum of population growth. *Demography*, 8:71–80, 1971.

[121] H. Kierstead and L.B. Slobodkin. The size of water masses containing plankton blooms. *Journal of Marine Research*, 12:141, 1953.

[122] S. Klorvuttimontara, C.J. McClean, and J.K. Hill. Evaluating the effectiveness of Protected Areas for conserving tropical forest butterflies of Thailand. *Biological Conservation*, 144:2534–2540, 2011.

[123] L.Y. Kolotilina. Lower bounds for the perron root of a nonnegative matrix. *Linear Algebra and its Applications*, 180:133–151, 1993.

[124] D.N. Koons, R.F. Rockwell, and J.B. Grand. Population momentum: implications for wildlife management. *Journal of Wildlife Management*, 70:19–26, 2006.

[125] M. Kot, M.A. Lewis, and M.G. Neubert. Integrodifference equations. In A. Hastings and L. Gross, editors, *Encyclopedia of Theoretical Ecology*. University of California Press, Berkeley, 2012.

[126] M. Kot, M.A. Lewis, and P. Van Den Driessche. Dispersal data and the spread of invading organisms. *Ecology*, 77:2027–2042, 1996.

[127] M. Kot, J. Medlock, T. Reluga, and D.B. Walton. Stochasticity, invasions, and branching random walks. *Theoretical Population Biology*, 66:175–184, 2004.

[128] M. Kot and A. Phillips. Bounds for the critical speed of climate-driven moving-habitat models. *Mathematical Biosciences*, 262:65–72, 2015.

[129] M. Kot and A. Phillips. Bounds for the critical speed of climate-driven moving-habitat models. *Mathematical Biosciences*, 262:65–72, 2015.

[130] M. Kot and W.M. Schaffer. Discrete-time growth-dispersal models. *Mathematical Biosciences*, 80:109–136, 1986.

[131] Mark Kot. *Elements of Mathematical Ecology*. Cambridge University Press, 2001.

[132] S. Kotz and K. Podgorski. *The Laplace Distribution and Generalizations: A Revisit With Applications to Communications, Economics, Engineering, and Finance*. Birkhauser, Boston, MA, 2001.

[133] A. Kubisch, R.D. Holt, H.-J. Poethke, and E.A. Fronhofer. Where am I and why? Synthesizing range biology and the eco-evolutionary dynamics of dispersal. *Oikos*, 123:5–22, 2014.

[134] H. Kujala, A. Moilanen, M.B. Araújo, and M. Cabeza. Conservation planning with uncertain climate change projections. *PloS One*, 8:e53315, 2013.

[135] J. Latore, P. Gould, and A.M. Mortimer. Spatial dynamics and critical patch size of annual plant populations. *Journal of Theoretical Biology*, 190:277–285, 1998.

[136] T.-T. Lee and Y.-F. Chang. Solutions of convolution integral and integral equations via double general orthogonal polynomials. *International Journal of Systems Science*, 19:415–430, 1988.

[137] S.J. Leroux, M. Larrivée, V. Boucher-Lalonde, A. Hurford, J. Zuloaga, J.T. Kerr, and F. Lutscher. Mechanistic models for the spatial spread of species under climate change. *Ecological Applications*, 23:815–828, 2013.

[138] M.A. Lewis, M.G. Neubert, H. Caswell, J.S. Clark, and K. Shea. A guide to calculating discrete-time invasion rates from data. In M.W. Cadotte, S.M. McMahon, and T. Fukami, editors, *Conceptual Ecology and Invasion Biology: Reciprocal Approaches to Nature*, pages 169–192. Springer, Dordrecht, 2006.

[139] J. Liira and T. Paal. Do forest-dwelling plant species disperse along landscape corridors? *Plant Ecology*, 214:455–470, 2013.

[140] S.R. Loarie, P.B. Duffy, H. Hamilton, G.P. Asner, C.B. Field, and D.D. Ackerly. The velocity of climate change. *Nature*, 462:1052–1055, 2009.

[141] A. LoPresti, A. Charland, D. Woodard, J. Randerson, N.S. Diffenbaugh, and S.J. Davis. Rate and velocity of climate change caused by cumulative carbon emissions. *Environmental Research Letters*, 10:095001, 2015.

[142] B. Lozowski, A. Kdziorski, M. Nakonieczny, and P. Laszczyca. Parnassius apollo last-instar larvae development prediction by analysis of weather condition as a tool in the species? conservation. *Comptes Rendus Biologies*, 337:325–331, 2014.

[143] M.L. Mallory and A.W. Ando. The perils of shortcuts in efficient conservation portfolio design. *Resource and Energy Economics*, 2014.

[144] K.V. Mardia. Measures of multivariate skewness and kurtosis with applications. *Biometrika*, 57:519–530, 1970.

[145] C.R. Margules and R.L. Pressey. Systematic conservation planning. *Nature*, 405:243–253, 2000.

[146] J.E. Marsden and A. Tromba. *Vector Calculus*. Macmillan, 2003.

[147] S. Martello, D. Pisinger, and P. Toth. New trends in exact algorithms for the 0–1 knapsack problem. *European Journal of Operational Research*, 123:325–332, 2000.

[148] Y. Maruyama. A measure of multivariate kurtosis with principal components. *Communications in Statistics–Theory and Methods*, 37:2116–2123, 2008.

[149] S.F. Matter, A. Doyle, K. Illerbrun, J. Wheeler, and J. Roland. An assessment of direct and indirect effects of climate change for populations of the rocky mountain apollo butterfly (parnassius smintheus doubleday). *Insect Science*, 18:385–392, 2011.

[150] S.F. Matter and J. Roland. An experimental examination of the effects of habitat quality on the dispersal and local abundance of the butterfly parnassius smintheus. *Ecological Entomology*, 27:308–316, 2002.

[151] S.F. Matter and J. Roland. Mating failure of female parnassius smintheus butterflies: a component but not a demographic allee effect. *Entomologia Experimentalis et Applicata*, 146:93–102, 2013.

[152] S.F. Matter, J. Roland, A. Moilanen, and I. Hanski. Migration and survival of parnassius smintheus: detecting effects of habitat for individual butterflies. *Ecological Applications*, 14:1526–1534, 2004.

[153] S.F. Matter, T. Roslin, and J. Roland. Predicting immigration of two species in contrasting landscapes: effects of scale, patch size and isolation. *Oikos*, 111:359–367, 2005.

[154] A.J. McConnachie, M.P. De Wit, M.P. Hill, and M.J. Byrne. Economic evaluation of the successful biological control of azolla filiculoides in south africa. *Biological Control*, 28:25–32, 2003.

[155] J. Merilä and A.P. Hendry. Climate change, adaptation, and phenotypic plasticity: the problem and the evidence. *Evolutionary Applications*, 7:1–14, 2014.

[156] C. Miyagawa and T. Seo. A new multivariate kurtosis and its asymptotic distribution. *SUT Journal of Mathematics*, 47:55–71, 2011.

[157] A. Moilanen. Reserve selection using nonlinear species distribution models. *The American Naturalist*, pages 695–706, 2005.

[158] A. Moilanen and M. Cabeza. Accounting for habitat loss rates in sequential reserve selection: simple methods for large problems. *Biological conservation*, 136:470–482, 2007.

[159] M.-A. Moritz, M.A .and Parisien, E. Batllori, M.A. Krawchuk, J. Van Dorn, D.J. Ganz, and K. Hayhoe. Climate change and disruptions to global fire activity. *Ecosphere*, 3:1–22, 2012.

[160] P.W. Mote and E.P. Salathe Jr. Future climate in the Pacific Northwest. *Climatic Change*, 102:29–50, 2010.

[161] P.J. Mumby, I.A. Elliott, C.M. Eakin, W. Skirving, C.B. Paris, H.J. Edwards, S. Enríquez, R. Iglesias-Prieto, L.M. Cherubin, and J.R. Stevens. Reserve design for uncertain responses of coral reefs to climate change. *Ecology Letters*, 14:132–140, 2011.

[162] M. Nakonieczny, K. Michalczyk, and A. Kedziorski. Midgut glycosidases activities in monophagous larvae of Apollo butterfly, Parnassius apollo ssp. frankenbergeri. *Comptes Rendus Biologies*, 329:765–774, 2006.

[163] R. Nathan, F.M. Schurr, O. Spiegel, A. Steinitz, O.and Trakhtenbrot, and A. Tsoar. Mechanisms of long-distance seed dispersal. *Trends in Ecology & Evolution*, 23:638–647, 2008.

[164] M.G. Neubert and H. Caswell. Alternatives to resilience for measuring the responses of ecological systems to perturbations. *Ecology*, 78:653–665, 1997.

[165] M.G. Neubert and H. Caswell. Demography and dispersal: calculation and sensitivity analysis of invasion speed for structured populations. *Ecology*, 81:1613–1628, 2000.

[166] M.G. Neubert, M. Kot, and M.A. Lewis. Dispersal and pattern formation in a discrete-time predator-prey model. *Theoretical Population Biology*, 48:7–43, 1995.

[167] T.A. Nuñez, J.J. Lawler, B.H. Mcrae, D.J. Pierce, M.B. Krosby, D.M. Kavanagh, P.H. Singleton, and J.J. Tewksbury. Connectivity planning to address climate change. *Conservation Biology*, 27:407–416, 2013.

[168] A. Okubo and S.A. Levin. *Diffusion and Ecological Problems: Modern Perspectives*, volume 14. Springer Science & Business Media, 2013.

[169] O. Ovaskainen and I. Hanski. Transient dynamics in metapopulation response to perturbation. *Theoretical Population Biology*, 61:285–295, 2002.

[170] C. Parmesan. Ecological and evolutionary responses to recent climate change. *Annual Review of Ecology, Evolution, and Systematics*, pages 637–669, 2006.

[171] C. Parmesan and G. Yohe. A globally coherent fingerprint of climate change impacts across natural systems. *Nature*, 421:37–42, 2003.

[172] A. Phillips and M. Kot. Persistence in a two-dimensional moving-habitat model. *Bulletin of Mathematical Biology*, 77:2125–2159, 2015.

[173] B.L. Phillips, G.P. Brown, and R. Shine. Life-history evolution in range-shifting populations. *Ecology*, 91:1617–1627, 2010.

[174] A.C. Pipkin. *A Course on Integral Equations*. Springer-Verlag, New York, 1991.

[175] F. Pithan and T. Mauritsen. Arctic amplification dominated by temperature feedbacks in contemporary climate models. *Nature Geoscience*, 7:181–184, 2014.

[176] V.D. Popescu, L. Rozylowicz, D. Cogălniceanu, I.M. Niculae, and A.L. Cucu. Moving into protected areas? setting conservation priorities for romanian reptiles and amphibians at risk from climate change. *PloS one*, 8:e79330, 2013.

[177] D. Porter and D.S.G. Stirling. *Integral Equations: A Practical Treatment, from Spectral Theory to Applications*. Cambridge University Press, 1990.

[178] A.B. Potapov and M.A. Lewis. Climate and competition: the effect of moving range boundaries on habitat invasibility. *Bulletin of Mathematical Biology*, 66:975–1008, 2004.

[179] F.M. Pouzols and A. Moilanen. A method for building corridors in spatial conservation prioritization. *Landscape Ecology*, 29:789–801, 2014.

[180] A.M. Prasad, J.D. Gardiner, L.R. Iverson, S.N. Matthews, and M. Peters. Exploring tree species colonization potentials using a spatially explicit simulation model: implications for four oaks under climate change. *Global Change Biology*, 19:2196–2208, 2013.

[181] W.H. Press, W.T. Teukolsky, S.A .and Vetterling, and B.P. Flannery. *Numerical Recipes 3rd Edition: The Art of Scientific Computing*. Cambridge University Press, New York, 2007.

[182] I. Quintero and J.J. Wiens. Rates of projected climate change dramatically exceed past rates of climatic niche evolution among vertebrate species. *Ecology Letters*, 16:1095–1103, 2013.

[183] A. Ricciardi and D. Simberloff. Assisted colonization is not a viable conservation strategy. *Trends in Ecology & Evolution*, 24:248–253, 2009.

[184] J. Roland, N. Keyghobadi, and S. Fownes. Alpine parnassius butterfly dispersal: effects of landscape and population size. *Ecology*, 81:1642–1653, 2000.

[185] J. Roland and S.F. Matter. Encroaching forests decouple alpine butterfly population dynamics. *Proceedings of the National Academy of Sciences*, 104:13702–13704, 2007.

[186] J. Roland and S.F. Matter. Variability in winter climate and winter extremes reduces population growth of an alpine butterfly. *Ecology*, 94:190–199, 2013.

[187] M.J. Samways. Insect conservation: a synthetic management approach. *Annu. Rev. Entomol.*, 52:465–487, 2007.

[188] B. Sandel and E.M. Dangremond. Climate change and the invasion of California by grasses. *Global Change Biology*, 18:277–289, 2012.

[189] G. Sansone. *Orthogonal Functions*. Dover Publications, Inc., Mineola, New York, 2004.

[190] D. Savage, M.J. Barbetti, W.J. MacLeod, M.U. Salam, and M. Renton. Timing of propagule release significantly alters the deposition area of resulting aerial dispersal. *Diversity and Distributions*, 16:288–299, 2010.

[191] D. Savage, M.J. Barbetti, W.J. MacLeod, M.U. Salam, and M. Renton. Can mechanistically parameterised, anisotropic dispersal kernels provide a reliable estimate of wind-assisted dispersal? *Ecological Modelling*, 222:1673–1682, 2011.

[192] M. Scheffer, S.R. Carpenter, T.M. Lenton, J. Bascompte, W. Brock, V. Dakos, J. Van De Koppel, I.A. Van De Leemput, S.A. Levin, E.H. Van Nes, et al. Anticipating critical transitions. *Science*, 338:344–348, 2012.

[193] K. Schiffers, E.C. Bourne, S. Lavergne, W. Thuiller, and J.M.J. Travis. Limited evolutionary rescue of locally adapted populations facing climate change. *Philosophical Transactions of the Royal Society B: Biological Sciences*, 368:20120083, 2013.

[194] C.A. Schloss, T.A. Nuñez, and J.J. Lawler. Dispersal will limit ability of mammals to track climate change in the western hemisphere. *Proceedings of the National Academy of Sciences*, 109:8606–8611, 2012.

[195] D.S. Schmeller, M. Dolek, A. Geyer, J. Settele, and R. Brandl. The effect of conservation efforts on morphological asymmetry in a butterfly population. *Journal for Nature Conservation*, 19:161–165, 2011.

[196] S.D. Schoville and G.K. Roderick. Alpine biogeography of parnassian butterflies during quaternary climate cycles in north america. *Molecular ecology*, 18:3471–3485, 2009.

[197] C.B. Schultz. Dispersal behavior and its implications for reserve design in a rare Oregon butterfly. *Conservation Biology*, 12:284–292, 1998.

[198] C.B. Schultz and E.E. Crone. Burning prairie to restore butterfly habitat: A modeling approach to management tradeoffs for the Fender's blue. *Restoration Ecology*, 6:244–252, 1998.

[199] C.B. Schultz and E.E. Crone. Edge-mediated dispersal behavior in a prairie butterfly. *Ecology*, 82:1879–1892, 2001.

[200] C.B. Schultz and E.E. Crone. Using ecological theory to develop recovery criteria for an endangered butterfly. *Journal of Applied Ecology*, 52:1111–1115, 2015.

[201] C.B. Schultz and P.C. Hammond. Using population viability analysis to develop recovery criteria for endangered insects: case study of the fender's blue butterfly. *Conservation Biology*, 17:1372–1385, 2003.

[202] A.J. Schwenk. Tight bounds on the spectral radius of asymmetric nonnegative matrices. *Linear Algebra and its Applications*, 75:257–265, 1986.

[203] J. Settele, E. Kuehn, and J. Thomas. *Studies on the Ecology and Conservation of Butterflies in Europe, Volume 1: General Concepts and Case Studies*. Pensoft Publishing, 2005.

[204] TA Severini. *Elements of Distribution Theory*. Cambridge University Press, Cambridge, UK, 2005.

[205] P.M. Severns. Exotic grass invasion impacts fitness of an endangered prairie butterfly, *icaricia icarioides fenderi*. *Journal of Insect Conservation*, 12:651–661, 2008.

[206] C.M. Sgrò, A.J. Lowe, and A.A. Hoffmann. Building evolutionary resilience for conserving biodiversity under climate change. *Evolutionary Applications*, 4:326–337, 2011.

[207] J.A. Sherratt, B.T. Eagan, and M.A. Lewis. Oscillations and chaos behind predator–prey invasion: mathematical artifact or ecological reality? *Philosophical Transactions of the Royal Society of London B: Biological Sciences*, 352:21–38, 1997.

[208] N. Shigesada and K. Kawasaki. *Biological Invasions: Theory and Practice*. Oxford University Press, UK, 1997.

[209] O. Skarpaas and K. Shea. Dispersal patterns, dispersal mechanisms, and invasion wave speeds for invasive thistles. *The American Naturalist*, 170:421–430, 2007.

[210] B.D. Smith and M.A. Zeder. The onset of the anthropocene. *Anthropocene*, 4:8–13, 2013.

[211] R.E. Snyder. What makes ecological systems reactive? *Theoretical Population Biology*, 77:243–249, 2010.

[212] M.S. Srivastava. A measure of skewness and kurtosis and a graphical method for assessing multivariate normality. *Statistics & Probability Letters*, 2:263–267, 1984.

[213] R. St. John and S.F. Tóth. Spatially explicit forest harvest scheduling with difference equations. *Annals of Operations Research*, pages 1–23, 2013.

[214] M.D. Staudinger, S.L. Carter, M.S. Cross, N.S. Dubois, J.E. Duffy, C. Enquist, R. Griffis, J.J. Hellmann, J.J. Lawler, J. O'Leary, et al. Biodiversity in a changing climate: a synthesis of current and projected trends in the us. *Frontiers in Ecology and the Environment*, 11:465–473, 2013.

[215] W. Steffen, J. Grinevald, P. Crutzen, and J. McNeill. The anthropocene: conceptual and historical perspectives. *Philosophical Transactions of the Royal Society of London A: Mathematical, Physical and Engineering Sciences*, 369:842–867, 2011.

[216] V.M. Stevens, C. Turlure, and M. Baguette. A meta-analysis of dispersal in butterflies. *Biological Reviews*, 85:625–642, 2010.

[217] C.A. Stockwell, A.P. Hendry, and M.T. Kinnison. Contemporary evolution meets conservation biology. *Trends in Ecology & Evolution*, 18:94–101, 2003.

[218] I. Stott, S. Townley, and D.J. Hodgson. A framework for studying transient dynamics of population projection matrix models. *Ecology Letters*, 14:959–970, 2011.

[219] N. Strange, B.J. Thorsen, and J. Bladt. Optimal reserve selection in a dynamic world. *Biological Conservation*, 131:33–41, 2006.

[220] J.-C. Svenning and B. Sandel. Disequilibrium vegetation dynamics under future climate change. *American Journal of Botany*, 100:1266–1286, 2013.

[221] C.D. Thomas. Climate, climate change and range boundaries. *Diversity and Distributions*, 16:488–495, 2010.

[222] C.D. Thomas, P.K. Gillingham, R.B. Bradbury, D.B. Roy, B.J. Anderson, J.M. Baxter, N.A.D. Bourn, H.Q.P. Crick, R.A. Findon, R. Fox, et al. Protected areas facilitate species' range expansions. *Proceedings of the National Academy of Sciences*, 109:14063–14068, 2012.

[223] W. Thuiller, L.J. Pollock, M. Gueguen, and T. Münkemüller. From species distributions to meta-communities. *Ecology Letters*, 18:1321–1328, 2015.

[224] M.T. Tinker, D.F. Doak, and J.A. Estes. Using demography and movement behavior to predict range expansion of the southern sea otter. *Ecological Applications*, 18:1781–1794, 2008.

[225] V. Todisco, P. Gratton, D. Cesaroni, and V. Sbordoni. Phylogeography of Parnassius apollo: hints on taxonomy and conservation of a vulnerable glacial butterfly invader. *Biological Journal of the Linnean Society*, 101:169–183, 2010.

[226] S.F. Tóth, R.G. Haight, and L.W. Rogers. Dynamic reserve selection: Optimal land retention with land-price feedbacks. *Operations Research*, 59:1059–1078, 2011.

[227] S. Townley, D. Carslake, O. Kellie-Smith, D. McCarthy, and D. Hodgson. Predicting transient amplification in perturbed ecological systems. *Journal of Applied Ecology*, 44:1243–1251, 2007.

[228] J.M.J. Travis and C. Dytham. Habitat persistence, habitat availability and the evolution of dispersal. *Proceedings of the Royal Society B: Biological Sciences*, 266:723–728, 1999.

[229] M.C. Urban. Accelerating extinction risk from climate change. *Science*, 348:571–573, 2015.

[230] R.W. Van Kirk and M.A. Lewis. Integrodifference models for persistence in fragmented habitats. *Bulletin of Mathematical Biology*, 59:107–137, 1997.

[231] R.W. Van Kirk and M.A. Lewis. Edge permeability and population persistence in isolated habitat patches. *Natural Resource Modeling*, 12:37–64, 1999.

[232] C. Van Swaay, S. Collins, G. Dušej, D. Maes, M.L. Munguira, L. Rakosy, N. Ryrholm, M. Šašić, J. Settele, J. Thomas, et al. Dos and don'ts for butterflies of the habitats directive of the european union. *Nature Conservation*, 1:73–153, 2012.

[233] C. van Swaay, M. Warren, and G. Lois. Biotope use and trends of european butterflies. *Journal of Insect Conservation*, 10:189–209, 2006.

[234] C.A.M.A. van Swaay and M.S. Warren. Prime butterfly areas of europe: An initial selection of priority sites for conservation. *Journal of Insect Conservation*, 10:5–11, 2006.

[235] J. VanDerWal, H.T. Murphy, A.S. Kutt, B.L. Perkins, G.C .and Bateman, J.J. Perry, and A.E. Reside. Focus on poleward shifts in species' distribution underestimates the fingerprint of climate change. *Nature Climate Change*, 3:239–243, 2013.

[236] R.R. Veit and M.A. Lewis. Dispersal, population growth, and the allee effect: dynamics of the house finch invasion of eastern north america. *The American Naturalist*, 148:255–274, 1996.

[237] P. Visconti, R.L. Pressey, D.B. Segan, and B.A. Wintle. Conservation planning with dynamic threats: the role of spatial design and priority setting for species? persistence. *Biological Conservation*, 143:756–767, 2010.

[238] M.E. Visser. Keeping up with a warming world; assessing the rate of adaptation to climate change. *Proceedings of the Royal Society B: Biological Sciences*, 275:649–659, 2008.

[239] J. Wang. A family of kurtosis orderings for multivariate distributions. *Journal of Multivariate Analysis*, 100:509–517, 2009.

[240] M.-L. Wang, R.-Y. Chang, and S.-Y. Yang. Double generalized orthogonal polynomial series for the solution of integral equations. *International Journal of Systems Science*, 19:459–470, 1988.

[241] G.N. Watson. *A Treatise on the Theory of Bessel functions*. Cambridge University Press, New York, 1995.

[242] J.J. Wiens, D.D. Ackerly, A.P. Allen, B.L. Anacker, L.B. Buckley, H.V. Cornell, E.I. Damschen, T. Jonathan Davies, S.P. Grytnes, J.-A.and Harrison, et al. Niche conservatism as an emerging principle in ecology and conservation biology. *Ecology Letters*, 13:1310–1324, 2010.

[243] R.J. Wilson and I.M.D. Maclean. Recent evidence for the climate change threat to lepidoptera and other insects. *Journal of Insect Conservation*, 15:259–268, 2011.

[244] M.C. Wimberly and Z. Liu. Interactions of climate, fire, and management in future forests of the pacific northwest. *Forest Ecology and Management*, 327:270–279, 2014.

[245] C. Wissel. A universal law of the characteristic return time near thresholds. *Oecologia*, 65:101–107, 1984.

[246] L.A. Wolsey. *Integer Programming*. Wiley New York, 1998.

[247] R.J. Wood and M. O'Neill. Finding the spectral radius of a large sparse non-negative matrix. *ANZIAM Journal*, 48:C330–C345, 2007.

[248] R.J. Wood and M.J. O'Neill. An always convergent method for finding the spectral radius of an irreducible non-negative matrix. *ANZIAM Journal*, 45:C474–C485, 2004.

[249] S.A. Woodin, T.J. Hilbish, B. Helmuth, S.J. Jones, and D.S. Wethey. Climate change, species distribution models, and physiological performance metrics: predicting when biogeographic models are likely to fail. *Ecology and Evolution*, 3:3334–3346, 2013.

[250] S. Yalçınbaş, M. Aynigül, and T. Akkaya. Legendre series solutions of fredholm integral equations. *Mathematical and Computational Applications*, 15:371–381, 2010.

[251] L. Yeh. Inequalities for the maximal eigenvalue of a nonnegative matrix. *Glasgow Mathematical Journal*, 39:276–284, 1997.

[252] Y. Zhou and M. Kot. Discrete-time growth-dispersal models with shifting species ranges. *Theoretical Ecology*, 4:13–25, 2011.

[253] Y. Zhou and M. Kot. Life on the move: Modeling the effects of climate-driven range shifts with integrodifference equations. In M.A. Lewis, P.K. Maini, and S.V. Petrovskii, editors, *Dispersal, Individual Movement and Spatial Ecology*, pages 263–292. Springer, Berlin, Germany, 2013.